Dissertation

Study on Electroplating and Electrochemical Properties of Dimethyl Sulfone-Aluminum Chloride Electrolyte with Ammonium Salt

（アンモニウム塩を添加したジメチルスルホン－塩化アルミニウム電解液のめっき特性と電気化学的特性に関する研究）

Junichi Matsuda

Student ID number: 20701987

Energy and Environment Science,

Graduate School of Engineering,

Nagaoka University of Technology

August 2023

Table of Contents

Chapter 1. Introduction

1.1. Background

1.1.1. Features of aluminum

Aluminum (Al) is a lightweight metal with a specific gravity of 2.7, excellent electrical and thermal conductivity, and good workability. It also offers good corrosion resistance because it forms a dense oxide film on its surface to prevent corrosion. In addition, its properties can be modified by alloying it with other metal elements. Al of the 1000 series, represented by 1100, 1N30, and so on, is a 99.00% pure soft material that has excellent abovementioned properties with a low strength. Nevertheless, its strength and softness can be improved by alloying it with elements, such as Cu and Mn. Al alloys are classified into forgings and castings. Table 1-1 summarizes the alloy species and main components of Al forgings alloys [1]. Al alloys in the 2000 series, including duralumin (2017) and super duralumin (2024), contain Cu and have higher strength but inferior corrosion resistance than pure Al. Al alloys in the 3000 series contain Mn and have high strength and similar level of workability and corrosion resistance as in pure Al. It is mainly used for building materials, containers, aircraft, and many more. Al alloys in the 4000 series contain Si and have excellent heat and wear resistance and are generally used in architectural panels as a brazing filler owing to its low melting temperature than that of pure Al. Al alloys in the 5000 series contain Mg and have good corrosion resistance and weldability, have relatively high strength, and are used in ships, vehicles, and pressure vessels. Al alloys in the 6000 series contain Mg and Si and have excellent strength and corrosion resistance. These alloys are widely used in aluminum sashes, railway vehicles, and automobiles. Al alloys in the 7000 series contain Zn. The strongest material among the Al alloys is 7075, called ultra-duralumin, which is mainly used in aircraft components. Al alloys in the 8000 series comprise alloys other than those in the 1000–7000 series. These alloys have good spreadability

and corrosion resistance and are often used as a foil for packaging and telecommunications. Thus, the characteristics of Al differ considerably based on the type and number of chemical components and heat treatment, indicating that Al has wide applications in different fields such as transportation, construction, electronic packaging.

Table 1-1. Aluminum alloy series and symbols and compositions [1].

Series	Symbols	Compositions
1000 series	1100, 1050, 1N30	Pure Al (purity >99.00%)
2000 series	2017, 2024	Al–Cu alloys
3000 series	3003	Al–Mn alloys
4000 series	4004, 4032	Al–Si alloys
5000 series	5052, 5083	Al–Mg alloys
6000 series	6061	Al–Mg–Si alloys
7000 series	7075	Al–Zn alloys
8000 series	8021, 8079	Alloys other than the above

1.1.2. Aluminum refining

Al is the most abundant metallic element in the Earth's crust and has more resources compared to Fe and Cu. It does not exist as a metal but as alumina (Al_2O_3) in bauxite, which is mainly produced in Australia, China, Guinea, Brazil, and Indonesia [2]. Bauxite contains 51%–57% Al_2O_3; highly pure Al_2O_3 can be purified (refined) from bauxite using the Bayer process. In this process, bauxite is first washed with sodium hydroxide solution at 250 °C to obtain aluminum hydroxide ($Al(OH)_3$) (Eqs. 1-1, 1-2). The extracted $Al(OH)_3$ is heated to 1050 °C to obtain high-purity Al_2O_3 (Eq. 1-3). Next, metallic Al can be obtained by smelting Al_2O_3 using the Hall–Héroult process [3,4]. In this process, Al_2O_3 is dissolved in cryolite (Na_3AlF_6) at about 1000 °C. Then metallic Al is formed on the cathode (carbon electrolyte) via the electrolysis (Eq. 1-4). The purity of the produced Al considerably depends on the purity of the raw material, i.e., Al_2O_3, and generally has about 99% purity. For further purification of Al ingots, i.e., to achieve a purity of 99.9%–99.99%, a three-layer electrolysis method or a segregation method is used [5]. The Bayer process and the Hall–Héroult process are currently the only practical smelting methods for Al ingots. However, these processes are associated with very high processing temperature of about 1000 °C and consume a large amount of electricity during the melting and electrolysis of Al_2O_3, along with adverse environmental impacts. Thus, recently, there is increased research on producing Al ingots from Al scrap using the electroplating method to contribute to a carbon-neutral society [6–11]. In this regard, the Al electroplating method has attracted much attention as a method for recycling Al from scrap.

$$Al_2O_3 + 2NaOH + 3H_2O \rightleftharpoons 2Na^+ + 2[Al(OH)_4]^- \quad (1\text{-}1)$$

$$2Na^+ + 2[Al(OH)_4]^- \rightleftharpoons Al(OH)_3\downarrow + Na^+ + OH^- \quad (1\text{-}2)$$

$$2Al(OH)_3 \rightleftharpoons Al_2O_3 + 3H_2O \quad (1\text{-}3)$$

$$Al_2O_3 + 3C \rightleftharpoons 2Al + 3CO \quad (1\text{-}4)$$

1.1.3. Aluminum coating

Various Al-coating methods can impart the thermal and electrical conductivities and corrosion resistance of Al on material surfaces. Thus, Al coating has wide applications. The major Al coating methods include hot-dip plating [12–16], thermal spraying [17,18], vapor deposition [19–23], and sputtering [24,25].

In the hot-dip plating method for Al coating, the material is immersed in a molten Al bath at 660 ℃ or higher, resulting in an Al coating of several hundred μm to several mm on the material surface. During hot-dip plating, an alloy layer of the material and Al is formed at the interface between the material and the Al film [12]. Molten Al plating is often used to enhance the corrosion resistance of steel materials, but a brittle Fe–Al alloy is formed at the interface between the steel material and Al, which may reduce the workability of steel materials. In such a case, Si may be added to the plating bath to suppress the formation of the alloy layer at the interface [13].

In the thermal spraying method, the Al is melted using a heat source, such as gas or electric arc, and spraying the molten Al on the material surface. The molten Al is atomized by a high-pressure gas, and fine droplets are pressed on the material surface, enabling its spread and solidification. Compared to the hot-dip plating method, the thermal spraying method does not form an alloy layer at the interface with the material but is associated with poor adhesion of the film and difficult-to-control film thickness. So, pretreatment and management of the material are essential steps in the thermal spraying method [17,18].

Vapor deposition methods are categorized into physical vapor deposition [19,20] and chemical vapor deposition [21–23]. In both cases, Al is heated and evaporated in a depressurized atmosphere, and the vapor is adsorbed on the material surface. This method is widely used top form an Al vapor deposition film on a plastic film. In the sputtering method of Al coating, the Al atoms released by colliding noble gas ions, such as Ar, form a film on the

target surface in a depressurized atmosphere [24,25]. In the vapor deposition method and sputtering method, Al with few impurities can be uniformly deposited at nm-order thickness. Nevertheless, these methods require equipment to maintain a high vacuum atmosphere and involve cumbersome processes. Since deposition occurs inside the equipment, deposition loss that cannot be ignored occurs as the thickness of the coating layer increases, with the increase of the process cost.

In recent years, electroplating (electrodeposition) has attracted attention as a coating method that can solve the problems of the abovementioned conventional coating methods. This method enables film formation at low temperature and normal pressure. In addition, Al can be coated in the μm-order, which is difficult to achieve via hot-dip plating or thermal spraying. This method also forms a dense film of Al at a faster speed and lower cost than the vapor deposition method. Nevertheless, the Al electrodeposition process has not yet been put to wide practical use. It potential applications include corrosion resistant coating [26], efforts to color by anodizing [26,27], production of current collector foil for lithium ion batteries [28–30], and Al batteries using electrodeposition and dissolution reaction of Al [31].

1.1.4. Aluminum electroplating

The electroplating process using the aqueous solution is widely used in diverse industrial fields for decoration, anti-corrosion, wear resistance because of its easy solution handling, waste liquid treatment, and low-cost. However, there are limited metal elements that can be electrodeposited in this process, and base metals, such as Al, Mg, and Ti, cannot be deposited. The feasibility of electrodeposition of metals in an aqueous solution is determined by the standard electrode potential (E^0) of the electrodeposition reaction and the hydrogen overvoltage for the electrodeposited metal. Table 1-2 summarizes the standard electrode potential (E^0) of metal electrodeposition reaction, the hydrogen overvoltage on the

electrodeposition metal [33], and the hydrogen evolution potential at each metal surface, considering the hydrogen overvoltage. The hydrogen overvoltage is the difference between the actual hydrogen evolution potential on each metal surface and the standard electrode potential of the hydrogen generation reaction. If the standard electrode potential is positive, as in the case of Ag or Cu, metal electrodeposition takes precedence over hydrogen generation. Therefore, Ag and Cu can be electrodeposited from an aqueous solution. The standard electrode potential of Zn electrodeposition reaction is −0.762 V vs. SHE, which is more negative potential than the standard electrode potential of the hydrogen generation reaction. However, since the hydrogen overvoltage on the Zn surface is 0.95 V, the actual hydrogen evolution potential at the Zn surface, taking into account the hydrogen overvoltage, is −0.95 V vs. SHE, which is more negative than the standard electrode potential of Zn electrodeposition. Therefore, the electrodeposition reaction of Zn in the aqueous solution takes precedence over the hydrogen generation reaction, and Zn can be electrodeposited from the aqueous solution. The standard electrode potential of Cr is −0.744 V vs. SHE, which is more negative than the hydrogen evolution potential (−0.5 V vs. SHE) and considers the hydrogen overvoltage at the Cr surface. However, since the difference is small, the electrodeposition reaction of Cr in an aqueous solution proceeds with hydrogen generation. Conversely, the standard electrode potential of Al is −1.676 V vs. SHE, which is more negative than the hydrogen generation potential (−0.7 V vs. SHE) that considers the hydrogen overvoltage at Al surface. Therefore, the hydrogen evolution reaction proceeds preferentially over the Al electrodeposition reaction in an aqueous solution, making it difficult to electrodeposit Al. Thus, a nonaqueous electrolyte should be used for electrodeposition of Al. Many types of electrolyte solutions have been reported for Al electrodeposition and are classified into molten salts [34–40], ionic liquids [41–52], organic solvents [53–62], and deep eutectic solvents [63–91].

The binary system of $NaCl–AlCl_3$ or the ternary system of $NaCl–KCl–AlCl_3$ molten salts is classified as molten salt systems [34–40]. They may be mixed with $NaAlCl_4$ or metal

chlorides. These electrolyte solutions are easy to obtain and inexpensive, and thus, the construction bath cost is relatively low. However, most studies have examined this system at 150 °C–200 °C and 20–50 mA cm^{-2}, and this system is associated with high temperature and slow speed. In addition, the molar concentration of $AlCl_3$ is relatively high at 56–64 mol%, and its vapor pressure is high, increasing the evaporation of $AlCl_3$ from the electrolyte solution.

The ionic liquid system, also called room temperature molten salt, generally has a low melting point and is in a liquid state under normal temperature and pressure. For example, electrolyte solutions using 1-butylpyridinium chloride (BPC) [41,42] and 1-ethyl-3-methylimidazolium chloride (EMIC) [43–52] have been reported. These systems can perform Al electrodeposition near room temperature but have a low current density of 10–20 mA cm^{-2} near room temperature [45,46]. Note that it is difficult to coat at high speed. Thus, the temperature needs to be increased above the room temperature to coat at high speed using an ionic liquid. In addition, since BPC and EMIC are expensive, the high bath cost of the electrolyte solution hinders the practical application of this process.

Examples of electrolyte solution classified as organic solvents system include those using aromatic hydrocarbons, such as toluene and benzene [53–55], and those using ether-based solutions, such as diethyl ether and tetrahydrofuran (THF) [56–62]. These organic solvent-based electrolyte solutions have low melting point, low viscosity, high conductivity, and low-cost compared to other systems. Studies have examined an electrolyte of toluene–triethylaluminum ($Al(C_2H_5)_3$)–NaF called the SIGAL (i.e., Simens Galvano–Aluminum) process in Simens, and an electrolyte of THF–$AlCl_3$–lithium aluminum hydride ($LiAlH_4$) called REAL (i.e., room temperature electroplated aluminum) bath in Philips [58]. Nevertheless, these organic solvent-based electrolytic solutions have high solvent volatility and flammability, indicating a major safety issue.

A deep eutectic solvent is similar to an ionic liquid obtained by mixing a polar organic compound and a salt, and properties, such as the melting point of the liquid, change depending

on the mixing ratio. In recent years, sulfone-based solvents [63–84], such as dimethyl sulfone ($(CH_3)_2SO_2$, $DMSO_2$), diethyl sulfone, and dipropyl sulfone, have been classified as deep eutectic solvents and have low volatility and flammability and are easy to handle. The electrolyte using $DMSO_2$ as a solvent has a melting point of 109 °C, so the processing temperature is slightly higher than that of other systems. However, it is cheaper than ionic liquids and can be processed with a current density of 50 mA cm^{-2} or more, suggesting the possibility of electrodeposition at high speed [70–72]. Other deep eutectic solvents include electrolytes using grime-based [85–88], amide-based [89], and urea-based [90,91] solvents that have a lower melting point than $DMSO_2$.

These electrolytes are prepared by mixing aluminum halides of Lewis acid, such as $AlCl_3$ and $AlBr_3$.

Table 1-2. Difference between E^0 and hydrogen generation potential for each electrodeposition reaction.

Electrode reaction	E^0/V vs. SHE	Hydrogen overvoltage* /V	Hydrogen evolution potential considering hydrogen overvoltage/V	Difference between E^0 and hydrogen generation potential/V
$Al^{3+} + 3e^- \rightleftharpoons Al$	−1.676	0.70	−0.70	−0.976
$Zn^{2+} + 2e^- \rightleftharpoons Zn$	−0.763	0.95	−0.95	0.187
$Cr^{3+} + 3e^- \rightleftharpoons Cr$	−0.744	0.50	−0.50	−0.244
$Fe^{2+} + 2e^- \rightleftharpoons Fe$	−0.440	0.35	−0.35	−0.090
$Ni^{2+} + 2e^- \rightleftharpoons Ni$	−0.257	0.30	−0.30	0.043
$Pb^{2+} + 2e^- \rightleftharpoons Pb$	−0.126	1.20	−1.20	1.074
$2H^+ + 2e^- \rightleftharpoons H_2$	0.000	0.00	0.00	0.000
$Cu^{2+} + 2e^- \rightleftharpoons Cu$	0.339	0.45	−0.45	0.789
$Ag^+ + e^- \rightleftharpoons Ag$	0.799	0.30	−0.30	1.099

*The hydrogen overvoltage is a typical value at 1 mA cm^{-2} in an acidic solution [33].

1.1.5. Electrodeposition reaction of aluminum

The electrodeposition reaction of Al varies greatly depending on the type of electrolyte. Ionic species are generated in the electrolyte in molten salts and ionic liquids systems according to Eq. 1-5. As shown in Eq. 1-6, $Al_2Cl_7^-$ is generated when the mole fraction of $AlCl_3$ exceeds 0.5 [43,44]. $Al_2Cl_7^-$ is reduced according to Eq. 1-7, and the metal Al is deposited. Here, RCl is an inorganic salt, such as NaCl, and an organic salt, such as 1-ethyl-3-methylimidazolium chloride.

$$AlCl_3 + RCl \rightleftharpoons R^+ + AlCl_4^- \quad (1\text{-}5)$$

$$AlCl_3 + AlCl_4^- \rightleftharpoons Al_2Cl_7^- \quad (1\text{-}6)$$

$$4Al_2Cl_7^- + 3e^- \rightleftharpoons Al + 7AlCl_4^- \quad (1\text{-}7)$$

In a deep eutectic solvent, Al cations and anions are generally produced according to Eqs. 1-8 and 1-9. The generated Al cation is electrochemically reduced to deposit Al. Here, base is a polar organic molecule such as $DMSO_2$ and urea.

$$2\ AlCl_3 + n\text{Base} \rightleftharpoons (AlCl_2 \cdot n\text{Base})^+ + AlCl_4^- \quad (1\text{-}8)$$

$$4\ AlCl_3 + n\text{Base} \rightleftharpoons (Al(\text{Base})n)^{3+} + 3AlCl_4^- \quad (1\text{-}9)$$

The ionic species and equilibrium state in the electrolyte change depending on the type of electrolyte and the mixing ratio with salt. Thus, it is important to determine the ionic species and equilibrium state in the electrolyte to understand the characteristics of the electrolyte and electrodeposition film for practical application of the Al electrodeposition process.

1.1.6. Dimethyl sulfone-aluminum chloride electrolyte solution

The Al electrolyte solution using $DMSO_2$ as a solvent has high safety and productivity and low bath cost; thus, it has a high potential for industrial use. This electrolyte solution primarily comprises $DMSO_2$ and $AlCl_3$. According to Legrand's report, the reaction equation of $DMSO_2$ and $AlCl_3$ is represented in Eq. 1-10, wherein $Al(DMSO_2)_3^{3+}$ and $AlCl_4^-$ are formed in the electrolyte solution [65–67]. During electrodeposition, as represented by Eq. 1-11, $Al(DMSO_2)_3^{3+}$ is reduced and Al is deposited on the cathode. When Al is used as the anode, $Al(DMSO_2)_3^{3+}$ is dissolved from the anode, as represented by Eq. 1-12, and the concentration of $Al(DMSO_2)_3^{3+}$ in the electrolyte solution remains constant.

$$4AlCl_3 + 3DMSO_2 \rightleftharpoons Al(DMSO_2)_3^{3+} + 3AlCl_4^- \quad (1\text{-}10)$$

$$Al(DMSO_2)_3^{3+} + 3e^- \rightleftharpoons Al + 3DMSO_2 \quad (1\text{-}11)$$

$$Al + 3DMSO_2 \rightleftharpoons Al(DMSO_2)_3^{3+} + 3e^- \quad (1\text{-}12)$$

Table 1-3 summarizes an example of an electrolyte solution using $DMSO_2$ as a solvent. Although the mixing ratio of $DMSO_2$ and $AlCl_3$ can be described in various ways, the mixing ratio of 1 mol to $DMSO_2$ is shown here for ease of comparison. When the mixing molar ratio of $DMSO_2$ and $AlCl_3$ is 1:0.1 (mol), black deposits are formed, adversely affecting the formation of good electrodeposition films [79,80]. These black deposits are defects that are not desired at all. Many studies have mixed 0.2–0.3 mol of $AlCl_3$ with 1 mol of $DMSO_2$ and have studied the process temperature of the $DMSO_2$–$AlCl_3$ electrolyte at 110 °C–130 °C since the melting point of $DMSO_2$ is about 109 °C. Some studies have reported that the melting point of the electrolyte solution can be decreased to 25 °C or less by setting the mixed molar ratio of $DMSO_2$ and $AlCl_3$ to 1:0.38–0.40 (mol) [70,76]. This electrolyte composition lowers the process temperature and prevents solidification of the electrolyte solution due to uneven

temperature in the tank and piping during operation, thereby suppressing a decline in production efficiency. The conductivity of the electrolyte also decreases with this composition, so that the tank voltage and power consumption increase. The conductivity of the $DMSO_2$–$AlCl_3$ electrolyte has been reported in terms of the effect of the mixing ratio of $DMSO_2$ and $AlCl_3$ and temperature [70,76], but the effect of additives has not been examined. Many previous studies have investigated the use of additives to improve film properties, such as high purity [26,28,72], glossing [71,74,77] and alloying [83]. Energy saving in this process requires not only high conductivity but also high Coulombic efficiency. Note that Coulombic efficiency is evaluated for the effect of mixing ratio and current density [70,80] but not for the effect of additives. In many studies, the current density is 50 mA cm^{-2} or less. Since current density directly affects the deposition rate, the conditions that allow plating at a higher current density are desired industrially. To surpass vapor deposition method and the sputtering method, the electrodeposition method should have a deposition rate of 1 μm min^{-1} or more. The Al electrodeposition film obtained from the $DMSO_2$–$AlCl_3$ electrolyte solution without additives contains carbon, sulfur, and chlorine as impurities; it is also harder and brittle than general Al materials [26,28,72,80]. The addition of ammonium salts, such as dimethylamine hydrochloride [26] and trimethylamine hydrochloride [28,72] is effective in reducing the amount of impurities and improving brittleness. Several cases of analysis of electrode reactions by electrochemical measurement and evaluation of Coulombic efficiency in additive-free systems have been reported [63,64,80]. However, the effects of these ammonium salts on electrodeposition reactions and Coulombic efficiency have not been clarified.

From the abovementioned studies, it is important to consider the study of additives aimed at increasing the conductivity of $DMSO_2$–$AlCl_3$ electrolyte solution and the evaluation of Coulombic efficiency and polarization characteristics using an electrolyte with additives.

Table 1-3. Composition ratio and conditions of $DMSO_2$–$AlCl_3$ electrolyte per 1 mol of $DMSO_2$.

$DMSO_2$ /mol	$AlCl_3$ /mol	Additive	Amount of additive /mol	Temperature /°C	Current density /mA cm^{-2}	Ref.
1	0.1	—	—	130	—	[63]
1	0.2	LiCl	0.1	130	—	[64]
1	0.1	—	—	130	—	[65]
1	0.1	—	—	130	—	[66]
1	0.1–0.4	—	—	100–150	50–200	[70]
1	0.3	Dimethylamine hydrochloride	0.01	110	50	[26]
1	0.3	Trimethylamine hydrochloride	0.01	95	50	[28]
1	0.2	$ZrCl_4$	0–0.0015	110	60	[71]
1	0.2, 0.3	Trimethylamine hydrochloride	0–0.04	110	20–80	[72]
1	0.3			110	15	[73]
1	0.2	Tetraethylenepentamine	0–0.02	110	40	[74]
1	0.3	—	—	110	30	[75]
1	0.2, 0.38	—	—	110	50	[76]
1	0.2	Diethylenetriamine, Triethkenetetramine, Tetraethylenepentamine, Pentaethylenehexamine	0–0.04	110	Hull-cell	[77]
1	0.2	—	—	110	40	[78]
1	0.11–0.25	LiCl	0.05–0.25	130	Constant potential	[79]
1	0.066–0.39	—	—	130	40	[80]
1	0.3	—	—	130	40	[81]
1	0.3	$SnCl_2$	0.00002–0.0005	110	30	[82]
1	0.3	$TiCl_4$, $CrCl_3$, $MnCl_2$, $FeCl_2$, $NiCl_2$, CuCl, $ZnCl_2$, $GaCl_3$	0.001	90–110	10–30	[83]
1	0.2, 0.3	Dimethylamine hydrochloride	0.001–0.01	110	40–80	[84]

1.2. Purpose and significance of this work

The main focus of this study was to establish an electrolyte composition that exhibited high electrical conductivity and allowed plating with high Coulombic efficiency. In addition, it aimed to elucidate the factors affecting the anodic dissolution process in $DMSO_2$–$AlCl_3$ electrolyte. Herein, the goal was to achieve a conductivity of 0.5 S m^{-1} or more at 100 °C and a Coulombic efficiency of 80% or more. As described above, when the mixed molar ratio of $DMSO_2$ and $AlCl_3$ is 1:0.38 (mol), the conductivity of the electrolyte is lower than the most reported composition of 1:0.20–0.30 (mol). Furthermore, the tank voltage and power consumption of the Al electrodeposition process increase. The increase in power consumption can be a major barrier to the practical application of the Al electrodeposition process. Hence, the conductivity of the electrolyte should be increased to save energy during this process. Herein, my aim was to make the conductivity of the electrolyte exceed that of the 1:0.2 (mol) composition, representing the highest conductivity of any Al electrodeposition capable composition. Generally, an additive that serves as supporting electrolyte is added to increase the conductivity of the electrolyte. In this study, additives were added to the basic composition ($DMSO_2$:$AlCl_3$ = 1:0.38 (mol)) to save the energy during this process. In addition to conductivity of the electrolyte, Coulombic efficiency is a crucial factor for energy saving. Thus, both high Coulombic efficiency and high conductivity in the electrolyte should be required simultaneously. The Coulombic efficiency was aimed at 80% or more considering the economic rationality. Moreover, the overvoltage of electrodeposition and dissolution reactions must be decreased to facilitate energy saving.

The significance of this study is that the author examined additives that are effective in improving conductivity of electrolyte and elucidated the mechanism by which these additives affect conductivity and Coulombic efficiency. Additionally, the elucidation of factors affecting the anodic dissolution process was studied through electrochemical measurements. Therefore,

this study offers a low-cost Al electrodeposition process because of the low power consumption and energy savings.

1.3. Outline of the dissertation

In Chapter 1, the features of Al, its coating method, and different types of electrolytes for Al electrodeposition were introduced. In addition, the reasons for selecting the electrolyte used in this study and that used in previous studies were described. Accordingly, the purpose and guidelines of this study were shown.

In Chapter 2, the author determined an electrolyte composition that exhibited high electrical conductivity and allows plating with high Coulombic efficiency. First, an effective additive for increasing conductivity of the electrolyte solution was determined, and then the mechanism to increase conductivity was examined. NH_4Cl and TMAC were found to be effective in increasing conductivity, and a decrease in viscosity was found to contribute to increased conductivity. In addition, from the ionic equilibrium change in the electrolyte due to their addition, the viscosity decreased with the increase in the amount of free $DMSO_2$. Next, the effects of the additive on Coulombic efficiency, film appearance, and purity were evaluated. The conductivity of the electrolyte was improved while the Coulombic efficiency was minimized by adding 0.02 mol NH_4Cl and 0.10 mol TMAC to the electrolyte solution. Moreover, the amount of power consumption required for Al electrolysis was decreased to about 1/3 compared to no additives. Furthermore, promising results were obtained with respect to the appearance and purity of the electrodeposition film.

In Chapter 3, cyclic voltammetry of $DMSO_2$–$AlCl_3$ electrolyte solution was performed using a microelectrode to clarify the effect of the addition of NH_4Cl or TMAC on the cathode reaction. NH_4Cl promoted Al electrodeposition reaction, but Coulombic efficiency decreased with the increasing NH_4Cl concentrations. Meanwhile, TMAC suppressed the Al

electrodeposition reaction in the potential region where the side reaction occurred. When adding both NH_4Cl and TMAC, the action of NH_4Cl took precedence over that of TMAC; the Al electrodeposition reaction was promoted and a large dissolution current was obtained. Therefore, electrolyte containing both NH_4Cl and TMAC has excellent electrochemical properties.

In Chapter 4, anodic dissolution chronopotentiometry was performed to clarify the factors affecting the anodic dissolution reaction of $DMSO_2$–$AlCl_3$ electrolyte solution. The $DMSO_2$–$AlCl_3$ electrolyte solution was found to undergo transition to another anodic dissolution reaction with a potential of 1.0V higher than the normal anodic dissolution reaction during the anodic dissolution reaction, producing $Al_2Cl_7^-$ from Al and $AlCl_4^-$. The mechanism of transition to another reaction is that $DMSO_2$ is depleted in the vicinity of the electrode due to insufficient supply of $DMSO_2$ via diffusion to the electrode surface. NH_4Cl and TMAC were found to promote the diffusion supply of $DMSO_2$ by decreasing the viscosity of the electrolyte.

In Chapter 5, the contents described in the above chapters were summarized, and the conclusions of this paper and the prospects for future were described.

1.4. References

[1] JIS H4000.

[2] U.S. Geological Survey, Mineral Commodity Summaries, Jan. (2023).

[3] T. Murakami, *Materia Jpn.*, **58**, 553 (2019).

[4] M. Takemoto, *J. Jpn. Inst. Light Met.*, **7**, 15 (1957).

[5] N. Tsuchimashi, *J. Jpn. Inst. Light Met.*, **44**, 406 (1994).

[6] J. Xu, J. Zhang, Z, Shi, B. Gao, Z. Wang, and Z. Hu, *T NONFERR METAL SOC*, **24**, 250 (2014).

[7] Y. Wang, R. G. Reddy, and R. Wang, *J. Clean. Prod.*, **287**, 125043 (2021).

[8] X. Liu, Z. Zhengyang, T. Hiraki, O. Takeda, H. Zhu, K. Matsubae, and T. Nagasaka, *Nature*, **606**, 511 (2022).

[9] J. Nunomura, H. Matsushima, Y. Kyo, Y. Kojima, and M. Ueda, *J. Electrochem. Soc.*, **169**, 082518 (2022).

[10] S. Oya, J. Nunomura, H. Matsushima, Y. Kyo, Y. Kojima, and M. Ueda, *Electrochemistry*, **90**, 127001 (2022).

[11] B. Adhikari, T. E. Lister, and R. G. Reddy, *Sustain. Prod. Consum.*, **33**, 932 (2022).

[12] T. Ohnishi, Y. Noguchi, M. Nishiyama, and T. Nakayama, *J. Japan Inst. Metals*, **56**, 198 (1992).

[13] J. Maki, T. Izaki, and K. Tano, *J. Surf. Finish. Soc. Jpn.*, **51**, 1229 (2000).

[14] W. Deqing, S. Ziyuan, and Z. Longjiang, *Appl. Surf. Sci.*, **214**, 304 (2003).

[15] D. Wang and Z. Shi, *Appl. Surf. Sci.*, **227**, 225 (2004).

[16] S. Kainuma, M. Yang, Y. Gao, and M. Hashimoto, *Constr Build Mater.*, **280**, 122516 (2021).

[17] R. G. Song, W. Z. He, and W. D. Huang, *Surf. Coat. Technol.*, **130**, 20 (2000).

[18] R. S. C. Paredes, S. C. Amico, and A. S. C. M. d'Oliveira, *Surf. Coat. Technol.*, **200**,

3049 (2006).

[19] J. C. S. Fernandes and M. G. S. Ferreira, *Surf. Coat. Technol.*, **52**, 289 (1992).

[20] C. Charrier, P. Jacquot, E. Denisse, J. P. Millet, and H. Mazille, *Surf. Coat. Technol.*, **90**, 29 (1997).

[21] D. Yang, R. Jonnalagadda, B. R. Rogers, J. T. Hillman, R. F. Foster, and T. S. Cale, *Thin Solid Films*, **332**, 312 (1998).

[22] T. Suzuki and H. Umehara, *Carbon*, **37**, 47 (1999).

[23] T. Nakajima and K. Yamashita, *J. Mol. Struct.*, **490**, 155 (1999).

[24] M. S. Chu and S. K. Wu, *Acta Mater.*, **51**, 3109 (2003).

[25] A. P. Baraban, M. A. Dobrotvorskii, D. I. Elets, I. E. Gabis, V. G. Kuznetsov, V. A. Piven, A. P. Voyt, and A. A. Selivanov, *Thin Solid Films*, **709**, 138217 (2020).

[26] H. Hoshi, A. Okamoto, and S. Ando, *Hitachi Metals Tech. Rev.*, **27**, 20 (2011).

[27] T. Hirai, H. Matsushima, and M. Ueda, *J. Surf. Finish. Soc. Jpn.*, **71**, 32 (2020).

[28] A. Okamoto, M. Morita, and N. Yoshimoto, *J. Surf. Finish. Soc. Jpn.*, **63**, 641 (2012).

[29] H. Sakaida, K. Goto, K. Kimura, K. Okuno, J. Nishimura, and A. Hosoe, *Sumitomo Electric Industries Tech. Rev.*, **190**, 78 (2017).

[30] K. Ui, S. Kobayashi, K, Sasaki, T. Takeguchi, T. Tsuda, M. Ueda, J. Nunomura, Y. Honkawa, and Y. Kojima, *J. Electrochem. Soc.*, **168**, 056510 (2021).

[31] T. Tsuda, I. Kokubo, M. Kawabata, M. Yamagata, M. Ishikawa, S. Kusumoto, A. Imanishi, and S. Kuwabata, *J. Electrochem. Soc.*, **161**, A908 (2014).

[32] M. C. Lin, M. Gong, B. Lu, Y. Wu, D. Y. Wang, M. Guan, M. Angell, C. Chen, J. Yang, B. J. Hwang, and H. Dai, *Nature*, **520**, 325 (2015).

[33] H. Kita and M. Honda, *DENKI KAGAKU*, **38**, 17 (1970).

[34] P. Fellner, M. Chrenkova-Paucirova, and K. Matiasovsky, *Surf. technol.*, **14**, 101 (1981).

[35] L. Qingfeng, H. A. Hjuler, R. W. Berg, and N. J. Bjerrum, *J. Electrochem. Soc.*, **137**, 2794 (1990).

[36] M. Jafarian, M. G. Mahjani, F. Global, and I. Danaee, *J. Electroanal. Chem.*, **588**, 190 (2006).

[37] M. Jafarian, M. G. Mahjani, F. Global, and I. Danaee, *J. Electroanal. Chem.*, **366**, 1169 (2006).

[38] M. Ueda, R. Inaba, and T. Ohtsuka, *Electrochim. Acta*, **100**, 281 (2013).

[39] K. Sato, H. Matsushima, and M. Ueda, *APPL SURF SCI.*, **388**, 794 (2016).

[40] F. Zhua, K. Li, W. Song, L. Li, D. Zhang, and K. Qiu, *Intermetallics*, **139**, 107341 (2021).

[41] J. Robinson and R. A. Osteryoung, *J. Electrochem. Soc.*, **127**, 122 (1980).

[42] S. Takahashi, K. Akimoto, and I. Saeki, *J. Surf. Finish. Soc. Jpn.*, **40**, 548 (1989).

[43] J. S. Wilkes, J. A. Levisky, R. A. Wilson, and C. L. Hussey, *Inorg. Chem.*, **17**, 2728 (1978).

[44] A. A. Fannin, D. A. Floreani, L. A. King, J. S. Landers, B. J. Piersma, D. J. Stech, R. L. Vaughn, J. S. Wilkes, and J. L. Williams, *J. Phys. Chem.*, **21**, 1263 (1984).

[45] T. Tsuda, T. Nohira, and Y. Ito, *Electrochim. Acta*, **47**, 2817 (2002).

[46] T. Yatsushiro, N. Koura, S. Nakano, K. Ui, and K. Takeuchi, *Electrochemistry*, **74**, 233 (2006).

[47] T. Jiang, M. J. Chollier Brym, G. Dubé, A. Lasia, and G. M. Brisard, *Surf. Coat. Technol.*, **201**, 1 (2006).

[48] T. Jiang, M. J. Chollier Brym, G. Dubé, A. Lasia, and G. M. Brisard, *Surf. Coat. Technol.*, **201**, 10 (2006).

[49] J. Tang and K. Azumi, *Electrochim. Acta*, **56**, 1130 (2011).

[50] A. Endo, M. Miyake, and T. Hirato, *Electrochim. Acta*, **137**, 470 (2014).

[51] Y. Fang, K. Yoshii, X. Jiang, X. Sun, T. Tsuda, N. Mehio, and S. Dai, *Electrochim. Acta*, **160**, 82 (2015).

[52] H. Matsushima, H. Takahashi, T. Suzuki, M. Ueda, and I. Mogi, *Electrochem Commun*,

115, 106733 (2020).

[53] G. A. Capuano and W. G. Davenport, *J. Electrochem. Soc.*, **118**, 1688 (1971).

[54] M. Yoshio, M. Matsuyuki, I. Iwasawa, and M. Nagamatsu, *Kinzoku Hyomen Gijutsu*, **26**, 416 (1975).

[55] F. S. Platis and G. A. Capuano, *J. Electrochem. Soc.*, **134**, 2425 (1987).

[56] M. Yoshio, N. Ishibashi, H. Waki, and T. Seiyama, *J. Inorg. Nucl. Chem.*, **34**, 2439 (1972).

[57] N. Ishibashi and M. Yoshio, *Electrochim. Acta*, **17**, 1343 (1972).

[58] J. F. M. van der Berg, T. E. G. Daenen, G. Krijl, and R. E. van de Leest, *Philips tech., Rev.*, **39**, 87 (1980).

[59] M. Galova, *Surf. Technol.*, **11**, 357 (1980).

[60] M. Galova and D. Kladekova, *Surf. technol.*, **11**, 371 (1980).

[61] M. Galova, D. Kladekova, and L. Lux, *Surf. technol.*, **13**, 315 (1981).

[62] Q. Chen, D. Tan, R. Liu, and W. Li, Surf. *Coat. Technol.*, **205** 4418 (2011).

[63] L. Legrand, A. Tranchant, and R. Messina, *Electrochim. Acta*, **39**, 1427 (1994).

[64] L. Legrand, A. Tranchant, and R. Messina, *J. Electrochem. Soc.*, **141**, 378 (1994).

[65] L. Legrand, M. Heintz, A. Tranchant, and R. Messina, *Electrochim. Acta*, **40**, 1711 (1995).

[66] L. Legrand, A. Tranchant, and R. Messina, *Electrochim. Acta*, **41**, 2715 (1996).

[67] L. Legrand, A. Tranchant, and R. Messina, *Inorg. Chem.*, **35**, 1310 (1996).

[68] L. Legrand, E. Chassaing, A. Chausse, and R. Messina, *Electrochim. Acta*, **43**, 3109 (1998).

[69] T. Hirato, J. Fransaer, and J. P. Celis, *J. Electrochem. Soc.*, **148**, C280 (2001).

[70] T. Jiang, M. J. Chollier Brym, G. Dube, A. Lasia, and G. M. Brisard, *Surf. Coat. Technol.*, **201**, 6309 (2007).

[71] S. Shiomi, M. Miyake, and T. Hirato, *J. Electrochem. Soc.*, **159**, D225 (2012).

[72] M. Miyake, H. Motonami, S. Shiomi, and T. Hirato, *Surf. Coat. Technol.*, **206**, 4225 (2012).

[73] I. Matsui, S. Ono, Y. Takigawa, T. Uesugi, and K. Higashi, *Mater. Sci. Eng. A*, **550**, 363 (2012).

[74] M. Miyake, Y. Kubo, and T. Hirato, *J. Surf. Finish. Soc. Jpn.*, **64**, 364 (2013).

[75] I. Matsui, Y. Hanaoka, S. Ono, Y. Takigawa, T. Uesugi, and K. Higashi, *Mater. Lett.*, **109**, 229 (2013).

[76] A. Okamoto, M. Morita, and N. Yoshimoto, *J. Surf. Finish. Soc. Jpn.*, **65**, 47 (2014).

[77] M. Miyake, Y. Kubo, and T. Hirato, *Electrochim. Acta*, **120**, 423 (2014).

[78] H. Okamoto, M. Miyake, and T. Hirato, *J. MMIJ*, **130**, 70 (2014).

[79] S. Kim, S. Kumeno, K. Kamebuchi, K. Kuroda, and M. Okido, *J. surf. eng. mater. Adv. Technol.*, **8**, 110 (2018).

[80] S. Kim, N. Matsunaga, K. Kuroda, and M. Okido, *J. Electrochem. Sci. Technol.*, **9**, 69 (2018).

[81] S. Kim, K. Kuroda, and M. Okido, *SN appl. Sci.*, **1**, 53 (2019).

[82] C. Kuma, K. Sato, I. Matsui, Y. Takigawa, T. Uesugi, and K. Higashi, *Mater. Lett.*, **244**, 192 (2019).

[83] C. Kuma, K. Sato, Y. Hanaoka, I. Matsui, Y. Takigawa, T. Uesugi, and K. Higashi, *J. Alloys Compd*, **783**, 919 (2019)."

[84] M. Miyake, M. Hirata, H. Okamoto, and T. Hirato, *J. Surf. Finish. Soc. Jpn.*, **70**, 523 (2019).

[85] A. Kitada, K. Nakamura, K. Fukami, and K. Murase, *Electrochemistry*, **82**, 946 (2014).

[86] A. Kitada, K. Nakamura, K. Fukami, and K. Murase, *Electrochim. Acta*, **211**, 561 (2016).

[87] A. Kitada, Y. Kato, K. Fukami, and K. Murase, *J. Surf. Finish. Soc. Jpn.*, **69**, 310 (2018).

[88] Z. Zhang, A. Kitada, T. Chen, K. Fukami, M. Shimizu, S. Arai, Z. Yao, and K. Murase, *ACS Appl. Mater. Interfaces*, **12**, 43289 (2020).

[89] M. Li, B. Gao, C. Liu, W. Chen, Z. Shi, X. Hu, and Z. Wang, *Electrochim., Acta*, **180**, 811 (2015).

[90] M. Malik, K. L. Ng, and G. Azimi, *Electrochim. Acta*, **354**, 136708 (2020).

[91] V. S. Cvetkovic, N. M. Vukicevic, N. Jovicevic, J. S. Stevanovic, and J. N. Jovicevic, *T NONFERR METAL SOC*, **30**, 823 (2020).

Chapter 2. Conductivity Enhancement and Evaluation of Electroplating Properties of Dimethyl Sulfone–Aluminum Chloride Electrolyte Solution containing Ammonium Salt

2.1. Introduction

The purpose of this chapter is to find an electrolyte composition that exhibits high electrical conductivity and allows plating with high Coulombic efficiency. The respective target values are a conductivity is 0.5 S m^{-1} or more at 100 °C, and a Coulombic efficiency of 80% or more. In this chapter, the author explored effective additives for increasing the conductivity of the electrolyte and clarified its mechanism of the conductivity increase.

Then, plating experiments were carried out under the conditions of 100 °C and 80 mA cm^{-2} using the electrolytic solution containing the discovered additives, and the Coulombic efficiency and film appearance were evaluated. By carrying out this study, it was confirmed that it is possible to obtain a plating film with a good appearance with a Coulombic efficiency exceeding the target when plating with the electrolytic solution of the found composition under the conditions.

As shown in Chapter 1, the $DMSO_2$–$AlCl_3$ electrolyte solution is main composed of $DMSO_2$ and $AlCl_3$. It is known that when $DMSO_2$ and $AlCl_3$ are mixed, $AlCl_4^-$ and $Al(DMSO_2)_3^{3+}$ were formed, as expressed in Eq. 2-1 [1–3]. $Al(DMSO_2)_3^{3+}$ is reduced to Al on the cathode in the electrodeposition reaction, as shown in Eq. 2-2. Using Al as the anode, $Al(DMSO_2)_3^{3+}$ is dissolved from the Al anode. The $Al(DMSO_2)_3^{3+}$ concentration in the electrolyte solution was maintained constant, as shown in Eq. 2-3.

$$4AlCl_3 + 3DMSO_2 \rightleftharpoons Al(DMSO_2)_3^{3+} + 3AlCl_4^- \quad (2\text{-}1)$$

$$Al(DMSO_2)_3^{3+} + 3e^- \rightleftharpoons Al + 3DMSO_2 \quad (2\text{-}2)$$

$$Al + 3DMSO_2 \rightleftharpoons Al(DMSO_2)_3^{3+} + 3e^- \quad (2\text{-}3)$$

The melting point of $DMSO_2$, a solvent, is 109 °C. Due to the need to study phenomena at temperatures higher than the melting temperature of solvents, most of the $DMSO_2$–$AlCl_3$ electrolyte solutions have been studied at temperatures above 109 °C. Some studies have shown that the melting point of the electrolyte solution drops significantly below 109 °C when the ratio of $AlCl_3$ to $DMSO_2$ is defined at 1:0.38–0.4 [4,5]. However, if the temperature is lowered too much, there is concern that the conductivity will be too low. In this study, 100 °C was selected as the minimum temperature at which the decrease in conductivity could be acceptable under conditions where Al can be electrodeposited. By lowering the temperature of the electrolyte, the energy required for heating can be reduced. Current density has been often studied at 20–100 mA cm^{-2} in previous studies on this electrolyte. A higher current density is advantageous from the viewpoint of productivity. There are also reports that the higher the current density, the lower the impurity concentration in the electrodeposited film [6]. Based on these past studies, the author decided to verify the effects of adding additive at a current density of 80 mA cm^{-2}.

To increase conductivity in the solution, it is generally beneficial to increase charge carrier density and charge carrier mobility. In order to increase the charge carrier density in the electrolyte, the additive must dissolve in the electrolyte and dissociate into anions and cations. In this study, ammonium salts and inorganic salts, that are soluble in $DMSO_2$–$AlCl_3$ electrolyte solution, were selected, referring to previous studies. The mobility of the charge carrier is affected by the size of

the charge carrier ion species. If the radius of the charge carrier ion is large, the mobility is decreased, and the conductivity will decrease. On the other hand, if the ionic radius is too small, the charge carrier becomes a solvated ion as a result of strong solvation with the solvent molecules. Therefore, candidate additive compounds with different ion sizes after dissociation were selected and compared. In order to simplify the composition of ion species in the electrolyte, chloride ions were selected as the anion species. In this study, ammonium chloride (NH_4Cl), tetramethylammonium chloride (TMAC), lithium chloride, and sodium chloride were investigated as additives for conductivity enhancement.

2.2. Experimental

2.2.1. Preparation of the electrolyte solution

300 g of $DMSO_2$ (Bergstrom Nutrition, purity > 99.0%) was placed in a 0.3 L glass vessel with an inner diameter of 75 mm and dissolved by heating to 110 °C or higher using a hot stirrer, a rubber heater, and a temperature regulator while supplying N_2 at a flow rate of 2 L min^{-1}. While stirring the dissolved $DMSO_2$, $AlCl_3$ (KANTO CHEMICAL CO., INC., purity > 98.0%) was added. The mixing ratio of $DMSO_2$ and $AlCl_3$ was 1:0.38 (molar ratio), this mixed molar ratio is the basic composition. Thereafter, NH_4Cl (KANTO CHEMICAL CO., INC., purity > 99.5%), TMAC (KANTO CHEMICAL CO., INC., purity > 96.0%), LiCl (KANTO CHEMICAL CO., INC., purity > 99.0%) or NaCl (KANTO CHEMICAL CO., INC., purity > 99.5%) was added and completely dissolved. The addition amounts of NH_4Cl and TMAC were in the range of 0.00–0.38 mol per 1 mol of $DMSO_2$. Hereinafter, the amount of NR_4Cl is expressed as the number of moles per 1 mol of $DMSO_2$, NH_4Cl and TMAC are referred to as NR_4Cl (R = H or CH_3). To suppress the water contamination of the electrolyte, each additive was dried at about 100 °C under a reduced pressure atmosphere prior to the experiments.

2.2.2. Conductivity, viscosity, and melting point of the electrolyte

A conductivity meter (DKK-TOA CO., MM-41DP) was employed to measure the electrolyte conductivity. The conductivity meter was placed in the heated electrolyte at 100 °C, and the measurement was taken when a stable value was achieved without stirring. The viscosity of the electrolyte was measured using an electromagnetically spinning sphere viscometer (KYOTO ELECTRONICS MANUFACTURING CO., LTD., EMS-1000S). The measurement was conducted with a spherical Al probe having a diameter of 2 mm. To suppress measurement variation due to corrosion of the probe, the probe was immersed in boiling pure water for 1 h to oxidize the probe surface before to the measurements. The target electrolyte solution was placed in a glass tube, heated to 100 °C, and measured at a probe rotation rate of 600–1000 rpm. The melting point of the electrolyte was gradually warmed from 20 °C to 110 °C, and the temperature at which the electrolyte began to melt was defined as the melting point.

2.2.3. Nuclear magnetic resonance (NMR) spectroscopy

The Al ions in the electrolyte were analyzed by NMR measurement (JEOL Ltd., JNM-ECZ400R). The measurement was conducted by placing the prepared electrolyte in a glass sample tube having a diameter of 5 mm and sealing it. The electrolyte was heated to 100 °C, and the ^{27}Al nuclei were measured by the single-pulse method. The chemical shift was based on the $Al(NO_3)_3$ signal (0 ppm). Since the ^{27}Al nucleus has a quadrupole interaction, ^{27}Al NMR analysis is not as quantitative as ^{1}H NMR or ^{13}C NMR. ^{27}Al NMR signals with poorly symmetric molecular structures tend to spread significantly, but in the solution state, the anisotropic interaction is canceled by the fast molecular motion and the signal appears to be relatively sharp. To further reduce the error, data processing was performed while also noting the settings of baseline correction and integral correction.

2.2.4. Electrodeposition

For the Al electrodeposition, a Cu sheet with a 1-mm thickness (The Nilaco CO., purity: 99.99%) was employed as the cathode, and an Al sheet with a 1-mm thickness (The Nilaco CO., purity: 99.99%) was employed as the anode. Each electrode was polished using a polishing paper of #1000 and dried after washing with water. The cathode and anode were masked with a polyimide adhesive tape (TERAOKA SEISAKUSHO CO., LTD., 652S#25) to afford an active electrode area of 30 mm × 30 mm. The electrodes were installed facing each other in the center of the glass vessel. The space between the cathode and the anode was 10 mm. The Al electrodeposition was conducted with a constant current using a DC power supply. During the Al electrodeposition, the temperature of the electrolyte was maintained at 95 °C–100 °C, and the current density was 80 mA cm^{-2}. The stirring rate of the electrolyte was 800 rpm. After the electrodeposition progressed for a predetermined time, the cathode on which Al was electrodeposited was taken out from the electrolyte, washed with water, and dried. The Al-electrodeposited film was peeled off from the cathode using tweezers when necessary. The tank voltage value displayed on the DC power supply was read at 1 min intervals, and the average value over a 10 min period was adopted as the voltage for the Al electrodeposition.

2.2.5. Coulombic efficiency

The cathodic Coulombic efficiency of the Al electrodeposition (Q_c) was determined using Eqs. 2-4, 2-5, and the anodic Coulombic efficiency of the Al dissolution (Q_a) was determined using Eqs. 2-6, 2-7.

$$Q_c = \frac{w_c}{T_c} \times 100 \tag{2-4}$$

$$T_c = \frac{ItM}{nF} \tag{2-5}$$

$$Q_a = \frac{w_a}{T_a} \times 100 \tag{2-6}$$

$$T_a = \frac{ItM}{nF} \tag{2-7}$$

where Q_c is the Coulombic efficiency of the Al electrodeposition (%), w_c is the measured electrodeposited weight of Al (g), T_c is the theoretical electrodeposited weight of Al (g), I is the current (A), t is the current application time (s), M is the atomic weight (g mol^{-1}), n is the valence number, F is Faraday's constant (A s mol^{-1}), Q_a is the Coulombic efficiency of the anodic dissolution (%), w_a is the measured anodic dissolution weight (g), and T_a is the theoretical anodic dissolution weight (g). The electrodeposition and the anodic dissolution weight were determined from the change in cathodic and anodic weight before and after plating.

2.2.6. Analysis of the Al-electrodeposited film

The surface morphologies of Al electrodeposition films were observed using a field-emission scanning electron microscope (FE-SEM, JEOL Ltd., JSM-7900F). The accelerated voltage of SEM observation was 5 kV, and the working distance was 10 mm. The crystal structure of Al electrodeposition films was analyzed by X-ray diffraction (XRD) using an X-ray diffractometer (Rigaku Co., SmartLab) with Cu Kα radiation (λ = 0.15418 nm). XRD was carried out at a beam diameter of 0.4 mm. The impurity content (C, S, and Cl) of the Al electrodeposition film peeled off from the cathode was measured. To ensure easy peeling of the Al-electrodeposited film from the cathode, a 1-mm thick Ti sheet was employed. The analysis area was the white portion of the

Al-electrodeposited film. The C and S contents were analyzed using a carbon and sulfur analyzer (Horiba Ltd., EMIA-820W), and the Cl content was analyzed using a fluorescent X-ray analyzer (Rigaku Co., RIX-2100).

2.3. Results and Discussion

2.3.1. Physical properties of the electrolyte

Figure 2-1a shows the conductivity of the electrolyte solution with additives added to the basic composition electrolyte. When NH_4Cl or TMAC was added, the conductivity increased in proportion to the amount added. On the other hand, when LiCl or NaCl was added, there was almost no change in conductivity even with an addition amount of 0.05 mol. The amount added exceeding 0.05 mol of LiCl or NaCl was not dissolved in the electrolyte solution. From these results, it was found that the inorganic salts such as LiCl and NaCl had a small effect on conductivity, and the ammonium salts such as NH_4Cl and TMAC were effective in increasing conductivity. To exceed the target value of 0.5 S m^{-1}, the addition of NH_4Cl or TMAC of 0.12 mol or more is required. Figure 2-1b shows the viscosity of the electrolyte solution with NH_4Cl or TMAC added. The viscosity of the electrolyte solution decreases with increasing addition of NH_4Cl or TMAC. In addition, no difference was observed between the two additives regarding the conductivity and viscosity values. A decrease in viscosity increases the mobility of ions that act as charge carriers. From these results, it was found that an increase in charge carrier mobility, that is, a decrease in viscosity, is more effective in increasing the conductivity of $DMSO_2$–$AlCl_3$ electrolyte than an increase in charge carrier density. Figure 2-1c shows the melting point of the electrolyte solution with NH_4Cl or TMAC added. The melting point of the basic composition was 20 °C or less. Therefore, the plot of the basic composition in Fig. 2-1c is indicated by a downward pointing arrow. The melting point of the electrolyte solution gradually increased with the addition of NH_4Cl and TMAC, and when the amount reached 0.38 mol, the melting points increased to approximately 45 °C and 65 °C for NH_4Cl and TMAC, respectively. When NR_4Cl exceeding 0.38 mol was added, they did not completely dissolve. Further, when the mixing ratio of $AlCl_3$ was changed, the limit dissolution amount of the additive changed according to the mixing ratio of $AlCl_3$, and it could not

dissolve beyond the molar ratio equivalent to the mixing ratio of $AlCl_3$. This suggests that the marginal dissolution amount of NR_4Cl depends on the abundance of Al ions.

Figure 2-2 shows the results of viscosity measurement of the $DMSO_2$–$AlCl_3$ electrolyte which a basic composition and 0.10 mol of NH_4Cl or TMAC was added by changing the probe rotation rate (shear rate). The probe rotation speed was 600–1000 rpm, and the measurement temperature was 100 °C. The horizontal axis in Fig. 2-2 indicates the shear rate. In any of the electrolyte solutions, the viscosity of the electrolyte was almost constant regardless of the shear rate. The measured viscosity of the basic composition appears to be slightly downward, but this is the effect of probe corrosion due to long-term measurement or the effect of measurement condition variation. This result suggests that the $DMSO_2$–$AlCl_3$ electrolyte is a Newtonian fluid regardless of whether NH_4Cl or TMAC is added.

The change in the conductivity of the electrolyte with the addition of NR_4Cl was considered as follows. The electrolyte conductivity (κ) is expressed by Eq. 2-8. The diffusion coefficient (D) of the ions in the electrolyte is expressed by the Stokes–Einstein equation (Eq. 2-9):

$$\kappa = \frac{F^2 CZD}{RT} \tag{2-8}$$

$$D = \frac{k_B T}{6\pi r \eta} \tag{2-9}$$

Here, κ is the conductivity (S m^{-1}), F is the Faraday constant (A s mol^{-1}), C is the concentration, Z is the valence number, D is the diffusion coefficient (m^2 s^{-1}), R is the gas constant (J K^{-1} mol^{-1}), T is the absolute temperature (K), k_B is the Boltzmann constant (J K^{-1}), r is the ionic radius (m), and η is the viscosity (Pa s). According to Eqs. 2-8 and 2-9, the conductivity depends on the reciprocal of the viscosity (η^{-1}). Figure 2-3 shows the relationship between η^{-1} and the electrolyte

conductivity. The conductivity of the electrolyte added with NH_4Cl or TMAC is almost proportional to η^{-1} in either case. This result indicates that the viscosity of the electrolyte has a dominant influence on the conductivity. Since the slope of the line at the electrolyte with NH_4Cl is about twice the slope at the electrolyte with TMAC, the Stokes radius of NH_4^+ is estimated to be about half that of $N(CH_3)_4^+$. Although no reports of the Stokes radii of these ions in $DMSO_2$-based electrolyte were observed, in aqueous solution it was reported that NH_4^+ hydrated ion radii have 148 pm and $N(CH_3)_4^+$ hydrated ion radii have 280 pm [7]. From the ratio of the Stokes radii of these ions in aqueous solution, the difference in slope of the conductivity compared to viscosity was the difference in Stokes radii. Therefore, it can be concluded that the reason for the increase in the conductivity with the addition of NR_4Cl is the decrease in the viscosity. The reason for the decrease in the viscosity with the NR_4Cl addition is described below. The difference in the degree of increase in the melting points between NH_4Cl and TMAC is probably due to the difference in the ionic radii between NH_4^+ and $N(CH_3)_4^+$.

Figure 2-4 shows the relationship between the conductivity and the melting point of the electrolyte solutions. Even for the electrolyte without additive (diamond), the conductivity and melting point change when the mixing ratio of $AlCl_3$ changes. The electrolyte with an $AlCl_3$ mixing ratio of 0.2 mol has a conductivity of 0.5 S m^{-1} and a melting point of 90 °C. As the $AlCl_3$ mixing ratio increases, the conductivity decreases. The melting point decreases to 62 °C at 0.3 mol, and 20 °C or less at 0.38 mol and 0.42 mol. With further increases in $AlCl_3$ mixing ratio, the melting point of the electrolyte increased; 60 °C when the mixing ratio of $AlCl_3$ was 0.46 mol. However, in the electrolyte with NH_4Cl (circle) or TMAC (square), the melting point increases only relatively slightly, and the conductivity increases significantly.

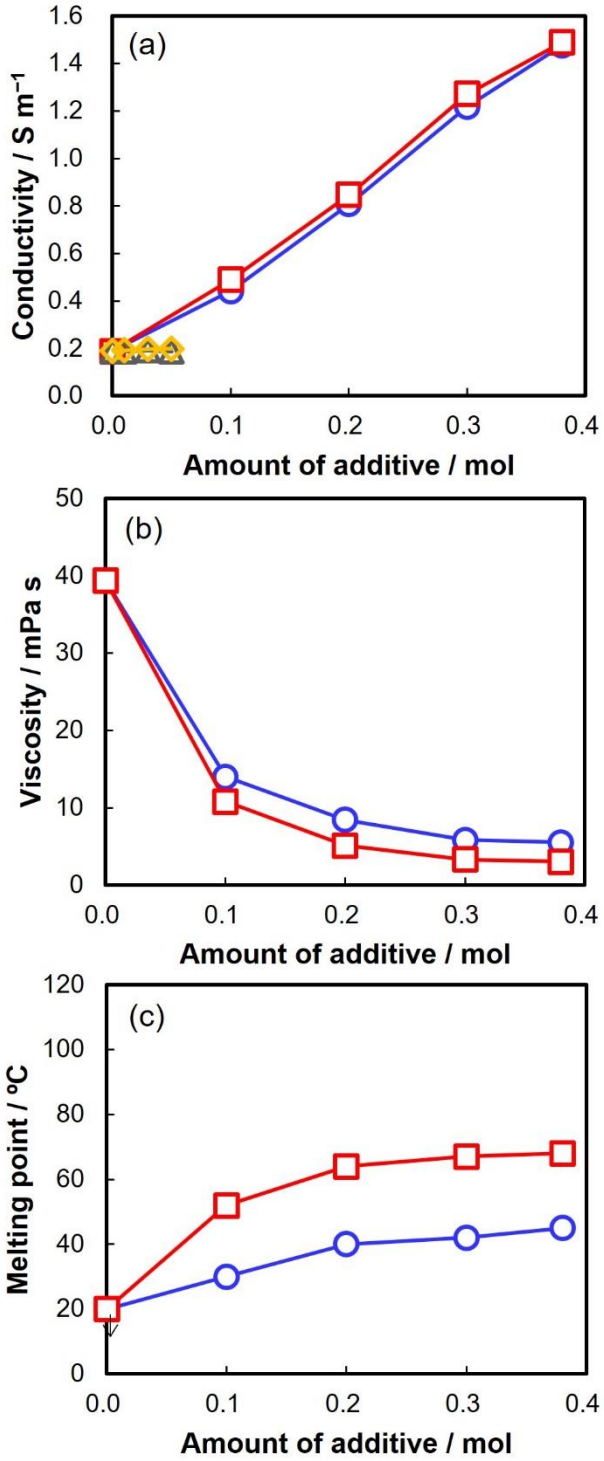

Figure 2-1. Dependence of the additives amount on the physical properties of the electrolyte. (a) Conductivity (100 °C), (b) viscosity (100 °C), and (c) melting point; $DMSO_2$:$AlCl_3$:additive = 1:0.38:*x* (mol), *x* = 0.00–0.38; (blue circles) NH_4Cl, (red squares) TMAC, (orange diamonds) NaCl, (gray triangles) LiCl.

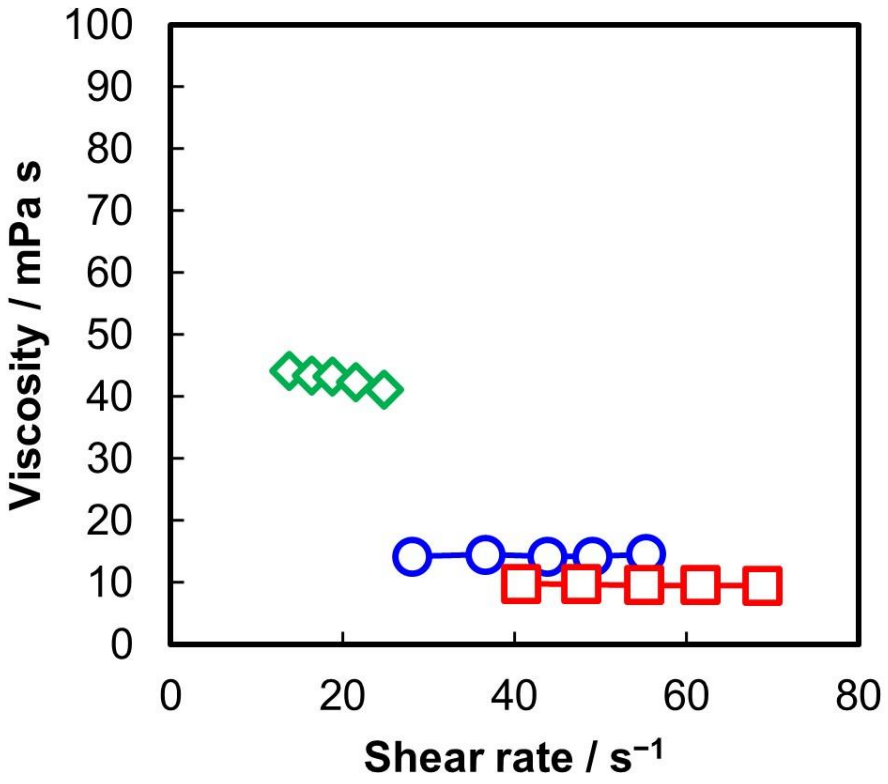

Figure 2-2. Relationship between the shear rate and the viscosity of the electrolyte. $DMSO_2$:$AlCl_3$ = 1:0.38 (mol), (green diamonds) no additive, (blue circles) NH_4Cl 0.10 mol, (red squares) TMAC 0.10 mol.

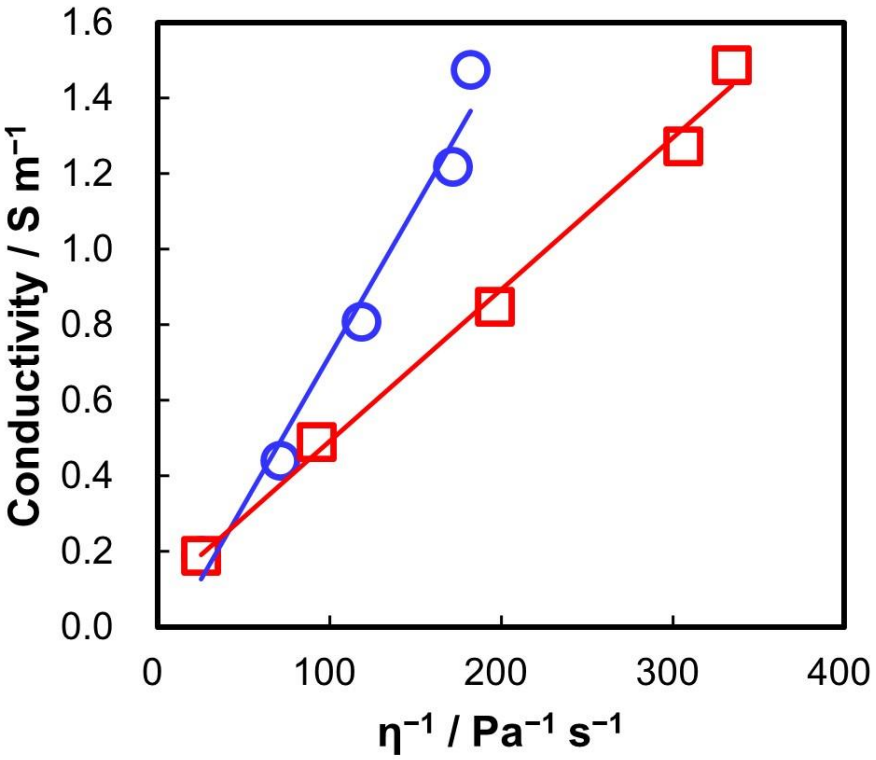

Figure 2-3. Relationship between η^{-1} and the electrolyte conductivity at 100 °C. $DMSO_2$:$AlCl_3$:additive = 1:0.38:*x* (mol), *x* = 0.00–0.38, (blue circles) NH_4Cl, (red squares) TMAC.

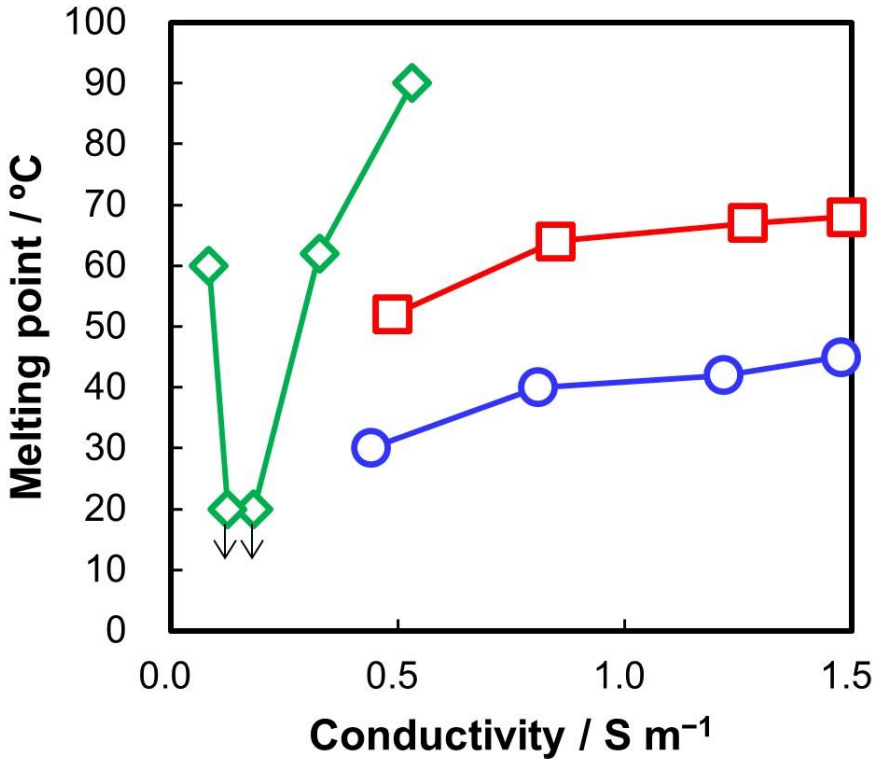

Figure 2-4. Relationship between the conductivity and the melting point of the electrolyte. (green diamonds) $DMSO_2$:$AlCl_3$ = 1:0.20–0.46 (mol), (blue circles) $DMSO_2$:$AlCl_3$:NH_4Cl = 1:0.38:0.10–0.38 (mol), (red squares) $DMSO_2$:$AlCl_3$:TMAC = 1:0.38:0.10–0.38 (mol).

2.3.2. Ionic species in $DMSO_2$-$AlCl_3$ electrolyte

In this study, ^{27}Al NMR measurements were performed to investigate the effects of NR_4Cl on the Al ion species in the electrolyte solution (see Fig. 2-5). For the additive-free electrolyte, peaks were confirmed at 103 ppm, −11 ppm, and −21 ppm. The intensities of the signals at −11 ppm and −21 ppm decreased as the amount of NR_4Cl increased, and the signals disappeared when the NR_4Cl amount reached 0.38 mol. Legrand reported that the signals near 103 ppm, −11 ppm, and −21 ppm correspond to $AlCl_4^-$, $Al(DMSO_2)_3^{3+}$, and $Al(DMSO_2)_n^{3+}$ ($n > 3$), respectively [1]. Furthermore, Kim reported that the intensity of the $Al(DMSO_2)_3^{3+}$ signals decreased upon adding LiCl to the electrolyte [8]. These results indicate that the addition of NR_4Cl decreases the concentration of the Al^{3+} species in the electrolyte involved in the Al electrodeposition, such as the solvated form of $Al(DMSO_2)_3^{3+}$.

Based on the results of ^{27}Al NMR results of the electrolyte solution shown in Fig. 2-5, the author discusses the change in the dissociation equilibrium of the ionic species in the electrolyte upon adding NR_4Cl. Generally, quaternary ammonium salts dissociate into cations and anions in polar non-aqueous solvents. NR_4Cl is considered to dissociate into NR_4^+ and Cl^- even in the $DMSO_2$-based electrolyte. As shown in Eq. 2-1, $AlCl_3$ produces and dissolves stable $AlCl_4^-$ in the $DMSO_2$–$AlCl_3$ mixed system. The surplus Al^{3+} is solvated with $DMSO_2$ and dissolved as $Al(DMSO_2)_3^{3+}$. When excess Cl^- is added here, it forms $AlCl_4^-$ with Al^{3+}, which is solvated as $Al(DMSO_2)_3^{3+}$ in the electrolyte. Therefore, presumably, the $Al(DMSO_2)_3^{3+}$ content in the electrolyte decreases as the amount of Cl^- increases. Consequently, the solvated $DMSO_2$ is released from the binding by Al^{3+} and can move freely. The above mechanism when m mol of NR_4Cl is added to the $DMSO_2$–$AlCl_3$ electrolyte is summarized in Eq. 2-10:

$$Al(DMSO_2)_3^{3+} + 3AlCl_4^- + mNR_4Cl$$

$$\rightleftharpoons (1 - \frac{m}{4})\, Al(DMSO_2)_3^{3+} + (3 + \frac{m}{4})\, AlCl_4^- + mNR_4^+ + \frac{3m}{4}DMSO_2. \quad (2\text{-}10)$$

Using Eq. 2-10, the amount of each ion in the electrolyte was estimated, and the results are summarized in Table 2-1.

In the NMR spectra shown in Fig. 2-5, the ratio of $AlCl_4^-$ and $Al(DMSO_2)_3^{3+}$ in the $DMSO_2$–$AlCl_3$ electrolyte is represented by the ratio of the area of the −11 ppm peak to the area of the 103 ppm peak. Figure 2-6 shows the result of comparing the ratio obtained from the peak of ^{27}Al NMR measurement and the ratio estimated from Eq. 2-10. The estimated value from Eq. 2-10 was almost the same as the peak area ratio from the NMR measurement. From these results, it was confirmed that the amounts of $Al(DMSO_2)_3^{3+}$ and $AlCl_4^-$ in the electrolyte changed according to Eq. 2-10 with the addition of NR_4Cl. According to Eq. 2-10, the solubility of NR_4Cl is related to the amount of Al in the electrolyte that can form $AlCl_4^-$. Additionally, the addition of NR_4Cl increases the amount of $DMSO_2$ not involved in the solvation (free $DMSO_2$). This might be the cause of the decrease in the electrolyte viscosity.

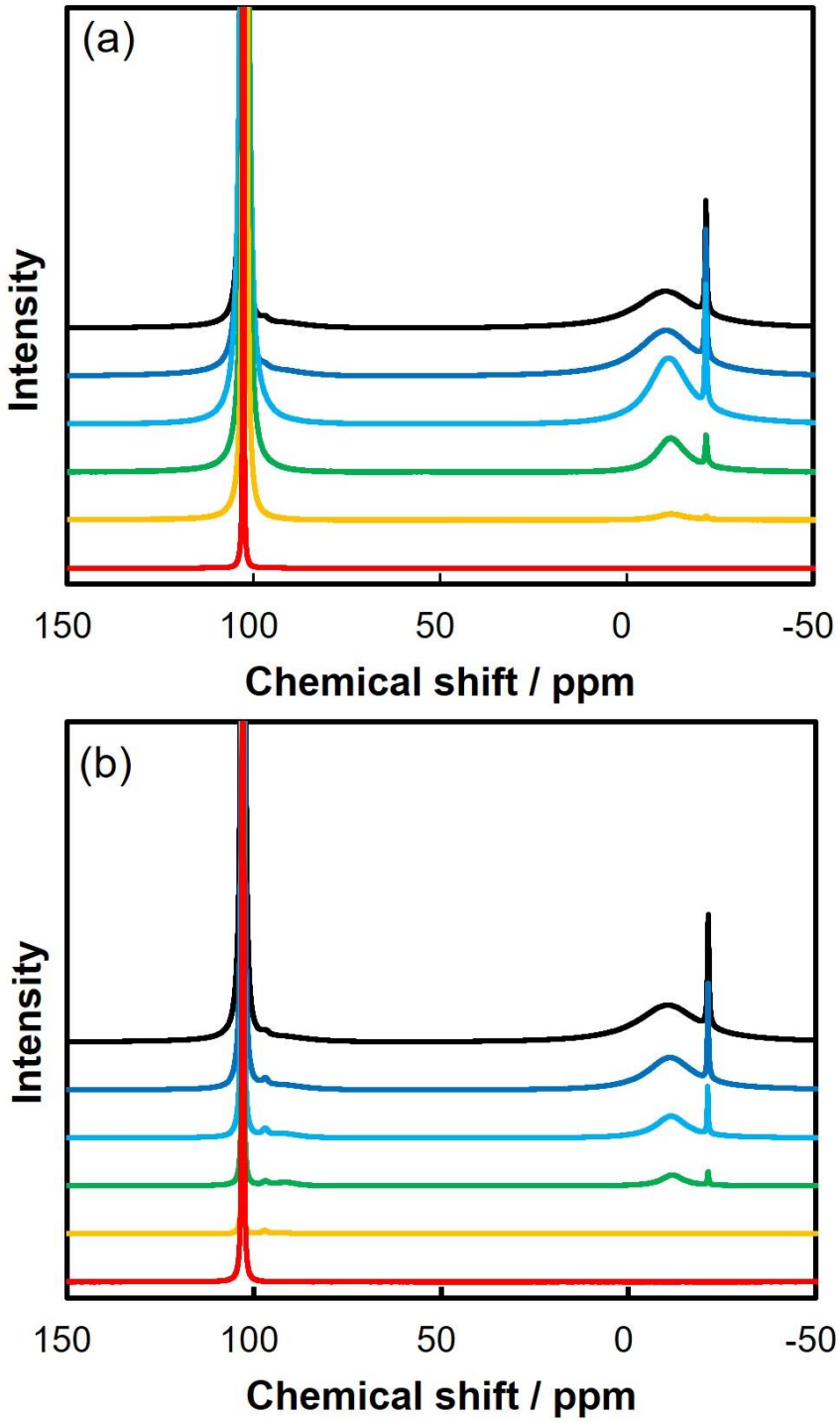

Figure 2-5. ^{27}Al NMR spectra of the $DMSO_2$–$AlCl_3$ electrolyte solution at 100 °C. $DMSO_2$:$AlCl_3$:additive = 1:0.38:*x* (mol), (a) NH_4Cl, *x* = (black) 0.00, (blue) 0.02, (light blue) 0.10, (green) 0.20, (orange) 0.30, (red) 0.38; (b) TMAC, *x* = (black) 0.00, (blue) 0.02, (light blue) 0.10, (green) 0.20, (orange) 0.30, (red) 0.38.

Table 2-1. Estimated amount of ions in the electrolyte containing 1 mol of $DMSO_2$.

Electrolyte composition			Estimated amount of ions				
$DMSO_2$ (mol)	$AlCl_3$ (mol)	NR_4Cl (mol)	Free $DMSO_2$ (mol)	$Al(DMSO_2)_3^{3+}$ (mol)	$AlCl_4^-$ (mol)	NR_4^+ (mol)	$Al(DMSO_2)_3^{3+}$ /$AlCl_4^-$
1	0.38	0.00	0.715	0.095	0.285	0.000	0.33
1	0.38	0.10	0.790	0.070	0.310	0.100	0.23
1	0.38	0.20	0.865	0.045	0.335	0.200	0.13
1	0.38	0.30	0.940	0.020	0.360	0.300	0.06
1	0.38	0.38	1.000	0.000	0.380	0.380	0.00

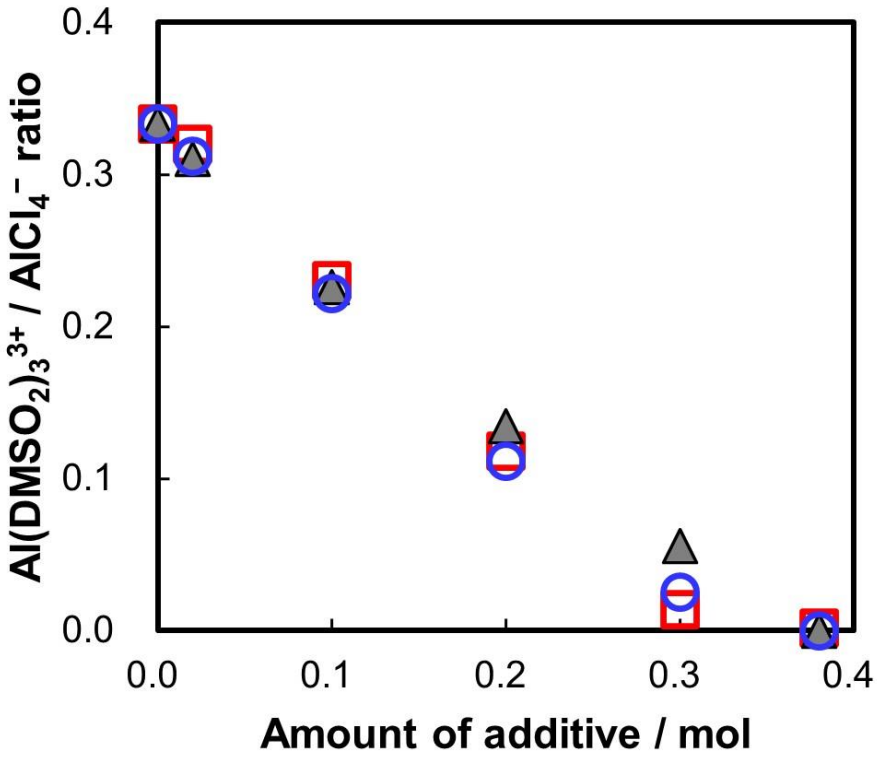

Figure 2-6. Comparison of the $Al(DMSO_2)_3^{3+}/AlCl_4^-$ ratio calculated from the peak area ratio of the ^{27}Al NMR spectrum and the ratio estimated from Eq. 2-10. $DMSO_2$:$AlCl_3$:NR_4Cl = 1:0.38:0.00–0.38 (mol); (blue circles) the peak area ratio of the ^{27}Al NMR spectrum of the electrolyte with NH_4Cl, (red squares) the peak area ratio of the ^{27}Al NMR spectrum of the electrolyte with TMAC, (gray triangles) the $Al(DMSO_2)_3^{3+}/AlCl_4^-$ ratio estimated from Eq. 2-10.

2.3.3. Coulombic efficiency

Figure 2-7 shows the results of measuring Coulombic efficiency during the Al electrodeposition using the electrolytes added with NH_4Cl and TMAC. The Coulombic efficiency decreased significantly as the amount of NR_4Cl increased.

First, the effect of the changes in the ionic equilibrium expressed in Eq. 2-10 on the Coulombic efficiency is discussed. As shown in Fig. 2-1b, the viscosity of the electrolyte decreases when NR_4Cl is added. Conversely, as shown in Fig. 2-5, it also decreases the amount of $Al(DMSO_2)_3^{3+}$ species involved in the Al electrodeposition. If the influence of the decrease in $Al(DMSO_2)_3^{3+}$ is significant, the supply of reactive species to the electrode surface will decrease; resultantly, the Coulombic efficiency is expected to decrease since the side reactions occur preferentially. If the diffusion transport of the reactive species to the electrode surface follows Fick's law, the transport amount in the diffusion rate-determining step is determined by the product of the bulk-ion concentration and the diffusion coefficient. The concentration of ions is almost proportional to the molar ratio of ions in the electrolyte. The diffusion coefficient (D) is proportional to the reciprocal of the viscosity according to the Stokes–Einstein equation as shown in Eq. 2-9. Therefore, the value obtained by dividing the molar ratio by the viscosity is an index of the diffusion supply limit. Here, the $Al(DMSO_2)_3^{3+}$ molar ratio divided by the viscosity is defined as the diffusion transport index of $Al(DMSO_2)_3^{3+}$. Figure 2-8 shows how the $Al(DMSO_2)_3^{3+}$ molar ratio and diffusion transport index change with the addition of NR_4Cl, with the value displayed as 1 without NR_4Cl addition. These values are calculated based on the ion-composition ratio obtained by the ^{27}Al NMR measurement, as shown in Fig. 2-5. As shown in Fig. 2-8, the diffusion transport index is the maximum value achieved with the addition amount is 0.10 mol or 0.20 mol. This is because the effect of the viscosity reduction is greater than the decrease in the Al^{3+} concentration due to the dissociation equilibrium change. These results suggest that the decrease in $Al(DMSO_2)_3^{3+}$ by

addition of NR_4Cl is not a direct influencing factor of the decrease in Coulombic efficiency.

Noticeably, in Fig. 2-7, there is a difference in the behavior of the decrease in Coulombic efficiency between NH_4Cl and TMAC. With NH_4Cl, the Coulombic efficiency decreases to 80% and 60% with the addition of 0.02 mol and 0.1 mol of NH_4Cl, respectively. Conversely, with TMAC, the Coulombic efficiency is about 90% even when 0.1 mol of TMAC is added, which is not significantly decreased. When NH_4Cl is added, more bubbles are generated from the cathodic surface during Al electrodeposition than when NR_4Cl-free or TMAC is added. The amount of bubbles generated tend to increase with the amount of NH_4Cl added. The measurement with the gas-detection tube revealed that the main component of the bubble is H_2. It was considered that the H_2-generation reaction is the cause of the decrease in the Coulombic efficiency. As shown in Eq. 2-10, NH_4Cl dissociates in the electrolyte and produces NH_4^+. Berkh reported that NH_4^+ is reduced at a less noble potential than the reduction potential of water in aqueous solutions (about −0.55 V vs. NHE) at the Pt electrode, and it generates $NH_4{}^0{}_{ads}$ adsorbed on the electrode surface, followed by H_2 and NH_3, as expressed in Eq. 2-11 [9]:

$$NH_4^+ + e^- \rightleftharpoons NH_4{}^0{}_{ads} \rightleftharpoons \frac{1}{2}H_2 + NH_3. \quad (2\text{-}11)$$

Since the standard electrode potential of Al in an aqueous solution is −1.67 V vs. NHE, the reduction reaction of NH_4^+ occurs at a more positive potential than the Al electrodeposition potential even in the $DMSO_2$–$AlCl_3$ electrolyte. Therefore, it is considered that NH_4^+ reduction occurs at the potential at which Al electrodeposition occurs. As the amount of NH_4Cl added increases, the reduction reaction of NH_4^+ also increases; consequently, the Coulombic efficiency decreases according to the amount of NH_4Cl added. Conversely, for TMAC, since the potential window of the cathodic side is wide, it hardly decomposes, unlike NH_4Cl. The cause of the decrease in the

Coulombic efficiency of the electrolyte solution due to the addition of TMAC is different from that of NH_4Cl. To clarify the difference in the effect of NH_4Cl and TMAC on Coulombic efficiency, the Coulombic efficiency was measured by changing the current density to 30–80 mA cm^{-2} using an electrolyte solution with NH_4Cl or TMAC of 0.20 mol. Figure 2-9 shows this result. In this experiment, the electrolysis time was adjusted to align the coulomb quantity. When NH_4Cl or TMAC is added, the effect on current density is different, respectively. The Coulombic efficiency seemed to decrease gradually with respect to the current density in the case of NH_4Cl addition, but decreased significantly with respect to the current density in the case of TMAC addition. In the case of NH_4Cl addition, as described above, since NH_4^+ reduction occurs at a positive potential than Al electrodeposition, the influence of current density is small in the region where the Al electrodeposition reaction sufficiently occurs. In the case of TMAC addition, there is a factor that decreasing Coulombic efficiency in the high current density region. Therefore, this result also suggests that the mechanism of decrease in Coulombic efficiency by adding NH_4Cl or TMAC is different. This will be discussed in Chapter 3.

The electrolyte composition indicating the target value of Coulombic efficiency of 80% or more was up to 0.02 mol for NH_4Cl and up to 0.10 mol for TMAC. As shown in Fig. 2-1a, to achieve the target conductivity of the electrolyte, an addition of 1.2 mol or more is required. Therefore, 0.02 mol of NH_4Cl and 0.10 mol of TMAC were both added, and the Coulombic efficiency was measured. The Coulombic efficiency of this electrolyte was 86.6%. The deviation from 100% in the Coulombic efficiency is due to H_2 generation. In the closed system, the generated H_2 accumulates in the plating vessel and leads to problems. As in this study, since the electrolyte can be electroplated under the conditions of N_2 gas flow, the generated H_2 is discharged with N_2, and H_2 does not accumulate in the plating vessel.

The Coulombic efficiency of anodic dissolution at the opposite electrode was almost 100% in any of the electrolyte compositions regardless of the addition of NR_4Cl addition. This result

suggests that NR_4Cl addition has negligible effects on anodic Coulombic efficiency. Since the cathodic Coulombic efficiency is less than 100%, the concentration of $Al(DMSO_2)_3^{3+}$ in the electrolyte solution is expected to increase as the electrolysis time lengthens. Even in that case, the concentration of $Al(DMSO_2)_3^{3+}$ in the electrolyte can be adjusted by adding $DMSO_2$.

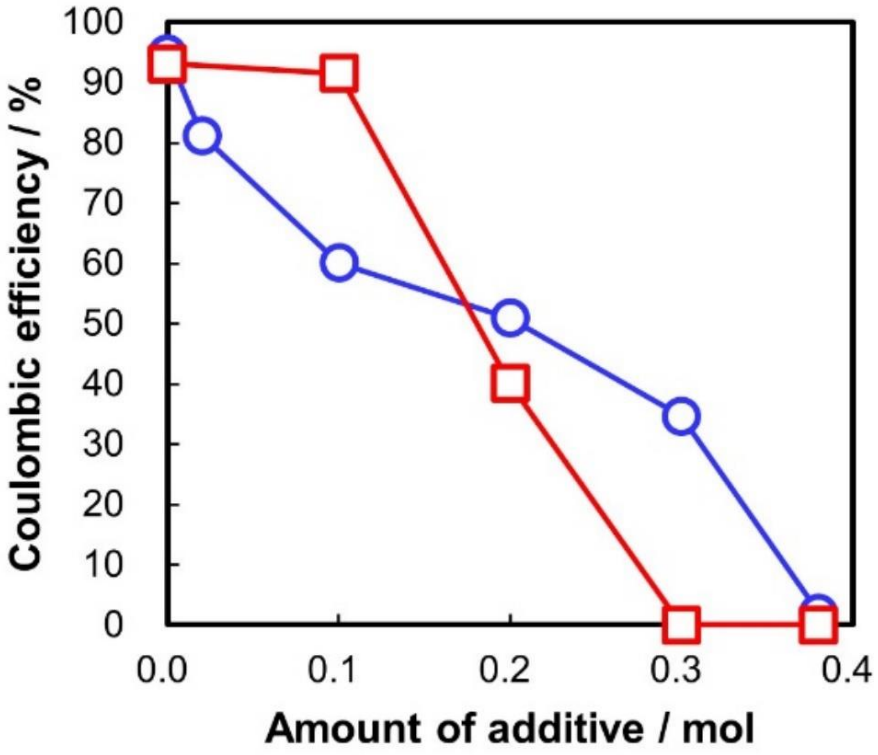

Figure 2-7. Relationship between the NR_4Cl addition amount and the Coulombic efficiency at 100 °C and 80 mA cm^{-2}. $DMSO_2$:$AlCl_3$:NR_4Cl = 1:0.38:*x* (mol), (blue circles) NH_4Cl, *x* = 0.00–0.38, (red squares) TMAC, *x* = 0.00–0.38.

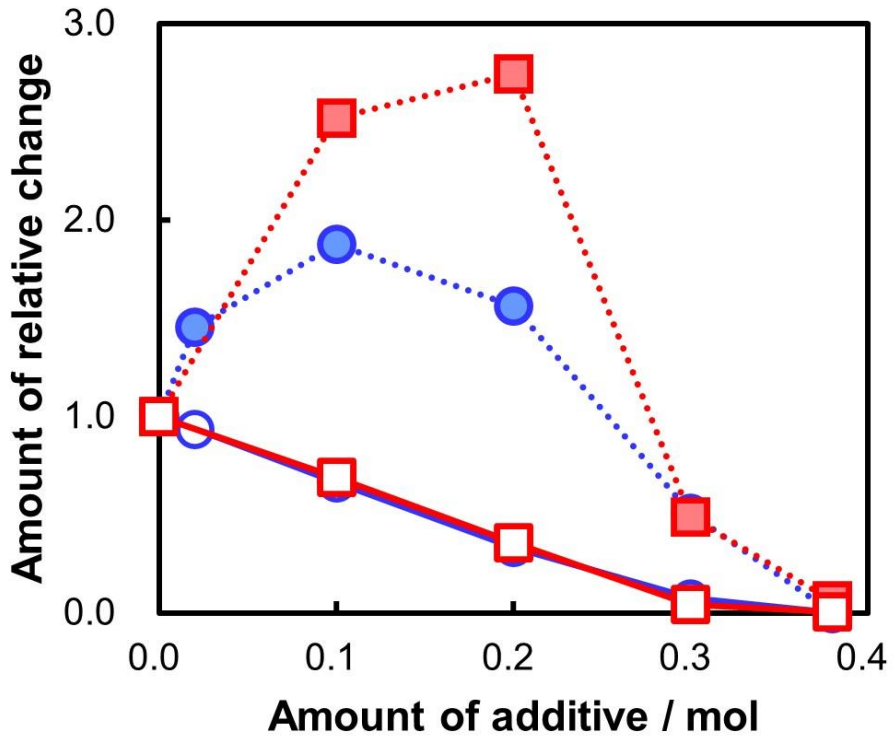

Figure 2-8. Change in the $Al(DMSO_2)_3^{3+}$ molar ratio and diffusion transport index with the addition of NR_4Cl (the value for the NR_4Cl-free electrolyte is 1). (Solid-symbol blue circles) change in the diffusion transport index with NH_4Cl, (solid-symbol red squares) change in the diffusion transport index with TMAC, (open-symbol blue circles) change in the $Al(DMSO_2)_3^{3+}$ molar ratio with NH_4Cl, (open-symbol red squares) change in the $Al(DMSO_2)_3^{3+}$ molar ratio with TMAC.

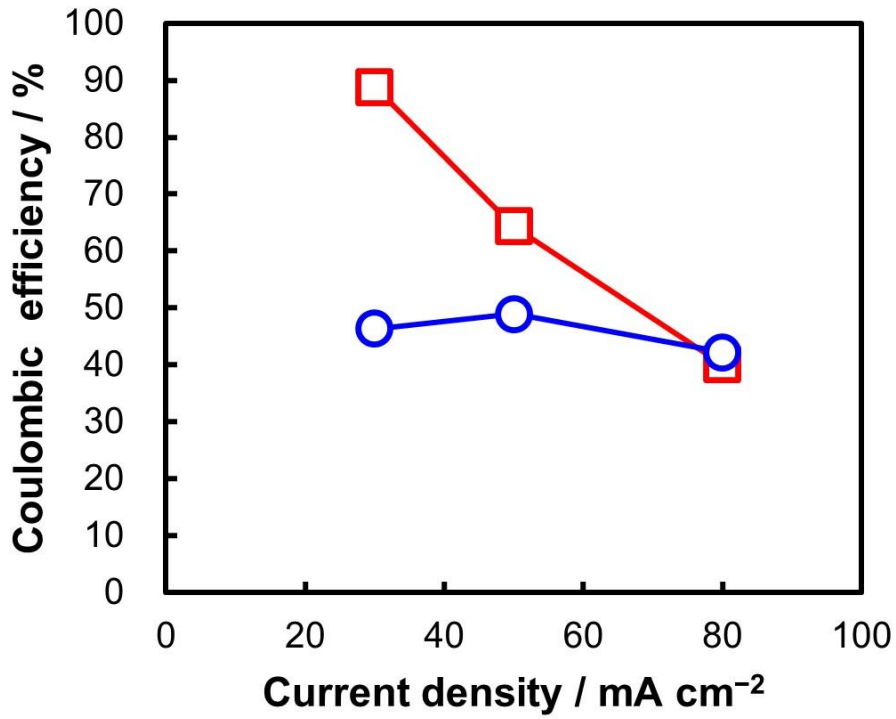

Figure 2-9. Relationship between current density and the Coulombic efficiency at 100 °C. $DMSO_2$:$AlCl_3$:additive = 1:0.38:0.20 (mol), (blue circles) NH_4Cl, (red squares) TMAC.

2.3.4. Properties of the deposits and electrolyte performance

For three different compositions shown in Fig. 2-7 with a Coulombic efficiency of 80% or more, the appearance of the Al-electrodeposited film, its impurity content, the electrolyte conductivity, and the tank voltage were evaluated. The results are shown in Fig. 2-10 and Table 2-2.

Composition (a) is an NR_4Cl-free electrolyte solution. The Al-electrodeposited film obtained using this electrolyte has a black portion in the peripheral area of the sample. Such a black portion has a bad appearance and is not desirable. The impurity contents of the Al-electrodeposited film are as follows: carbon: 0.31 wt%, sulfur: 0.40 wt%, and chlorine: 0.36 wt%. The Coulombic efficiency was 93.1%. The conductivity of this electrolyte composition was 0.19 S m^{-1}. Kim reported a case where a black Al film is precipitated from the $DMSO_2$–$AlCl_3$ electrolyte with a low $AlCl_3$ ratio [8]. The reason why the plating film turns black is probably the insufficient supply of $Al(DMSO_2)_3^{3+}$, which causes rough deposition at the peripheral area where the current is concentrated.

In composition (b) formed by the addition of 0.10 mol of TMAC to composition (a), the area of the black portion of the sample peripheral area decreased. The impurity content of the Al-electrodeposited film was slightly lower than that in (a). The Coulombic efficiency was 91.5%, which was slightly lower than that in (a). The conductivity increased by approximately 2.5 times to 0.49 S m^{-1}. Consequently, it was confirmed that the tank voltage was 0.44 times that in (a), and a 56% reduction was achieved. The area of the black portion in the plated sample reduced because the viscosity of the electrolyte decreased and the diffusion transport index increased with the addition of TMAC. Furthermore, with the decreased viscosity, the diffusion-limited current increased. The threshold of the blackening current density should shift toward higher values.

In composition (c), formed by the addition of 0.02 mol of NH_4Cl to composition (a), no blackening portion was observed, and a white Al-electrodeposited film was obtained on the entire surface of the sample. The impurity content was significantly decreased compared to the cases for

(a) and (b); however, the conductivity increased only slightly to 0.22 S m^{-1} because of the small amount added. NH_4Cl influenced the impurity reduction and improved the appearance of the Al-electrodeposited film. However, the conductivity could not be sufficiently increased because of the small amount of NH_4Cl added. The tank voltage was 0.86 times that in (a), and a 14% reduction was achieved; the Coulombic efficiency was 81.2%.

The addition of NH_4Cl was quite effective for preventing the generation of black portions and decreasing the concentration of impurities. To achieve the target conductivity of electrolyte solution and reduce the tank voltage to a sufficient level, NR_4Cl of 0.12 mol or more should be added. However, adding more than 0.10 mol of NH_4Cl is significantly below the target Coulombic efficiency of 80%. Therefore, the author formed co-addition composition (d) by adding 0.02 mol of NH_4Cl and 0.10 mol of TMAC together. In composition (d), as in composition (c), black portions were not observed in the peripheral area, the impurity content was low, and the conductivity was 0.54 S m^{-1}. The tank voltage was 0.34 times that in (a), and a 65% reduction was achieved. The Coulombic efficiency in (d) was 86.6%, which was higher than that in (b). By adding both NH_4Cl and TMAC, it is possible to increase the conductivity and significantly decrease the tank voltage while suppressing the decrease in Coulombic efficiency. Furthermore, with the proposed electrolyte, the Al-electrodeposited film exhibited good plating appearance with an Al purity of 99% or more.

Figures 2-11–2-13 show SEM images and XRD analysis of the four plating films shown in Fig. 2-10. Figure 2-11 shows the SEM image of the white portion of the Al-electrodeposited films prepared by each electrolyte. For the (a) composition, a black portion in the peripheral area was also observed, which is shown in Fig. 2-11a'. The surface morphology of the white portion in composition (a) was dense and rough, and the grain size was about 3–10 μm. The surface morphology of the black portion in composition (a) was a crude plating film as compared to the white portion. In composition (b), the roughness of the crystal surface was slightly reduced compared to (a). The grain size in (b) was almost the same as (a). In composition (c), the grain size was slightly smaller than

(a), 3–5 μm. The grain size in (d) appears to be slightly smaller than (c). The stepped structure indicating the existence of twins is clearly visible in the order of (b) < (c) < (d). Figure 2-12 shows XRD patterns of each Al-electrodeposited film. All electrodeposited films showed the crystalline structure of Al, but the crystal orientation of the black portion was different than the white portion. Figure 2-13 shows the orientation index calculated using the Wilson formula. The white portion of the Al-electrodeposited film was oriented to (220). The orientation index of the (220) plane increased in the order of (a) < (b) < (c) < (d). The black portion showed priority orientation to (200), which differed from the white portion.

By co-adding NH_4Cl and TMAC, it is possible to increase the conductivity and significantly decrease the tank voltage while suppressing the decrease in the Coulombic efficiency. Furthermore, with the proposed electrolyte, the Al-electrodeposited film exhibited a good plating appearance, with an Al purity of 99% or more.

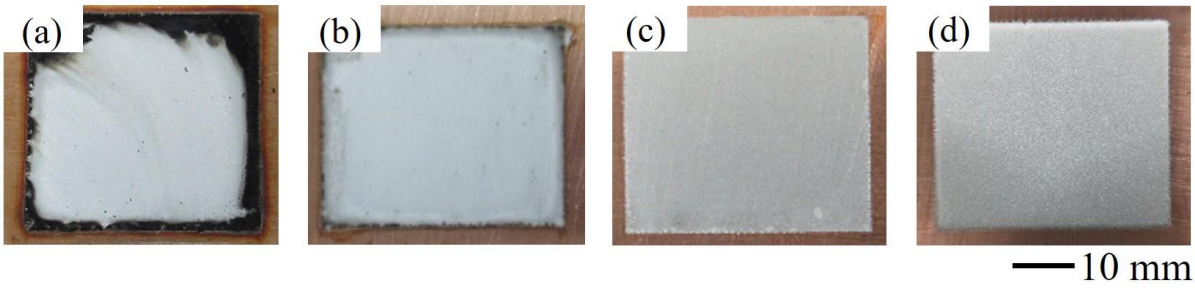

Figure 2-10. The appearance of Al-electrodeposited films prepared with different electrolytes at 100 °C and 80 mA cm^{-2}. (a) $DMSO_2$:$AlCl_3$ = 1:0.38 (mol), (b) $DMSO_2$:$AlCl_3$:TMAC = 1:0.38:0.10 (mol), (c) $DMSO_2$:$AlCl_3$:NH_4Cl = 1:0.38:0.02 (mol), (d) $DMSO_2$:$AlCl_3$:NH_4Cl:TMAC = 1:0.38:0.02:0.10 (mol).

Table 2-2 Performance comparison of the electrolytes containing different additives at 100 °C and 80 mA cm^{-2}.

Electrolyte composition		(a)	(b)	(c)	(d)
Amount of additive/mol	NH_4Cl	0.00	0.00	0.02	0.02
	TMAC	0.00	0.10	0.00	0.10
Impurity content /wt%	Carbon	0.31	0.23	0.05	0.05
	Sulfur	0.40	0.09	0.01	0.01
	Chlorine	0.36	0.28	0.11	0.07
Viscosity/mPa s		39.4	10.8	25.4	9.3
Conductivity/S m^{-1}		0.19	0.49	0.22	0.54
Tank voltage/V		48.8	21.5	41.8	16.9
Coulombic efficiency/%		93.1	91.5	81.2	86.6

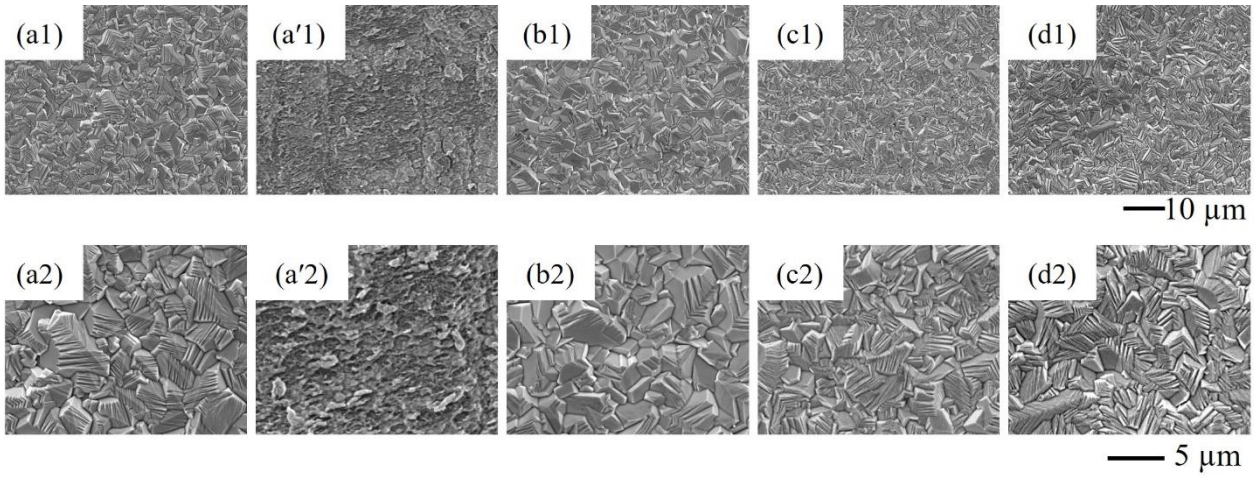

Figure 2-11. Surface morphology of Al electrodeposited films prepared with different electrolytes at 100 °C and 80 mA cm^{-2}. (a), (a') $DMSO_2$:$AlCl_3$ = 1:0.38 (mol), (b) $DMSO_2$:$AlCl_3$:TMAC = 1:0.38:0.10 (mol), (c) $DMSO_2$:$AlCl_3$:NH_4Cl = 1:0.38:0.02 (mol), (d) $DMSO_2$:$AlCl_3$:NH_4Cl:TMAC = 1:0.38:0.02:0.10 (mol), (a)–(d) evaluated the white portion, (a') evaluated the black portion.

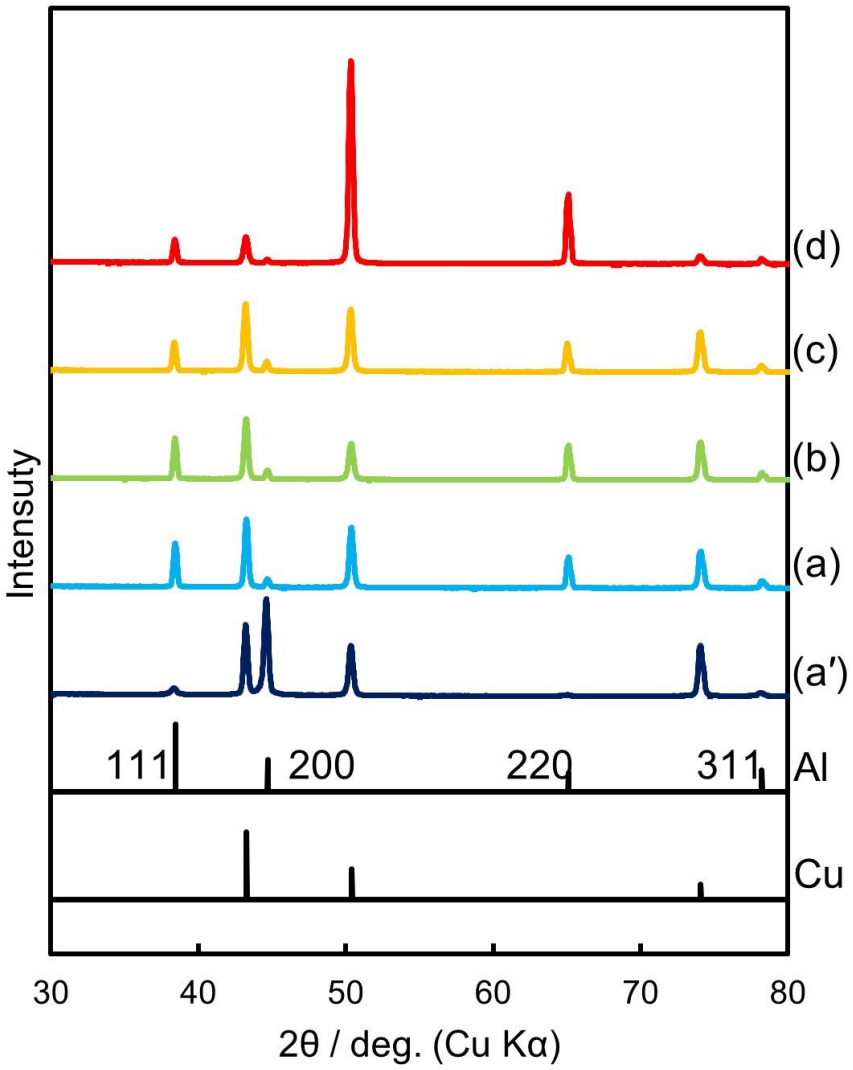

Figure 2-12. XRD pattern of Al-electrodeposited films prepared with different electrolyte at 100 °C and 80 mA cm^{-2}. (a), (a') $DMSO_2$:$AlCl_3$ = 1:0.38 (mol), (b) $DMSO_2$:$AlCl_3$:TMAC = 1:0.38:0.10 (mol), (c) $DMSO_2$:$AlCl_3$:NH_4Cl = 1:0.38:0.02 (mol), (d) $DMSO_2$:$AlCl_3$:NH_4Cl:TMAC = 1:0.38:0.02:0.10 (mol), (a)–(d) evaluated the white portion, (a') evaluated the black portion.

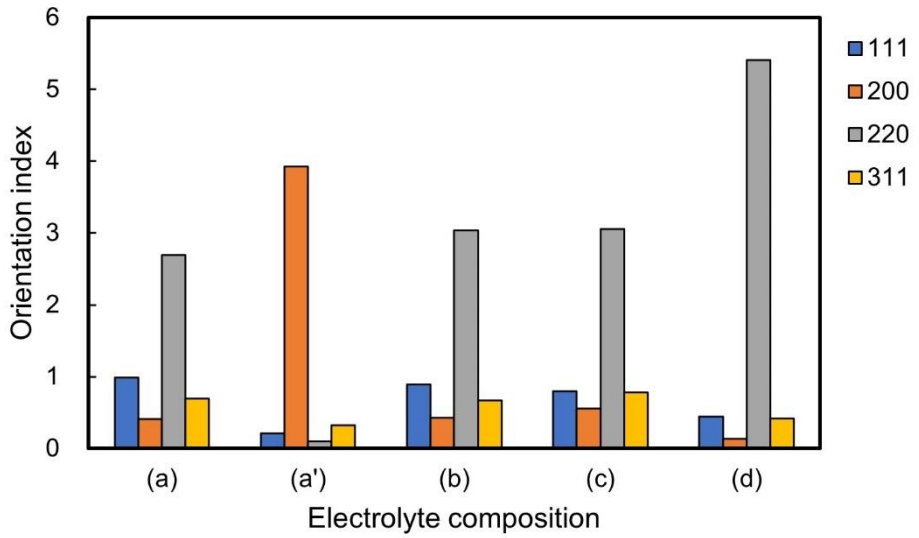

Figure 2-13. Orientation index of Al-electrodeposited films prepared with different electrolytes at 100 °C and 80 mA cm^{-2}. (a), (a') $DMSO_2$:$AlCl_3$ = 1:0.38 (mol), (b) $DMSO_2$:$AlCl_3$:TMAC = 1:0.38:0.10 (mol), (c) $DMSO_2$:$AlCl_3$:NH_4Cl = 1:0.38:0.02 (mol), (d) $DMSO_2$:$AlCl_3$:NH_4Cl:TMAC = 1:0.38:0.02:0.10 (mol), (a)–(d) evaluated the white portion, (a') evaluated the black portion.

2.4. Summary of findings

In this chapter, the author evaluated the electroplating properties of the additive-added $DMSO_2$–$AlCl_3$ electrolyte to find an electrolyte composition that exhibits high electrical conductivity and allows plating with high Coulombic efficiency. The conclusions are as follows.

1. NH_4Cl and TMAC are effective additives that increase the conductivity of the electrolyte for Al electrodeposition by decreasing the viscosity of the $DMSO_2$–$AlCl_3$ electrolyte.
2. The reason for the decrease in the electrolyte viscosity is the increase in the concentration of non-solvating $DMSO_2$ species.
3. NH_4Cl and TMAC had different effects on the Coulombic efficiency. When 0.1 mol of NH_4Cl was added to the electrolyte, the Coulombic efficiency decreased by approximately 60%, while TMAC maintained at least 90% of the Coulombic efficiency. With the addition of both 0.02 mol of NH_4Cl and 0.10 mol of TMAC to the $DMSO_2$-based electrolyte ($DMSO_2$:$AlCl_3$ = 1:0.38), the conductivity increased to approximately three times that of the additive-free electrolyte while minimizing the decrease in Coulombic efficiency. During Al electrodeposition, the tank voltage was decreased to approximately 1/3 times that without the additives. By adding both NH_4Cl and TMAC, the author found an electrolyte composition that achieves the target values of conductivity and Coulombic efficiency. Compared to the additive-free electrolyte, this electrolyte consumes about 1/3 times, and Al energy saving in the electrodeposition process has been achieved.
4. The addition of TMAC does not adversely affect the appearance and purity of the film. In contrast, advantages such as decreased crude plating area and high purity plating films were obtained via the addition of NH_4Cl.

2.5. References

[1] L. Legrand, M. Heintz, A. Tranchant and R. Messina, *Electrochim. Acta*, **40**, 1711 (1995).

[2] L. Legrand, A. Tranchant and R. Messina, *Electrochim. Acta*, **41**, 2715 (1996).

[3] L. Legrand, A. Tranchant and R. Messina, *Inorg. Chem.*, **35**, 1310 (1996).

[4] T. Jiang, M. J. Chollier Brym, G. Dube, A. Lasia, and G. M. Brisard, *Surf. Coat. Technol.*, **201**, 6309 (2007).

[5] A. Okamoto, M. Morita, and N. Yoshimoto, *J. Surf. Finish. Soc. Jpn.*, **63**, 641 (2012).

[6] A. Okamoto, M. Morita, and N. Yoshimoto, *J. Surf. Finish. Soc. Jpn.*, **65**, 47 (2014).

[7] M. C. Simoes, K. J. Hughes, D. B. Ingham, L. Ma, and M. Pourkashanian, *Inorg. Chem.*, **56**, 7566 (2017).

[8] S. Kim, S. Kumeno, K. Kamebuchi, K. Kuroda, and M. Okido, *J. Surf. Engineered Mater. Adv. Technol.*, **8**, 110 (2018).

[9] O. Berkh, Y. Shacham-Diamand, and E. Gileadi, *J. Electrochem. Soc.*, **155**, F223 (2008).

Chapter 3. Evaluation of Electrochemical Properties of Dimethyl Sulfone–Aluminum Chloride Electrolyte with Ammonium Salt using an Ultramicro Disk Electrode

3.1. Introduction

Al-electrodeposited films manufactured using $DMSO_2$–$AlCl_3$ electrolyte solutions have been reported to include sulfur, carbon, and chlorine as impurities [1–4]. Chapter 2 revealed that adding NH_4Cl and TMAC as additives to the $DMSO_2$–$AlCl_3$ electrolyte solution had different effects on the Coulombic efficiency and the amount of impurities in the Al-electrodeposited film. In the $DMSO_2$–$AlCl_3$ electrolytes without NH_4Cl, caused black portion at corners of sample where the current concentration is present. The addition of NH_4Cl suppresses the generation of this black portion and improves the Al purity and appearance of the Al-electrodeposited film; however, it also decreases the Coulombic efficiency when added in large quantities. When TMAC is added to the basic composition electrolyte, the purity of the Al-electrodeposited film is lower than when NH_4Cl is added; but its influence on the Coulombic efficiency is low, reaching up to 0.1 mol of TMAC per 1 mol of $DMSO_2$. In addition, both ammonium salts decrease the viscosity of the electrolyte solution and increase its electrical conductivity. Using 0.02 mol of NH_4Cl and 0.1 mol of TMAC together increase the conductivity of the electrolyte and the purity of the Al-electrodeposited film while suppressing negative impacts on Coulombic efficiency. Thus, clarified the effects of the addition of ammonium salts on the $DMSO_2$–$AlCl_3$ electrolyte and Al-electrodeposited film; however, the mechanism by which each of the ammonium salts influences the Al electrodeposition reaction has not yet been elucidated. The purpose of this chapter is to clarify the Al electrodeposition mechanism from $DMSO_2$–$AlCl_3$ electrolyte by evaluating electrochemical polarization properties. When conducting electrochemical measurements of organic electrolytes, the

conductivity of the electrolyte is an important factor. $DMSO_2$–$AlCl_3$ electrolytes have higher viscosities and lower electrical conductivities than common water-based plating electrolytes, even when ammonium salts are added. To analyze the electrode reaction of a plating electrolyte with low conductivity in a high current density region, such as the electrodeposition reaction, a microelectrode may be employed as the working electrode for electrochemical measurements [5].

In this chapter, cyclic voltammetry was performed using microelectrodes on $DMSO_2$–$AlCl_3$ electrolyte solution (molar ratio 1:0.38) and electrolyte solution containing NH_4Cl and TMAC at different concentrations. The author clarified the mechanism by which NH_4Cl and TMAC influenced the electroplating properties such as Coulombic efficiency and purity of Al-electrodeposited film.

3.2. Experimental

3.2.1. Preparation of the electrolyte

For electrochemical measurement, a glass cell with a capacity of 0.06 L was used. 20.00 g of $DMSO_2$ (Bergstrom Nutrition, purity > 99.0%) and 10.77 g of $AlCl_3$ (KANTO CHEMICAL CO., INC., purity > 98.0%) were placed in the cell, which was then closed. The cell was placed in an oil bath and heated above 110 °C to dissolve the reagents. Subsequently, the electrolyte solution was stirred using a magnetic stirrer so that the electrolyte solution was uniform. The mixing ratio of $DMSO_2$ to $AlCl_3$ was 1:0.38 (molar ratio); hereafter, this is termed the electrolyte of basic composition. Then, depending on the purpose of the experiment, predetermined amounts of NH_4Cl (KANTO CHEMICAL CO., INC., purity > 98.0%) and TMAC (KANTO CHEMICAL CO., INC., purity > 99.5%) were added, and thoroughly stirred until complete dissolved. The amount of NH_4Cl and TMAC added ranged from 0.00– 0.30 mol per 1 mol of $DMSO_2$. Before performing the measurement, the electrolyte was bubbled with N_2 gas for 0.5 h. N_2 gas constantly flowed into the measurement cell at 0.1 L min^{-1} until the end of the experiment.

3.2.2. *Volume change of electrolyte and evaluation of molar concentration of ammonium ions*

The relationship between the electrochemical reaction current and physical properties such as the diffusion coefficient is usually discussed in terms of molality. When NH_4Cl and TMAC are added to the $DMSO_2$–$AlCl_3$ electrolyte solution, the volume of the electrolyte increases by a non-negligible amount. Therefore, it is necessary to measure the volume of the electrolyte solution for each additional amount of NH_4Cl and TMAC and calculate the molarity based on that value. A graduated cylinder with a capacity of 0.1 L was used to measure the volume of the electrolyte solution. The electrolyte solutions were prepared by adding 26.91 g of $AlCl_3$, 50.00 g of $DMSO_2$, and a predetermined amount of either NH_4Cl or TMAC into a graduated cylinder, then heating, dissolving, and mixing. The volume of the electrolyte solution at 100 °C was measured by reading the value of the scale when the temperature was 100 °C, and the volume of the electrolyte solution was calculated considering the volume change of the graduated cylinder due to thermal expansion. The volume change of the graduated cylinder due to thermal expansion was measured by heating silicone oil (Shin-Etsu Chemical Co., Ltd., KF54) from room temperature to 100 °C, then corrected using the volume expansion coefficient of the silicone oil.

As described in Chapter 2, the concentration of ionic species in the electrolyte solution changes with the addition of NH_4Cl or TMAC. Equation 3-1 shows the change in ionic equilibrium in the electrolyte solution when m mol of NR_4Cl is added. Here, R is H or CH_3.

$$\begin{aligned} &Al(DMSO_2)_3^{3+} + 3AlCl_4^- + \ mNR_4Cl \\ &\rightleftharpoons \ (1 - \tfrac{m}{4})\, Al(DMSO_2)_3^{3+} + (3 + \tfrac{m}{4})\, AlCl_4^- + \ mNR_4^+ + \tfrac{3m}{4}DMSO_2 \end{aligned} \tag{3-1}$$

Tables 3-1a, 3-1b, and 3-1c summarize the number of charged moles of the electrolyte

solutions, volume, ionic equilibrium change, molar concentration, viscosity, and conductivity. Composition A is a basic composition electrolyte, compositions B to E are electrolytes with added NH_4Cl, compositions F to H are electrolytes with added TMAC, and composition I is an electrolyte to which NH_4Cl and TMAC are added together. The molar ratio of ionic equilibrium in Table 3-1c shows the ratio to 1 mol of $DMSO_2$. NH_4Cl and TMAC are assumed to have completely dissociated, and the dissociated ammonium cations are denoted by NH_4^+ and TMA^+, respectively. The ion concentrations involved in the electrode reaction are discussed using the molar concentrations calculated after considering the volume change.

Table 3-1a. The number of charged moles and volume of electrolyte solutions.

Electrolyte composition	Number of charged mole/mol (molar ratio)				Volume/mL (change ratio)
	$DMSO_2$	$AlCl_3$	NH_4Cl	TMAC	
A	0.53 (1.00)	0.20 (0.38)	0.00 (0.00)	0.00 (0.00)	51.67 (1.00)
B	0.53 (1.00)	0.20 (0.38)	0.01 (0.02)	0.00 (0.00)	51.85 (1.00)
C	0.53 (1.00)	0.20 (0.38)	0.05 (0.10)	0.00 (0.00)	54.25 (1.05)
D	0.53 (1.00)	0.20 (0.38)	0.11 (0.20)	0.00 (0.00)	57.68 (1.12)
E	0.53 (1.00)	0.20 (0.38)	0.16 (0.30)	0.00 (0.00)	60.56 (1.17)
F	0.53 (1.00)	0.20 (0.38)	0.00 (0.00)	0.05 (0.10)	57.53 (1.11)
G	0.53 (1.00)	0.20 (0.38)	0.00 (0.00)	0.11 (0.20)	64.01 (1.23)
H	0.53 (1.00)	0.20 (0.38)	0.00 (0.00)	0.16 (0.30)	70.13 (1.36)
I	0.53 (1.00)	0.20 (0.38)	0.01 (0.02)	0.05 (0.10)	59.91 (1.16)

Table 3-1b. Ionic equilibrium of electrolyte solutions.

Electrolyte composition	Ionic equilibrium/mol (molar ratio)			
	$Al(DMSO_2)_3^{3+}$	$AlCl_4^-$	NH_4^+	TMA^+
A	0.051 (0.095)	0.151 (0.285)	0.000 (0.000)	0.000 (0.000)
B	0.048 (0.090)	0.154 (0.290)	0.011 (0.020)	0.000 (0.000)
C	0.037 (0.070)	0.165 (0.310)	0.053 (0.100)	0.000 (0.000)
D	0.024 (0.045)	0.178 (0.335)	0.106 (0.200)	0.000 (0.000)
E	0.011 (0.020)	0.191 (0.360)	0.159 (0.300)	0.000 (0.000)
F	0.037 (0.070)	0.165 (0.310)	0.000 (0.000)	0.053 (0.100)
G	0.024 (0.045)	0.178 (0.335)	0.000 (0.000)	0.106 (0.200)
H	0.011 (0.020)	0.191 (0.360)	0.000 (0.000)	0.159 (0.300)
I	0.035 (0.065)	0.167 (0.315)	0.011 (0.020)	0.053 (0.100)

Table 3-1c. Molar concentration and viscosity of electrolyte solutions.

Electrolyte composition	Molar concentration/mol L^{-1}			Viscosity	Conductivity
	$Al(DMSO_2)_3^{3+}$	NH_4^+	TMA^+	/mPa s	/S m^{-1}
A	0.977	0.000	0.000	39.40	0.19
B	0.922	0.205	0.000	25.40	0.22
C	0.685	0.979	0.000	14.00	0.44
D	0.414	1.842	0.000	8.43	0.81
E	0.175	2.631	0.000	5.82	1.22
F	0.646	0.000	0.923	10.80	0.49
G	0.373	0.000	1.660	5.09	0.85
H	0.151	0.000	2.272	3.27	1.27
I	0.576	0.164	0.887	9.30	0.54

3.2.3. *Electrochemical measurements*

Cyclic voltammetry was performed according to the three-electrode method using a potentiostat (BAS Inc., ALS-802B). The electrodes used for measurement were glass-enclosed Pt-micro disk electrodes with a diameter of 20 μm (hereafter Pt-micro electrode), or Pt-flag electrodes with a diameter of 4 mm for the WE, Al-wire for the RE, Al-coil for the CE. The temperature of the electrolyte solution was 100 °C. The potential was swept in the negative direction with a rate of 50 mV s^{-1} and reversed at a predetermined potential. The horizontal axis of voltammograms indicates the potential of the Al-wire reference (i.e., *versus* Al-wire), and the vertical axis indicates the current density obtained by dividing current by electrode area. The Coulombic efficiency Q_{eff} was calculated using Eq. 3-2, where Q_{eff} is Coulombic efficiency (%), Q_{o} is the Coulomb number of oxidation, and Q_{r} is the Coulomb number of reduction. Q_{o} and Q_{r} were determined by integrating the oxidation or reduction currents during one cycle.

$$Q_{\mathrm{eff}} = \frac{Q_{\mathrm{o}}}{Q_{\mathrm{r}}} \times 100 \tag{3-2}$$

The electrodes used to measure the potential window of $DMSO_2$ were Pt-micro electrodes for the WE, $Ag|AgNO_3$ for the RE, and Al-coil for the CE. Since $DMSO_2$ has low conductivity, 0.01 mol of $LiBF_4$ was added as a supporting electrolyte. The temperature of the $DMSO_2$-$LiBF_4$ electrolyte was 115 °C. The potential of a voltammogram of the $DMSO_2$-$LiBF_4$ electrolyte was shown by correcting vs. Al-wire. The potential was converted to potential against Al-wire by comparing the voltammogram of the basic composition electrolyte measured with $Ag|AgNO_3$ and that measured with Al-wire.

3.3. Results

3.3.1. *Cyclic Voltammetry of $DMSO_2$–$AlCl_3$ electrolyte without Ammonium salts*

Figure 3-1 shows cyclic voltammograms of the basic composition measured using working electrodes of different sizes. The electrodes used were a Pt-micro electrode with a diameter of 20 μm and a Pt-flag electrode with a diameter of 4 mm. The current value when using Pt-micro electrodes is displayed on the left axis, and that when using Pt-flag electrodes is displayed on the right axis. The current density and current change slope of the voltammograms measured using the Pt-flag electrode are smaller than those using the Pt-micro electrode when swept over the same potential range.

In the voltammogram with the Pt-micro electrode, the reduction current rises from approximately −0.5 V (vs. Al-wire) during the negative direction sweep (solid blue line), peaks around −0.8 V and decreases on the negative side. The peak current density is approximately −2.2 mA mm^{-2}. Reversing the sweep direction at −1.0 V causes the current to increase again (dotted blue line). The reduction current shows a larger reduction current peak than during the negative direction sweep, then decreases. At around 0.0 V, a change in exponential current specific to the electrode reaction was observed, in which the oxidation current flows toward a positive potential from 0.0 V. The oxidation current peaks around +0.3 V, then decreases gradually to 0.0 mA mm^{-2} at around +1.3 V. The peak current density of the oxidation current was approximately 2.6 mA mm^{-2}.

In the voltammogram with the Pt-flag electrode, the reduction current rises from −0.3 V during the negative direction sweep. The reduction current increased monotonically without exhibiting a peak. During the positive direction sweep, the reduction current decreased monotonically to an oxidation current at 0.0 V. The maximum current density was approximately 0.2 mA mm^{-2}, which is one order of magnitude lower than when using the Pt-micro electrode. The current around 0.0 V does not exhibit an exponential change peculiar to the electrode reaction; rather, it shows a linear change. The oxidation current peaked at 1.0 V

and then decreased rapidly, reaching 0.0 mA mm^{-2} after a slight shoulder effect.

Figure 3-2 shows voltammograms of the basic composition electrolyte measured by changing the reversal potential on the negative side using a Pt-micro electrode. In the negative direction sweep, the reduction current began to flow from −0.5 V and peaked at −0.8 V, then increased again at −1.2 V. In the positive direction sweep, the reduction current followed almost the same trajectory until −0.8 V. The reduction current within the potential range of −0.8 to 0.0 V was increased in the reverse positive direction sweep relative to the negative direction sweep. When the reversal potential was more negative than −1.0 V, the reduction current of the positive direction sweep peaked at around −0.7 V, and its peak current increased as the reversal potential became more negative.

The waveform of the oxidation current changed systematically with reversal potential. The oxidation current began to flow from 0.0 V and decreased after reaching its peak. When the reversal potential became more negative, the peak current of oxidation increased, and the peak potential shifted to the positive side. The current on the positive potential side of the peak decreased gradually as the reversal potential became negative, and the potential at which the oxidation current became 0.0 mA mm^{-2} shifted in the positive direction. Moreover, when the reversal potential became more negative than −1.1 V, a second peak appeared after the first peak. When the reversal potential became more negative, both the second peak potential and the potential at which the current began to increase again were shifted to positive values. The bottom current value between the first and second peaks became smaller than that when the reversal potential became more negative.

Figure 3-3 shows the reduction and oxidation Coulomb numbers obtained from the voltammograms shown in Fig. 3-2. Figure 3-4 shows the Coulombic efficiency calculated from the ratio of the reduction and oxidation Coulomb numbers. The reduction Coulomb number increased monotonically as the reversal potential became negative. When the reversal potential was within the range of −0.6 to −0.8 V, the oxidation Coulomb number was the same as the reduction Coulomb number; however, when the reversal potential became more negative than −0.8 V, the deviation of the oxidation Coulomb number from the reduction Coulomb number

increased. The Coulombic efficiency was 90% or more when the range of the reversal potential was −0.6 to −0.8 V; however, when the reversal potential was more negative than −0.8 V, the Coulombic efficiency decreased.

The potential window of the $DMSO_2$ solvent was evaluated by cyclic voltammetry of a solution in which $LiBF_4$ was added to $DMSO_2$ using a Pt-micro electrode. Fig. 3-5 shows the cyclic voltammograms of the $DMSO_2$–$LiBF_4$ swept to −1.8 V. The reduction current measured with the $DMSO_2$–$LiBF_4$ electrolyte was less than 10^{-2} mA mm^{-2} order, which was considerably lower than the deposition current shown in Fig. 3-2 (10^{1} mA mm^{-2} order).

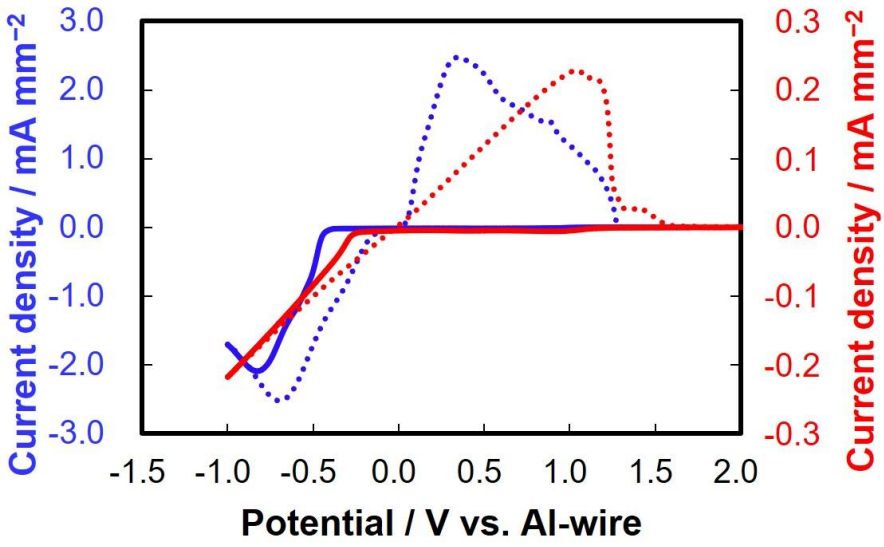

Figure 3-1. Cyclic voltammograms of $DMSO_2$–$AlCl_3$ electrolyte using a Pt electrode. (Blue line) Pt-micro electrode; (red line) Pt-flag electrode; (solid line) negative direction sweep; (dotted line) positive direction sweep; sweep rate, 50 mV s^{-1}; temperature, 100 °C.

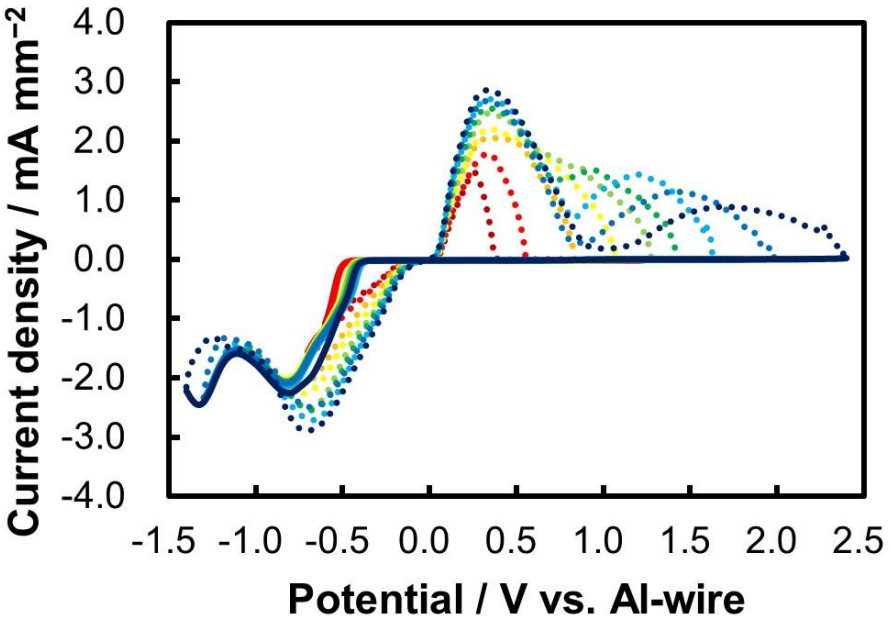

Figure 3-2. Cyclic voltammograms of $DMSO_2$–$AlCl_3$ electrolyte using a Pt-microelectrode. The sweep range at the negative side was varied from −0.6 to −1.4 V. Solid line, negative sweep; dotted line, positive sweep; Reversal potential, (brown line) −0.6 V, (red line) −0.7 V, (orange line) −0.8 V, (yellow line) −0.9 V, (light green line) −1.0 V, (green line) −1.1 V, (light blue line) −1.2 V, (blue line) −1.3 V, (violet line) −1.4 V; sweep rate, 50 mV s^{-1}; temperature, 100 °C.

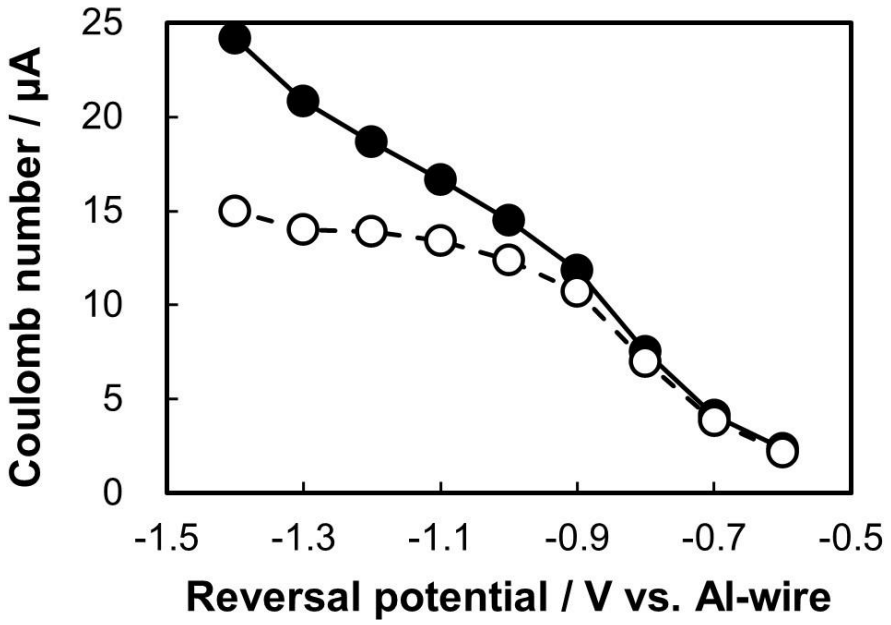

Figure 3-3. Change in the reduction and oxidation Coulomb number for various reversal potentials. (Solid-symbol circles) reduction Coulomb; (open-symbol circles) oxidation Coulomb.

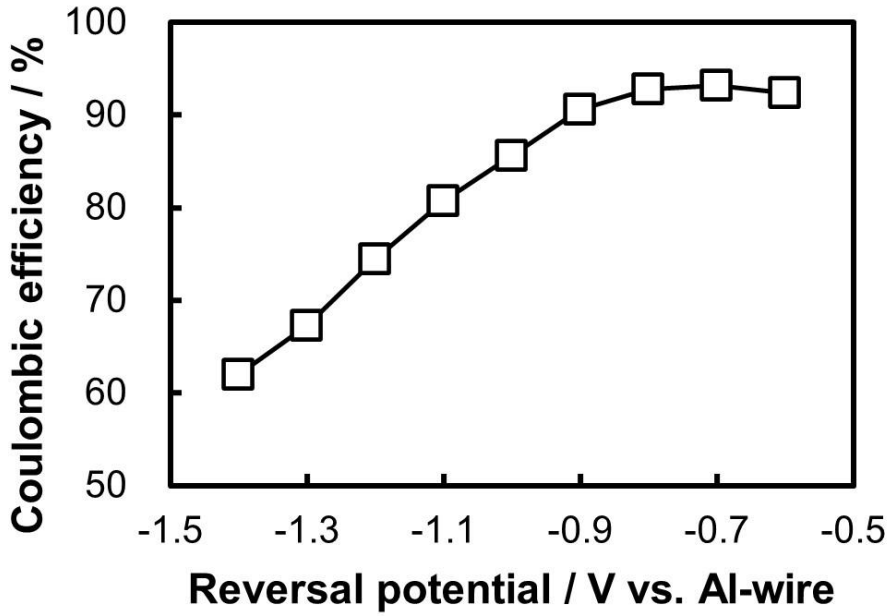

Figure 3-4. Relationship between reversal potential and Coulombic efficiency.

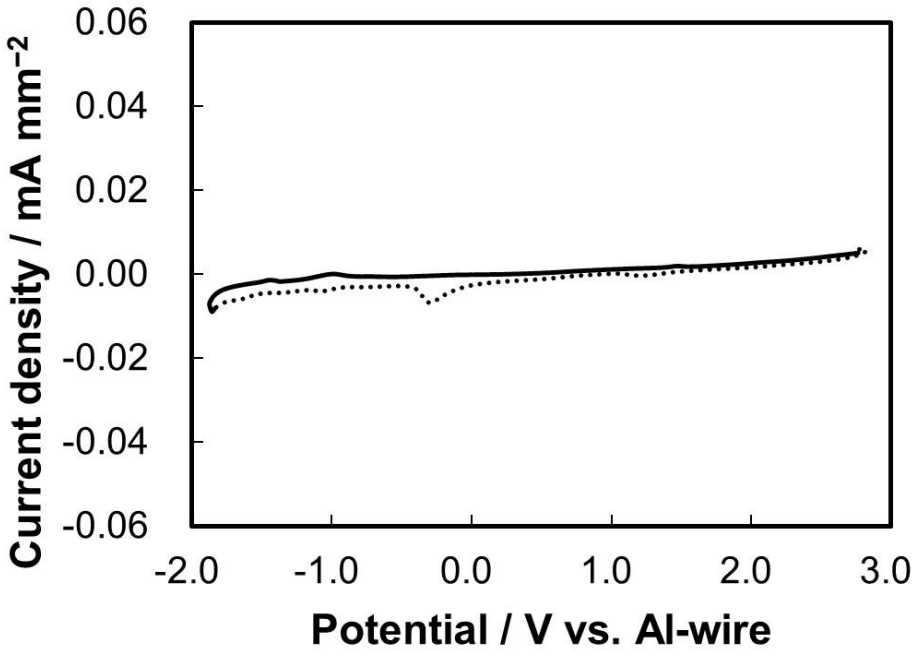

Figure 3-5. Cyclic voltammograms of $DMSO_2$–$LiBF_4$ electrolyte using a Pt-micro electrode. (Solid line) negative sweep; (dotted line) positive sweep; sweep rate, 50 mV s^{-1}; temperature, 115 °C.

3.3.2. *Cyclic Voltammetry of $DMSO_2$–$AlCl_3$ electrolyte with NH_4Cl addition*

Figures 3-6a–3-6e shows cyclic voltammograms of electrolyte solutions with different NH_4^+ concentrations measured using a Pt-micro electrode. The NH_4^+ concentrations were set at 0.00, 0.20, 0.98, 1.84, and 2.63 mol L^{-1}. Figures 3-7a–3-7b show the negative direction sweep voltammograms for different NH_4^+ concentrations. Figure 3-7c shows the positive direction sweep voltammograms for different NH_4^+ concentrations. Figure 3-7b provides an enlarged view of the range up to −2 mA mm^{-2} on the vertical axis of Fig. 3-7a.

The onset potential of the reduction current changed considerably with the addition of NH_4Cl. It was about −0.4 V, which was more positive than that in the basic composition electrolyte without NH_4Cl. The reduction current did not reach a peak as in the case of the basic composition electrolyte but continued to increase rapidly. When polarized to a more negative potential than shown in Figs. 3-6–3-7, the reduction current increased to 10 mA mm^{-2} or more. When polarized to a more negative potential, appropriate analysis becomes difficult because deposits Al with a thickness on the μm-order and changes the electrode shape. This is a limitation of microelectrode for electrodeposition measurements. Therefore, in this study, the sweep range was limited to the aforementioned potentials, even though the observed current density range is very high compared to normal-size disk electrodes. In the positive direction sweep, after reversing the sweep direction on the negative side, the reduction current did not reach a peak, but decreased monotonously. When it exceeded 0.0 V, it became an oxidation current.

Moreover, as shown in Fig. 3-7b, for the electrolyte with NH_4Cl, a small reduction current of about −0.1 to −1.5 mA mm^{-2} was observed in the potential range from +0.8 V to −0.3 V. The reduction current of this potential range has peaks at +0.5 V and +0.1 V, and its values increased with increasing NH_4^+ concentration. Figure 3-8 shows the voltammograms corresponding to this potential range in the electrolyte solution with an NH_4^+ concentration of 0.20 mol L^{-1}. When the sweep direction was reversed at −0.3 V, the reduction current increased,

and an oxidation current was observed on the positive side of 0.0 V. In contrast, when the sweep direction was reversed at −0.26 V, no oxidation current was observed in the positive direction sweep after reversal.

Figure 3-9 shows an enlarged view of the oxidation current for voltammograms of the positive direction sweep for different NH_4^+ concentrations, indicating that the oxidation current peaked at 0.3 V. When the NH_4^+ concentration was 0.20 mol L^{-1}, the oxidation current decreased after reaching its peak and flowed to +1.1 V while oscillating. At NH_4^+ concentrations equal to or greater than 0.98 mol L^{-1}, the current after exceeding the peak rapidly decreased to 0.0 mA mm^{-2}. Furthermore, the oxidation current peak was extremely small when using NH_4^+ concentration of 2.63 mol L^{-1}.

Figure 3-10 shows the Coulombic efficiency obtained from Fig. 3-6 *versus* NH_4^+ concentrations. The Coulombic efficiency decreased monotonically with increasing NH_4^+ concentrations up to 1.84 mol L^{-1}. The voltammogram of NH_4^+ concentration 2.63 mol L^{-1} is shown in Fig. 3-6e, the sweep range of the negative side is narrow, and the reduction current of Al electrodeposition is small. Therefore, it cannot properly evaluate the Coulombic efficiency.

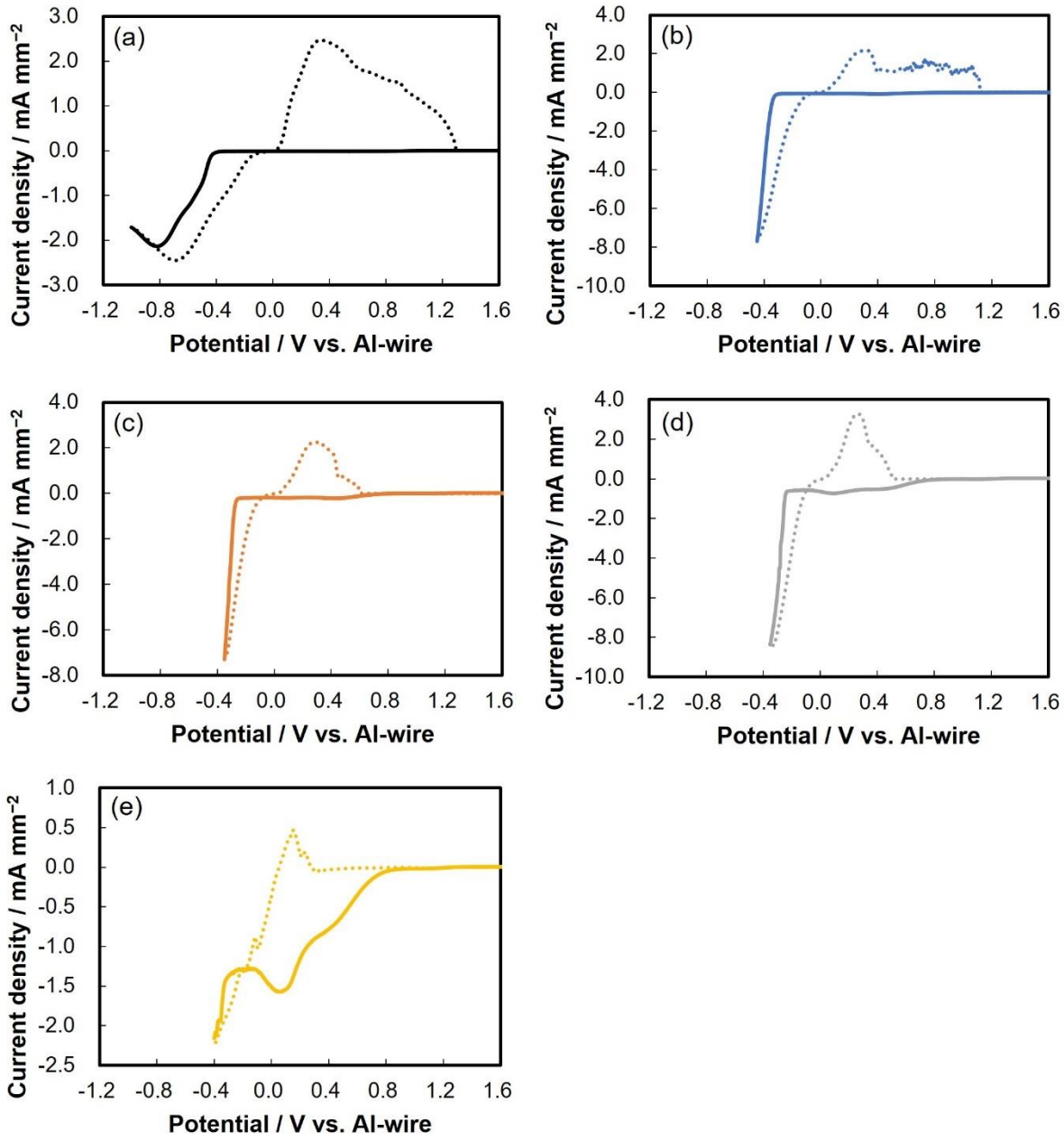

Figure 3-6. Cyclic voltammograms of the $DMSO_2$–$AlCl_3$ electrolyte with added NH_4Cl using a Pt-microelectrode. (a) NH_4^+ 0.00 mol L^{-1}, (b) NH_4^+ 0.20 mol L^{-1}, (c) NH_4^+ 0.98 mol L^{-1}, (d) NH_4^+ 1.84 mol L^{-1}, and (e) NH_4^+ 2.63 mol L^{-1}; (solid line) negative sweep; (dotted line) positive sweep; sweep rate, 50 mV s^{-1}; temperature, 100 °C.

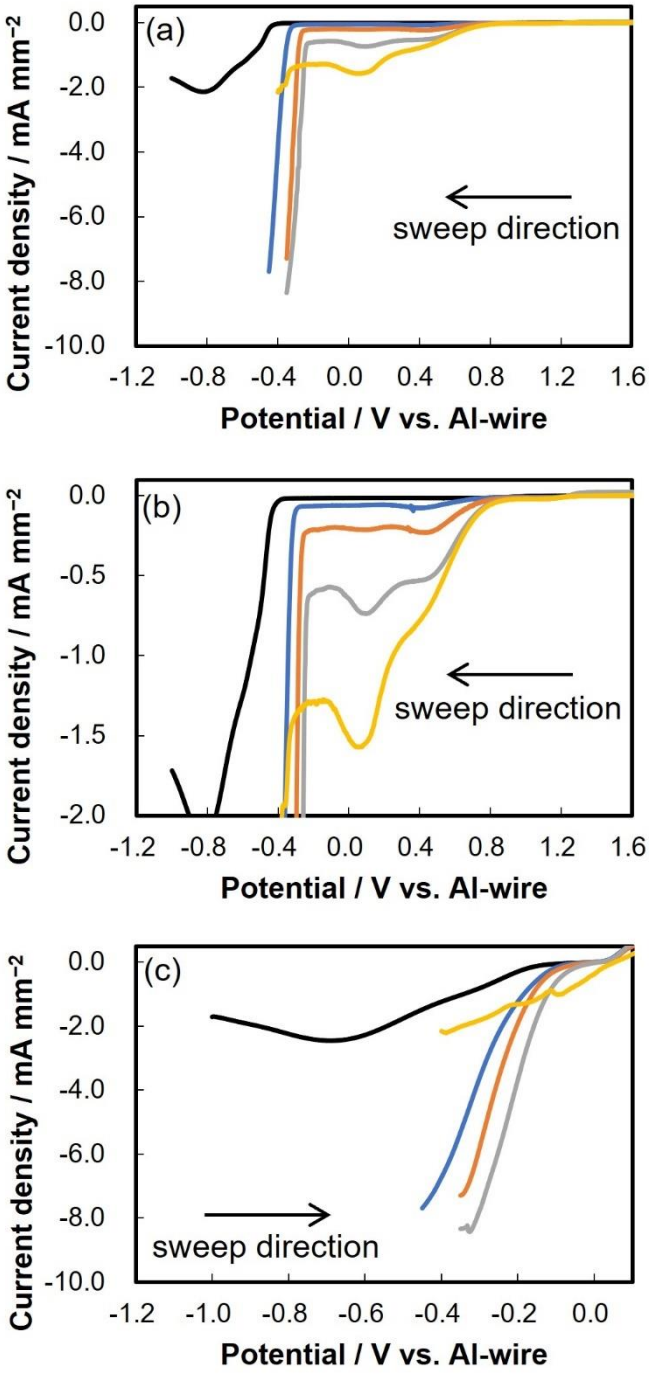

Figure 3-7. Reduction current in linear sweep voltammograms of $DMSO_2$–$AlCl_3$ electrolyte with added NH_4Cl using a Pt-microelectrode. (a) Negative direction sweep voltammograms, (b) expansion of the Y-axis of (a), and (c) positive direction sweep voltammograms; (black line) NH_4^+ 0.00 mol L^{-1}, (blue line) NH_4^+ 0.20 mol L^{-1}, (orange line) NH_4^+ 0.98 mol L^{-1}, (grey line) NH_4^+ 1.84 mol L^{-1}, (yellow line) NH_4^+ 2.63 mol L^{-1}; sweep rate, 50 mV s^{-1}; temperature, 100 °C.

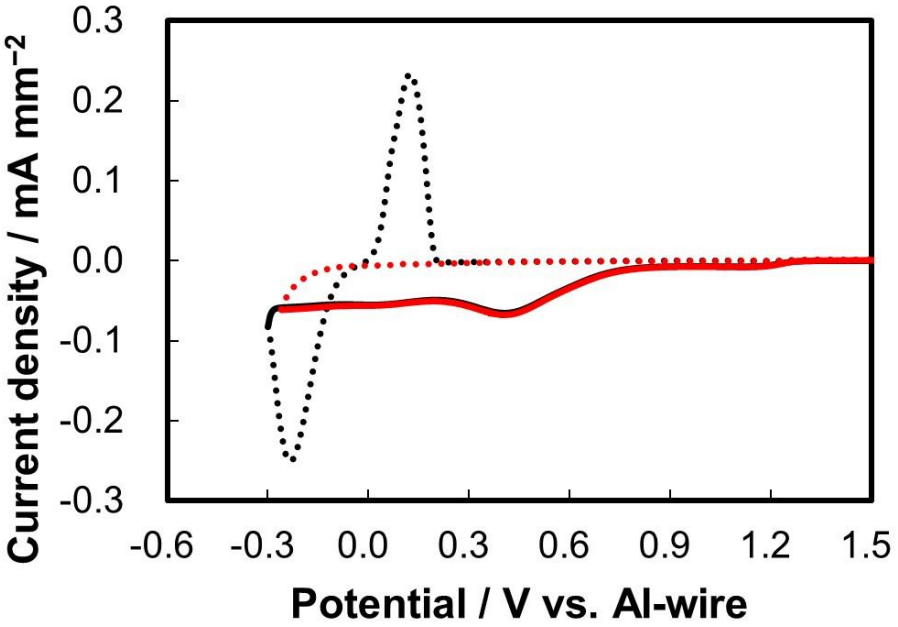

Figure 3-8. Cyclic voltammograms of $DMSO_2$–$AlCl_3$–NH_4Cl electrolyte solution using a Pt-microelectrode. NH_4^+ 0.20 mol L^{-1}; (solid line) negative sweep; (dotted line) positive sweep; reversal potential, (red line) −0.26 V, (black line) −0.3 V; sweep rate, 50 mV s^{-1}; temperature, 100 °C.

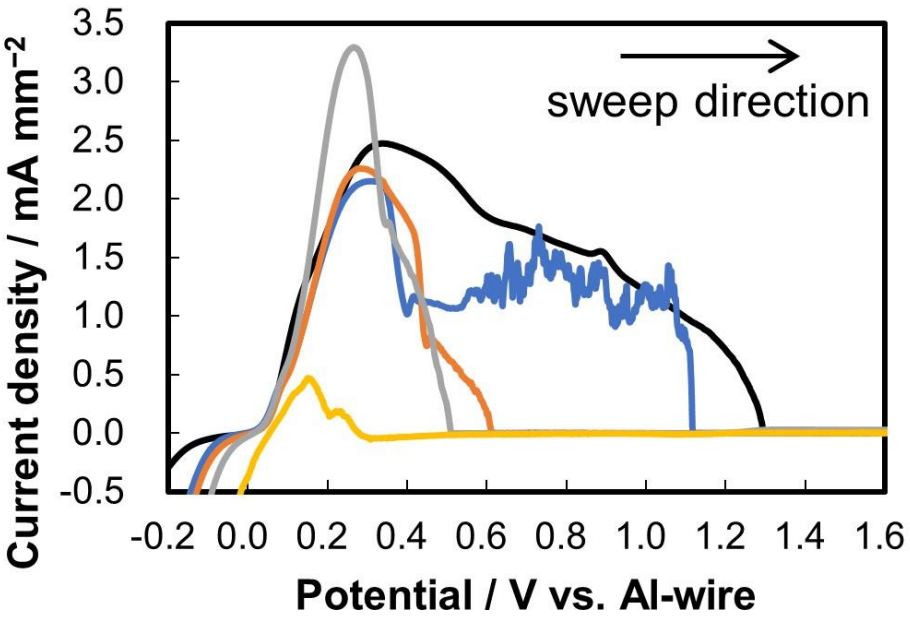

Figure 3-9. Oxidation current in positive direction linear sweep voltammograms of $DMSO_2$–$AlCl_3$ electrolyte with added NH_4Cl using a Pt-microelectrode. (Black line) NH_4^+ 0.00 mol L^{-1}, (blue line) NH_4^+ 0.20 mol L^{-1}, (orange line) NH_4^+ 0.98 mol L^{-1}, (grey line) NH_4^+ 1.84 mol L^{-1}, (yellow line) NH_4^+ 2.63 mol L^{-1}; sweep rate, 50 mV s^{-1}; temperature, 100 °C.

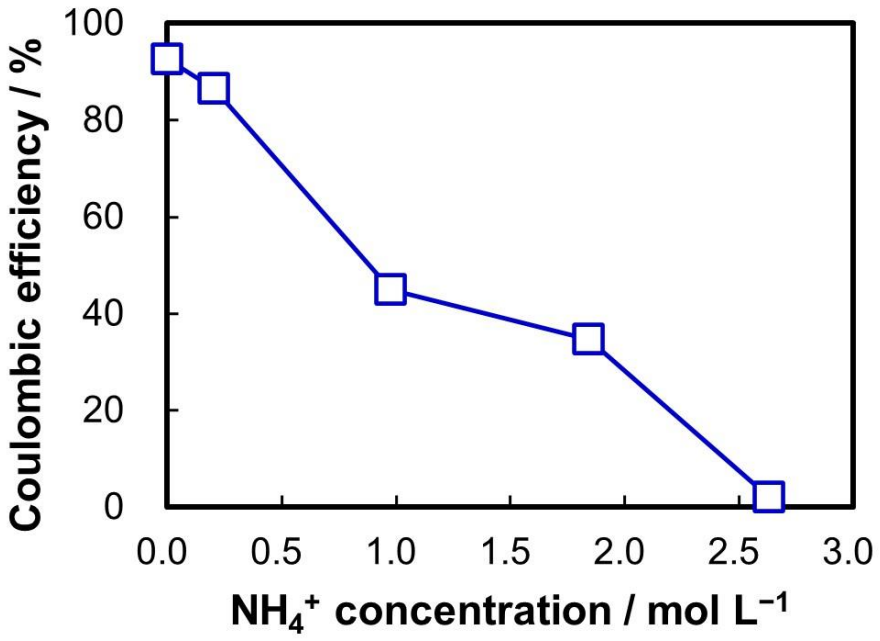

Figure 3-10. Relationship between NH_4^+ concentration and Coulombic efficiency.

3.3.3. *Cyclic Voltammetry of $DMSO_2$–$AlCl_3$ electrolyte with TMAC addition*

Figures 3-11a–3-11d shows cyclic voltammograms of the $DMSO_2$–$AlCl_3$ electrolyte with different TMA^+ concentrations measured using a Pt-micro electrode. The TMA^+ concentration was set at 0.00, 0.92, 1.66, and 2.27 mol L^{-1}. Figure 3-12a shows the negative direction sweep voltammograms for different TMA^+ concentrations. Figure 3-12b shows the positive direction sweep voltammograms for different TMA^+ concentrations. Figure 3-12c provides an enlarged view of the oxidation current of voltammograms of the positive direction sweep for different TMA^+ concentrations.

In Fig. 3-12a, the reduction current increases from about −0.4 V in the basic composition electrolyte without TMAC. When TMAC is added, the reduction current rises from a more negative potential, reaches a peak, decreases slightly, then gradually increases. The reduction current value decreased with increasing TMA^+ concentration. At potentials more positive than −0.7 V, no reduction current was observed as in the case of NH_4^+ addition shown in Fig. 3-7b. In a positive direction sweep after reversing potential, peaks at −0.7 V are observed regardless of TMA^+ concentration. The current value decreased with increasing TMA^+ concentration. For the oxidation current shown in Fig. 3-12c, the slope of oxidation current increased regardless of the TMA^+ concentration and was larger than that of the basic composition electrolyte at any concentration.

Coulombic efficiency calculated using Fig. 3-11 is plotted against TMA^+ concentration in Fig. 3-13. The Coulombic efficiency decreased monotonically as TMA^+ concentration increased, reaching about 40% in a TMA^+ concentration of 2.27 mol L^{-1}.

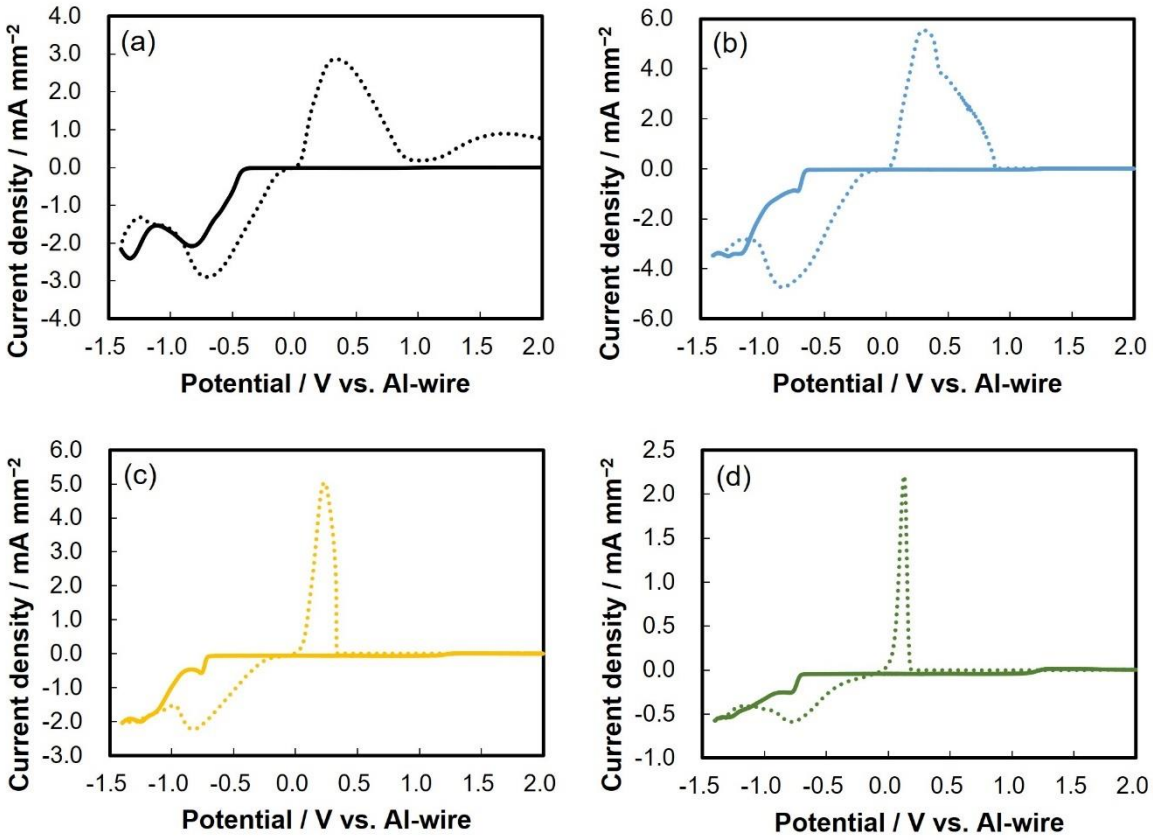

Figure 3-11. Cyclic voltammograms of $DMSO_2$–$AlCl_3$ electrolyte with added TMAC using a Pt-microelectrode. (a) TMA^+ 0.00 mol L^{-1}, (b) TMA^+ 0.92 mol L^{-1}, (c) TMA^+ 1.66 mol L^{-1}, (d) TMA^+ 2.27 mol L^{-1}; (solid line) negative sweep; (dotted line) positive sweep; sweep rate, 50 mV s^{-1}; temperature, 100 °C.

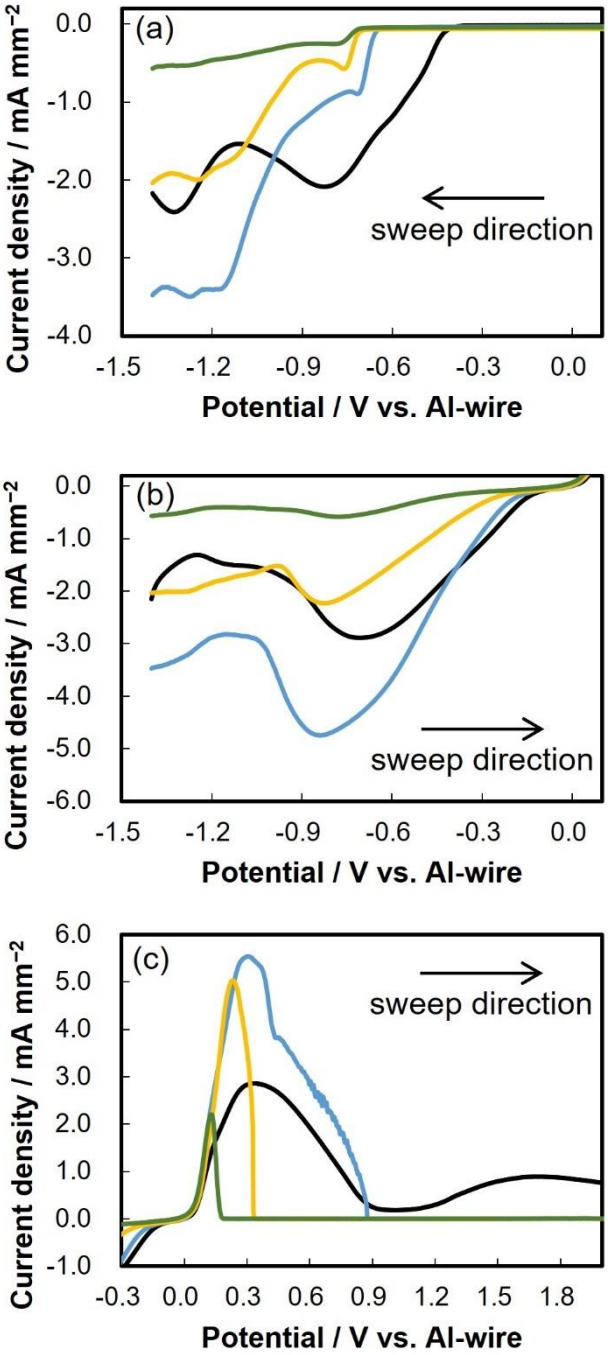

Figure 3-12. Linear sweep voltammograms of $DMSO_2$–$AlCl_3$ electrolyte with added TMAC using a Pt-microelectrode. (a) Reduction current voltammograms of negative direction sweep, (b) reduction current voltammograms of positive direction sweep, and (c) oxidation current voltammograms of positive direction sweep; (black line) TMA^+ 0.00 mol L^{-1}, (blue line) TMA^+ 0.92 mol L^{-1}, (yellow line) TMA^+ 1.66 mol L^{-1}, (green line) TMA^+ 2.27 mol L^{-1}; sweep rate, 50 mV s^{-1}; temperature, 100 °C.

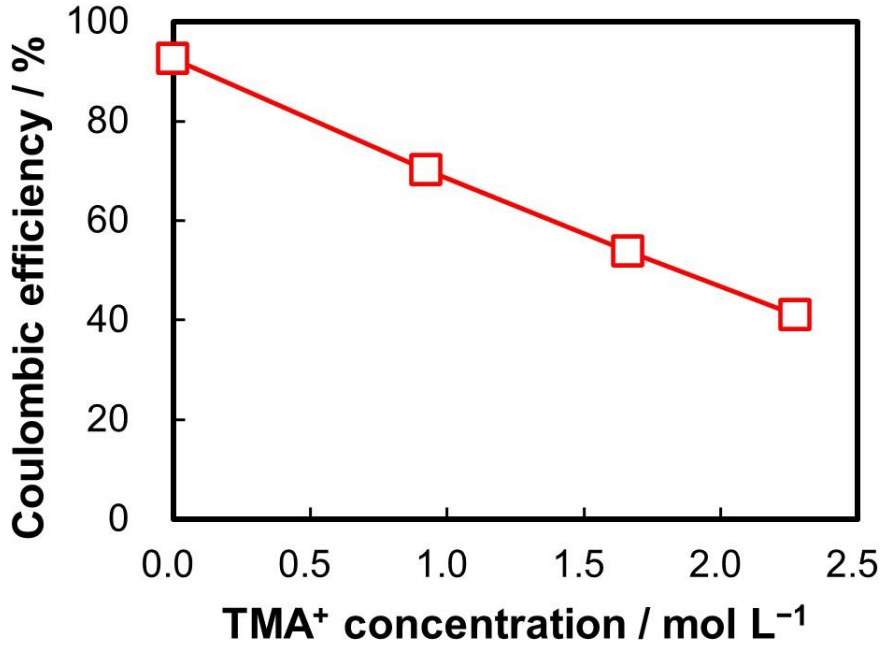

Figure 3-13. Relationship between the TMA^+ concentration and Coulombic efficiency.

3.3.4. *Cyclic Voltammetry of $DMSO_2$–$AlCl_3$ electrolyte with NH_4Cl and TMAC combined addition*

Figure 3-14 shows the voltammograms of the electrolyte solution added both NH_4Cl and TMAC measured using a Pt-micro electrode. The NH_4^+ concentration was 0.16 mol L^{-1} and the TMA^+ concentration was 0.88 mol L^{-1}. For comparison, the voltammograms of the basic composition electrolyte, only NH_4^+ 0.20 mol L^{-1}, and only TMA^+ 0.92 mol L^{-1} are shown in the same graph. Figure 3-15a shows the negative direction sweep linear sweep voltammograms, Fig. 3-15b shows the positive direction sweep linear sweep voltammograms, and Fig. 3-15c shows an enlarged view of the oxidation current portion of Fig. 3-14.

The behavior of the reduction current of the electrolyte solution with both NH_4Cl and TMAC was found to be similar to that when adding only NH_4Cl. In the electrolyte containing no NH_4Cl (i.e., the basic composition electrolyte and only TMAC), the maximum current value was small, about −2 mA mm^{-2}, even when the potential was swept to a potential value more negative than −1.0 V. Conversely, in the electrolyte containing NH_4Cl (i.e., combined addition and only NH_4Cl), a large reduction current was observed to flow with a small polarization.

The oxidation and the reduction currents exhibited different behavior. The oxidation current of the electrolyte solution added both NH_4Cl and TMAC showed similar behavior to the case in which only TMAC was added. Without TMAC (i.e., the basic composition electrolyte, and only NH_4Cl), the oxidation current peak was about 2–2.5 mA mm^{-2}. In contrast, in the electrolyte with TMAC (combined addition, and only TMAC), the oxidation current peak was about 4 mA mm^{-2}, i.e., 1.5–2.0 times higher than the electrolyte solution without TMAC. In the voltammogram of the electrolyte solution with both NH_4Cl and TMAC, the Coulombic efficiency was 75.3% when the reversal potential was −0.4 V. This value is lower than the Coulombic efficiency (86.6%) of the electrolyte solution in which NH_4^+ 0.20 mol L^{-1} is added alone shown in Fig. 3-10, but higher than the Coulombic efficiency (70.1%) of the electrolyte solution in which TMA^+ 0.92 mol L^{-1} is added alone shown in Fig. 3-13.

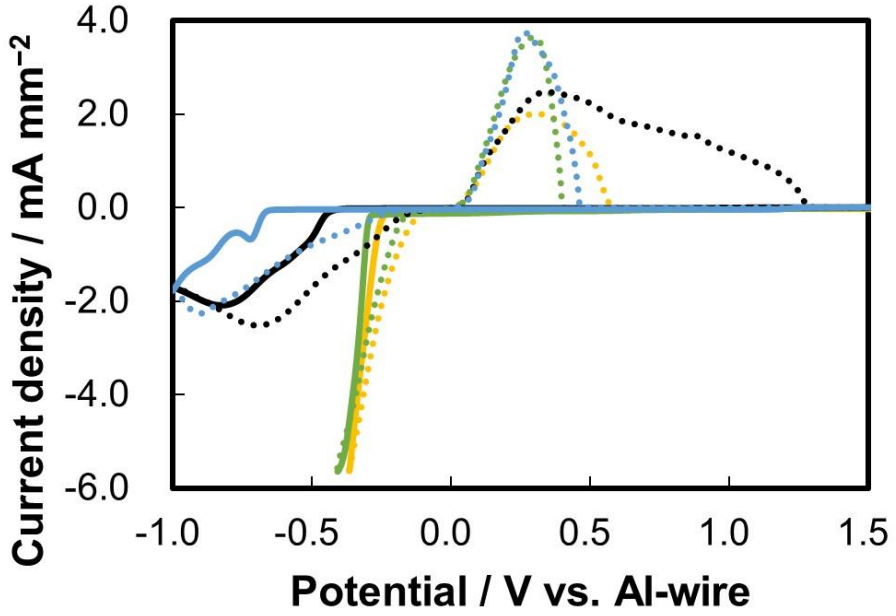

Figure 3-14. Cyclic voltammograms of $DMSO_2$–$AlCl_3$ electrolyte with added NH_4Cl and TMAC using a Pt-microelectrode. (Black line) no additive, (blue line) TMA^+ 0.92 mol L^{-1}, (yellow line) NH_4^+ 0.20 mol L^{-1}, (green line) NH_4^+ 0.16 mol L^{-1} and TMA^+ 0.89 mol L^{-1}; (solid line) negative sweep; (dotted line) positive sweep; sweep rate, 50 mV s^{-1}; temperature, 100 °C.

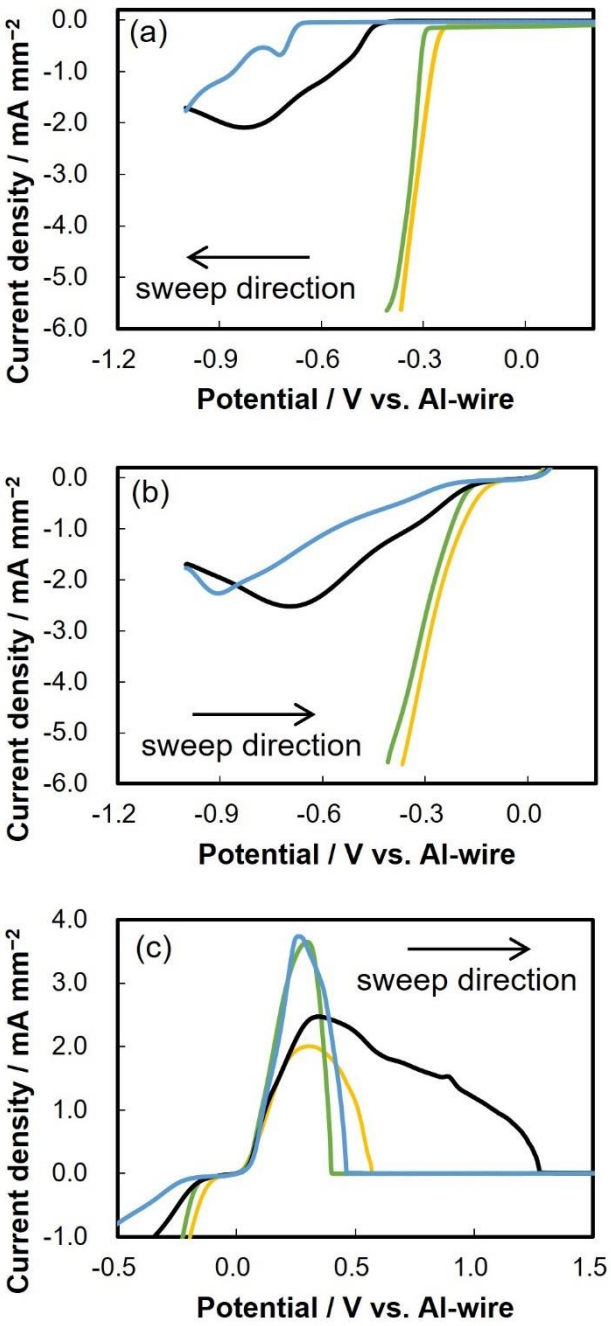

Figure 3-15. Linear sweep voltammograms of $DMSO_2$–$AlCl_3$ electrolyte with added NH_4Cl and TMAC using a Pt-microelectrode. (a) Reduction current voltammograms of negative direction sweep, (b) reduction current voltammograms of positive direction sweep, and (c) oxidation current voltammograms of positive direction sweep; (black line) no additive, (blue line) TMA^+ 0.92 mol L^{-1}, (yellow line) NH_4^+ 0.20 mol L^{-1}, (green line) NH_4^+ 0.16 mol L^{-1} and TMA^+ 0.89 mol L^{-1}; sweep rate, 50 mV s^{-1}; temperature, 100 °C.

3.4. Discussion

3.4.1. *Effect of electrode size*

As shown in Fig. 3-1, the current density obtained with the Pt-flag electrode, which is commonly used for electrochemical measurements, is an order of magnitude lower than that obtained with the Pt-micro electrode at the same potential. Pt-flag electrodes with a large electrode area generate large currents during electrochemical measurement. The potential drop during electrochemical measurement is large in low-conductivity solutions, such as the $DMSO_2$–$AlCl_3$ electrolyte solution, and the set potential is not correctly applied to the electrodes. In the case of the three-electrode electrochemical measurement using a potentiostat, the potential of the reference electrode is controlled to avoid the potential drop effect due to solution resistance between the working electrode and the counter electrode; however, it is difficult to avoid a potential drop between the working electrode and the reference electrode. For electrolytes with low conductivity, this causes a problem when the correct set potential is not applied, especially for measurements at high current densities. Since microelectrodes have extremely small electrode areas, the current values during electrochemical measurement are also extremely small, and the effect of potential drop due to solution resistance can be avoided even with a low-conductivity electrolyte solution. As shown in Fig. 3-1, the current density measured using the Pt-flag electrode was much smaller than that measured using the Pt-micro electrode with a diameter of 20 μm at the same potential. This is because the potential of the Pt-flag electrode is much smaller than the set potential by the influence of the solution resistance. For example, the current density of the disk electrode at −0.8 V is 0.17 mA mm^{-2}, while the current value of the microelectrode at the same potential is 2.30 mA mm^{-2}. Here, the respective actual current values are 4.2×10^{-3} A for disk electrodes and 7.2×10^{-7} A for microelectrodes. The current value of the disk electrode is approximately 6,000 times larger than that of the microelectrode. The potential drop of the disk electrode is significantly larger than that of the microelectrode because the magnitude of the potential drop due to the solution resistance increases in proportion to the current value. In addition, since the magnitude of the

potential drop due to solution resistance varies proportionally with the current value, the change in current value due to the potential sweep also changes the magnitude of the potential drop and the shape of the voltammogram. For measurements using a Pt-micro electrode as shown in Fig. 3-1, an exponential current change specific to the electrode reaction system was observed in a small region of the current value. In contrast, the voltammogram obtained by measuring the Pt-flag electrode exhibits a linear ohmic waveform. This indicates that microelectrodes have significant advantages in analyzing electrode reactions of $DMSO_2$–$AlCl_3$ electrolyte solutions.

For a reversible reaction system in an aqueous solution, the cyclic voltammograms measured using a microelectrode is known to exhibit a sigmoidal waveform saturated with a diffusion-limiting current [6]. However, the waveform of the reduction current shown in Figs. 3-1, 3-2, and 3-11 does not have much saturated current; rather, it has a distinct peak. A sigmoidal diffusion saturation current is observed when the electrode diameter is sufficiently smaller than the thickness of the diffusion layer determined by the diffusion coefficient. When the diffusion coefficient becomes small, this condition is not satisfied, and it exhibits a peak waveform, similar to a typical cyclic voltammogram in a typical disk electrode. According to the simulation by Aoki et al., the cyclic voltammogram becomes a sigmoidal saturation current curve without a peak only when Eq. 3-3 is satisfied [6]:

$$\left(\frac{nFa^2v}{RTD}\right)^{\frac{1}{2}} < 1.0 \tag{3-3}$$

where n is the valence of the reaction species, F is the Faraday constant, a is the electrode radius, v is the sweep speed, R is the gas constant, T is the temperature, and D is the diffusion coefficient of the reactive species. When measured at 50 mV s^{-1} using a microelectrode with a diameter of 20 μm, the conditions of Eq. 3-3 are satisfied if the diffusion coefficient D is 4.66×10^{-10} m^2 s^{-1} or greater. Conversely, for lower diffusion coefficients, the waveform may exhibit a peak even if a microelectrode with a diameter of 20 μm is used. To confirm this, the

diffusion coefficient of Al^{3+} was calculated using the Stokes-Einstein equation. Using the basic composition electrolyte viscosity of 39.4 mPa s from Table 3-1c and the ion radius of Al^{3+} (0.054 nm [7]), the diffusion coefficient of Al^{3+} is 1.28×10^{-10} m^2 s^{-1}. This value does not satisfy the conditions of Eq. 3-3. Furthermore, since Al^{3+} is coordinated with $DMSO_2$, the Stokes radius of $Al(DMSO_2)_3^{3+}$ is expected to be larger and the diffusion coefficient of $Al(DMSO_2)_3^{3+}$ is expected to be smaller. Therefore, when using a microelectrode with a diameter of 20 μm, the waveform may exhibit a peak rather than a sigmoidal waveform.

As shown in Fig. 3-6b, for the voltammogram corresponding to an NH_4^+ concentration of 0.20 mol L^{-1}, the reduction current exceeds the peak current value shown in Figs. 3-1 and 3-2. Table 3-1c shows that the viscosity of an electrolyte with an NH_4^+ concentration of 0.20 mol L^{-1} is reduced to approximately 64% of that of the basic composition electrolyte, and the diffusion coefficient is expected to be approximately 1.6 times that of the basic composition electrolyte according to the Stokes-Einstein equation. Under such conditions, since the current peak of the cyclic voltammetry of the reversible process is proportional to the 1/2 power of the diffusion coefficient, the increase in peak current due to the viscosity decrease is expected to be approximately 25%. Furthermore, the dissociation equilibrium in the electrolyte changes following the addition of NH_4Cl as shown in Table 3-1c, and the $Al(DMSO_2)_3^{3+}$ concentration is reduced by approximately 5%. The increase in the diffusion-controlled current expected from these changes is at most 1.2-fold, and the large reduction current seen in Figs. 3-6b–3-6d contradicts the assumption that the reduction peak current in Fig. 3-2 is diffusion-controlled. As such, the reduction current peaks seen in Figs. 3-1 and 3-2 are not caused by the effect of potential sweep conditions and diffusion; rather, the surface reaction may be rate-determining due to the action of a potential-dependent reaction inhibitor. In the case of reversible diffusion-controlled reduction reactions, cyclic voltammetry theory cannot explain the cathodic peak current observed in the forward sweep; however, considering the potential-dependent surface rate-determining reaction system, it is possible to explain the phenomenon by which the reduction current peak is observed even during sweeping in the positive direction.

3.4.2. *Cathodic deposition of Al*

In the $DMSO_2$–$AlCl_3$ electrolyte without additives shown in Fig. 3-2, the reduction current increased under potential levels exceeding −0.5 V. This current is the Al electrodeposition current. During the positive sweep, an oxidation current peak due to the anodic dissolution of Al is observed on the positive side of 0.0 V. The fact that the Al electrodeposition current does not flow down to −0.5 V indicates that the overpotential of the Al electrodeposition reaction to the Pt electrode surface is large. Conversely, when sweeping in the positive direction after the Al deposition, a reduction in the electrodeposition current corresponding to the potential was observed even in the range of −0.4 V–0.0 V because the overvoltage for the Al deposition on Al is smaller than that on Pt. However, in the range of −0.4 V–−0.8 V, the deposition current flows during the negative direction sweep, but it is larger during the positive direction sweep after reversal than during the negative direction sweep. This is due to a typical nucleation-controlled deposition mechanism, in which the current increases with the time from the start of deposition rather than with the potential. The reduction peak in the positive direction sweep shown in Fig. 3-8 is also based on the nucleation mechanism.

In the negative direction sweep, the reduction current increases from around −0.5 V, then decreases after a peak at around −0.8 V. This peak is not generated from the diffusion process and potential sweep as discussed in the preceding paragraph; instead, the author consider that it is the result of the surface reaction rate, which is dependent on the potential. That is, when the potential becomes more negative than −0.8 V, a change occurs on the electrode surface that suppresses the electrodeposition reaction of Al. As shown in Fig. 3, the number of reduced Coulombs not involved in Al electrodeposition increases when the potential is swept to the negative side from −0.9 V. This indicates that a side reaction that suppresses the Al electrodeposition reaction occurs under these conditions. $DMSO_2$ does not show reductive decomposition at least until −1.8 V (Fig. 3-5). It has a sufficiently wide potential window against the Al electrodeposition reaction. The same kind of results appeared in the reports of Legrand [8]. However, some $DMSO_2$ is present as a solvating form with Al^{3+}. Although the

nature of the side reaction is unclear, it may involve the reductive decomposition of $DMSO_2$ in solvating with Al^{3+}. In the positive directional sweep voltammogram, the reduction current in the range of −0.8 V–−1.2 V is the same trajectory as the negative directional sweep, indicating that potential-dependent inhibition of the reaction occurs on the negative side than −0.8 V, rather than the effect of nucleation-controlled deposition mechanism. Thus, when the basic composition electrolyte without ammonium ions is polarized to more negative potential to obtain a large reduction current, a side reaction occurs, and impurities are likely mixed into the electrodeposited film due to this side reaction.

As shown in Fig. 3-2, the reduction current decreases and then increases at potentials more negative than −1.2 V because the side reaction accelerates. As described in Chapter 2, when performing the electroplating evaluation on a test piece, the basic composition electrolyte without ammonium salts, and burned plating develops at the four corners where current concentration occurs. This may occur because the polarization is increased in the high current density portion and because the plating is performed in the negative potential region where the Coulombic efficiency is low.

3.4.3. *Effects on the cathodic deposition of Al by NH_4Cl addition*

In contrast, the addition of NH_4Cl to the basic composition electrolyte significantly changes its reduction current waveform. As shown in Figs. 3-6a and 3-6b, even at an NH_4^+ concentration of 0.20 mol L^{-1}, the Al electrodeposition onset potential shifted significantly in the positive direction compared to the basic composition electrolyte, and the slope of the rise of the reduction current also increased and was large even during the positive sweep after reversal. Moreover, the reduction current value rose rapidly to 8 mA mm^{-2} or greater, exceeding the peak current value of the basic composition electrolyte (2 mA mm^{-2}). This potential is approximately −0.3 to −0.5 V and does not reach a peak at the potential on the negative side of −0.8 V, which is thought to cause the side reaction. As a result, it is expected that electrolytes with NH_4Cl can avoid contamination by impurities due to side reactions, even

at high current densities of several mA mm^{-2} or more. As reported in Chapter 2, the impurity concentration in the electrodeposited film obtained from an electrolyte with an NH_4^+ concentration of 0.20 mol L^{-1} was lower than that obtained from the basic composition electrolyte containing no NH_4Cl. Also, in the electrolyte with an NH_4^+ concentration of 0.20 mol L^{-1}, no burned plating occurred even in the four corners where the current concentration tends to occur. Although the detailed mechanisms for these differences are not clear, it is believed that the presence of NH_4Cl promoted Al electrodeposition at a potential more positive than −0.8 V, which contributed to the elimination of burned plating and the reduction of impurity concentrations in the film. Even the addition of a small amount of NH_4Cl significantly increases the reduction current, and the difference due to NH_4^+ concentration is small. This suggests that the roles of NH_4^+ on the Al electrodeposition reaction are not due to the conversion of the reaction species for Al deposition into compounds involving NH_4^+, but rather that the NH_4^+ adsorption on the electrode surface promotes the electron transfer of $Al(DMSO_2)_3^{3+}$.

3.4.4. *Effects on the cathodic deposition of Al by TMAC addition*

As shown in Figs. 3-11a–3-11d, when using the electrolyte with TMAC, the Al electrodeposition onset potential shifts significantly in the negative direction, contrary to that in the case of adding NH_4Cl. In addition, as shown in Fig. 3-11a, the current is suppressed compared to the basic composition electrolyte even for the more positive potential range from −0.8 V, which results in the inhibition of side reactions in the basic composition electrolyte. Higher TMA^+ concentrations result in stronger inhibition. This indicates that the presence of TMA^+ suppresses the Al deposition reaction on the Pt surface. Since TMA^+ has a larger molecular size than NH_4^+, TMA^+ adsorbed on the Pt electrode surface is considered to inhibit the reduction of $Al(DMSO_2)_3^{3+}$, contrary to the case of NH_4^+. As shown in Fig. 3-12a, in linear sweep voltammograms of the electrolyte with TMAC, regardless of TMA^+ concentration, the waveforms exhibit a reduction current peak at approximately −0.8 V during the positive direction sweep. This feature is similar to that observed in the basic composition electrolyte.

This indicates that, in addition to suppressing the Al deposition reaction by TMA^+, a potential-dependent side reaction suppresses the deposition reaction at potentials more negative than −0.8 V. As shown in Fig. 3-11b, the voltammogram of the electrolyte with TMA^+ concentrations of 0.92 mol L^{-1}, a higher current density than the basic composition electrolyte is obtained. This result reflects an increase in the $Al(DMSO_2)_3^{3+}$ diffusion coefficient resulting from the decreasing viscosity due to the addition of TMAC. In addition, the adsorption of TMA^+ and the inhibition of the precipitation reaction on the Al surface are weaker than those on the Pt surface. The potential of the current density of 4 mA mm^{-2} is approximately −0.6 V, remaining on the positive side of −0.8 V, and is thought to reflect the absence of potential-dependent side reactions. Therefore, it is expected that contamination of impurities due to side reactions is unlikely to occur. According to the results of analyzing impurities in an electrodeposited film in Chapter 2, a plating electrolyte containing a 0.1 molar ratio of TMAC to $DMSO_2$ (TMA^+ concentration of 0.92 mol L^{-1}) can produce a film with a lower impurity concentration than the basic composition electrolyte. This result corresponds to the polarization characteristics observed in this study.

Contrastingly, the TMA^+ concentration is higher (1.66 mol L^{-1} and 2.27 mol L^{-1}), indicating that the reduction current is strongly suppressed. This is because the effect of suppressing the reaction exceeds that of increasing the diffusion coefficient due to the decrease in viscosity. Avchukir has reported that tetrabutylammonium in an aqueous electrolyte inhibits the electrodeposition reaction of metals by adsorption on electrodes [9]. Furthermore, Sankara has reported that the concentration and alkyl chain length of quaternary ammonium ions inhibit electrodeposition reactions [10]. Based on these findings, TMAC can effectively inhibit the electrodeposition reaction of Al in $DMSO_2$ solvents. Therefore, when performing plating at the same current density as Chapter 2, it occurs in the potential region in which the side reaction occurs actively. As a result, it is the Coulombic efficiency is expected to decrease, and the resulting film will contain many impurities.

3.4.5. *Effects on Cathodic deposition of Al by NH_4Cl and TMAC combined addition*

As shown in Figs. 3-15a–3-15b, the voltammogram in the electrolyte containing both TMA^+ (0.90 mol L^{-1}) and NH_4^+ (0.16 mol L^{-1}) is almost the same as for the electrolyte with only 0.20 mol L^{-1} NH_4^+. The effect of TMAC coexistence is, thus, very small. The potential of the current density at −0.8 mA mm^{-2} is approximately −0.4 V, which is the same as that of the electrolyte containing only NH_4^+ 0.20 mol L^{-1}. It is expected that the concentration of impurities in the electrodeposited film is low. This agrees with the analytical results of the electrodeposited film obtained in an electrolyte with the same composition as Chapter 2.

3.4.6. *Reduction current before Al deposition*

In the voltammograms of the electrolyte with NH_4Cl shown in Figs. 3-7a and 3-7b, an increase in the reduction current is observed at potentials more positive than −0.4 V, which is more positive than the Al electrodeposition reaction. The reduction current in this potential region has two peaks around +0.5 V and +0.1 V and the reduction peak currents increase with increasing NH_4^+ concentration. Also, as shown in Fig. 3-8, when reversed at potentials more positive than that of Al electrodeposition, the oxidation current was not observed during the positive direction sweep. Therefore, the reduction currents observed at +0.5 V and +0.1 V are considered to be reduction reaction currents involving NH_4Cl, and are not related to Al electrodeposition. Berkh reported an aqueous solution system in which the reduction of NH_4Cl on Pt proceeds *via* adsorption on Pt electrodes of NH_4^0 [11]. If the $DMSO_2$-$AlCl_3$ electrolyte undergoes the same reaction processes as the aqueous solution, the reduction reactions at +0.5 V and +0.1 V are thought to be due to the adsorption of NH_4^0 and the generation of NH_4^+. The Coulombic efficiency of the reduction and oxidation currents measured on the electrolyte containing NH_4Cl decreases with increasing NH_4^+ concentration, as shown in Fig. 3-10. This is because the NH_4Cl reduction reaction proceeded together with the Al electrodeposition reaction. In contrast, when TMAC is added, as shown in Fig. 3-12a, there is no clear increase

in the reduction current in the region to the positive side of the rising potential of the Al deposition current, as observed in the case of NH_4Cl. As shown in Fig. 3-13, the Coulombic efficiency with TMAC also decreases with increasing TMA^+ concentration. This is thought to be due to a different mechanism, i.e., not the reduction of TMA^+. As noted above, the reduction current was greatly suppressed when TMAC was added at a high concentration. As a result, the electrodeposition potential for obtaining the same current density was shifted to more negative values. In the case of the basic composition electrolyte, shown in Fig. 3-4, the Coulombic efficiency decreased when the potential sweep range was expanded to the negative side. Similarly, when the TMA^+ concentration was increased, the deposition potential shifted to the negative side, and the ratio of the side reaction increased, leading to a decrease in Coulombic efficiency.

3.4.7. *Anodic behavior*

The first oxidation current observed to the positive side of 0.0 V is the anodic dissolution current of the deposited Al. Except for Al, there are no oxidizable species within the measured potential region in this electrolyte. Therefore, the oxidation current goes from peak to zero, when all Al on the electrode is completely eluted. In such cases, the formation of an oxidation current peak is due to the Al electrodeposition amount, it is unrelated to the dissolution characteristics. This is important when comparing the voltammograms of the oxidation current under different conditions. Considering Fig. 3-2, when the reversal potential at the negative side is −0.6 V or −0.7 V, the oxidation current reaches a peak and then rapidly decreases to zero. This behavior is attributed to the insufficient deposition amount on the electrode. Therefore, to discuss the behavior of the first peak, it is necessary to compare the voltammograms where the anode current continues to flow to a more positive potential (Fig. 3-2); that is, the reversal potential should be <−0.9 V. In voltammograms under this condition, the first anode peak is almost constant regardless of the reversal potential value. When the reversal potential is shifted to negative, the time of the electrodeposition reaction

increases, thereby increasing the Al electrodeposition amount. The first anode peak waveform is constant regardless of the amount of electrodeposition, indicating that there are factors other than the amount of electrodeposition that limits the peak current.

When reversed at the negative side of −1.1 V, the oxidation current decreases after a peak around +0.4 V and increases again to a second peak. The presence of this second current peak suggests the existence of another Al anodic dissolution reaction at a more positive potential, in addition to the Al dissolution reaction that occurs around 0.0 V. As the negative side sweep reversal potential is widened toward the negative side, the current reduction after the first peak is of greater magnitude, and the second peak potential shifts to the more positive side. It is not clear from this measurement alone whether this is due to the sweep to a more negative potential, or, to an increase in the amount of electrodeposition.

In the electrolyte with NH_4Cl shown in Fig. 3-6b, after the oxidation current decreases beyond the first peak, the oxidation current at approximately 1.0 mA mm^{-2} continues to flow up to +1.1 V with current oscillation. The current oscillation seen over the potential range of +0.4 to +1.1 V is a characteristic phenomenon only when NH_4Cl is added. In general, such current oscillations are considered to occur in the following cases: (1) when the adsorption and desorption of the electrode surface by the gas-generating reaction occurs continuously; and (2) when the formation and destruction of some insoluble species covering the electrode surface occur continuously. In this system, when all Al is dissolved and the Pt surface is exposed, no oxidation current is observed, and gas generation in the anodic dissolution reaction of Al does not occur. This allows us to speculate that this phenomenon is not due to the gas generation reaction, but due to the formation of some insoluble species in (2). In the presence of NH_4^+, the anodic dissolution reaction of Al is thought to be followed by unstable layer formation of some insoluble species involving NH_4^+. In Figs. 3-6c, 3-6d, and 3-6e, when the NH_4^+ concentration is high, the oxidation current attenuates to zero before the potential region in which current oscillation occurs due to the small amount of precipitation is observed.

When using a TMA^+ concentration of 0.92 mol L^{-1} as shown in Fig. 3-11b, the oxidation current gradually decreases to around +1.0 V after the first oxidation current peak,

following which no further current oscillation was observed; this is similar to the case of the basic composition electrolyte. This also suggests that the current oscillation of the anodic oxidation current is a phenomenon specific to the addition of NH_4Cl. The slope of the current increase toward the first oxidation current peak in the electrolyte with TMAC is steeper than that in the basic composition electrolyte. The peak current for the electrolyte with a TMA^+ concentration of 0.92 mol L^{-1} is approximately two times larger than that of the basic composition electrolyte. As shown in Table 3-1c, electrolytes with TMA^+ concentrations of 0.92 mol L^{-1} or greater have significantly lower viscosities. Therefore, the oxidation peak current value is considered to increase due to the high diffusion coefficient of the reactive species.

The oxidation current waveform of the electrolyte with both TMA^+ (0.89 mol L^{-1}) and NH_4^+ (0.16 mol L^{-1}) as shown in Fig. 3-15c is almost the same as that of the electrolyte with only 0.92 mol L^{-1} TMA^+. As noted above, the reduction current waveform is greatly affected by the addition or non-addition of NH_4Cl. In contrast, the oxidation current waveform greatly depends on the presence or absence of TMA^+. This is believed to correspond to the viscosity change of the electrolyte following the addition of TMAC. The electrolyte with TMA^+ 0.89 mol L^{-1} and NH_4^+ 0.16 mol L^{-1} has desirable properties as a electrolyte solution because it has a small deposition overvoltage on the reducing side and a large dissolution current on the oxidation side.

3.5. Summary of findings

In this chapter, cyclic voltammetry using a microelectrode was performed on a $DMSO_2$–$AlCl_3$ electrolyte (molar ratio 1:0.38) and with ammonium salts. The purpose of this chapter is to clarify the mechanisms by which ammonium salts influence the electrolyte, as identified in Chapter 2. The conclusions are as follows.

1. By using a microelectrode in the reaction analysis, it is possible to evaluate the electrode reaction behavior, which was difficult to evaluate with conventional flag electrodes.
2. In the $DMSO_2$–$AlCl_3$ plating electrolyte, a side reaction occurs at potentials more negative than −0.8 V *versus* Al-wire, i.e., suppressing the Al electrodeposition reaction. The Coulombic efficiency of Al electrodeposition is found to be greatly decreased in regions where the electrodeposition potential is more negative than −0.8 V.
3. NH_4Cl promotes the Al electrodeposition reaction. In electrolytes with NH_4Cl, a large reduction current flows at a small overvoltage, and Al electrodeposition is possible at potentials where side reactions do not occur; this was confirmed using an electrolyte with a basic composition. This is considered to contribute both to the improvement of the appearance of the electrolyte and the decrease of the number of impurities in the Al-electrodeposited film.
4. TMAC has the effect of suppressing the Al electrodeposition reaction. To obtain sufficient reduction currents in the electrolyte with TMAC, a larger overvoltage than that in the basic composition electrolyte is required. However, when both NH_4Cl and TMAC are added, the action of NH_4Cl appears to occur preferentially over that of TMAC, and plating with a low overvoltage become possible.
5. In the $DMSO_2$–$AlCl_3$ electrolyte with NH_4Cl, the Coulombic efficiency of Al electrodeposition decreases due to the reduction reaction of NH_4Cl. The cyclic voltammetry results demonstrate that the reduction of NH_4Cl was the cause of the decrease in Coulombic efficiency in the plating experiments with solutions containing

NH_4Cl reported in Chapter 2. Conversely, the Coulombic efficiency also decreased with the addition of TMAC. This is because, in the TMAC-containing electrolyte, the Al electrodeposition reaction proceeds at negative potentials where the side reaction also occurs.

6. The plating electrolyte containing both TMA^+ (0.89 mol L^{-1}) and NH_4^+ (0.16 mol L^{-1}) has desirable properties as a plating electrolyte, such as a small deposition overvoltage on the reductive deposition side and a large dissolution current in the oxidative dissolution side.

3.6. References

[1] H. Hoshi, A. Okamoto, and S. Ando, *Hitachi Metals Tech. Rev.*, **27**, 20 (2011).

[2] A. Okamoto, M. Morita, and N. Yoshimoto, *J. Surf. Finish. Soc. Jpn.*, **63**, 641 (2012).

[3] M. Miyake, H. Motonami, S. Shiomi and T. Hirato, *Surf. Coat. Technol.*, **206**, 4225 (2012).

[4] S. Kim, N. Matsunaga, K. Kuroda, and M. Okido, *J. Electrochem. Sci. Technol.*, **9**, 69 (2018).

[5] K. Aoki, H. Takeuchi, J. Chen, and T. Nishiumi, *Rev. Polarogr.*, **57**, 101 (2011).

[6] K. Aoki, *DENKI KAGAKU*, **56**, 608 (1988).

[7] M. C. Simoes, K. J. Hughes, D. B. Ingham, L. Ma, and M. Pourkashanian, *Inorg. Chem.*, **56**, 7566 (2017).

[8] L. Legrand, A. Tranchant, and R. Messina, *Electrochim. Acta*, **39**, 1427 (1994).

[9] K. Avchukir, N. N. Yessaly, B. D. Burkitbayeva, *Eurasian Chem.-Technol. J.*, **21**, 157, (2019).

[10] T. S. N. Sankara Narayanan, *Met. Finish.*, **97**, 94, (1999).

[11] O. Berkh, Y. Shacham-Diamand, and E. Gileadi, *J. Electrochem. Soc.*, **155**, F223 (2008).

Chapter 4. Chronopotentiometric Analysis of the Anodic Dissolution Process in Dimethyl Sulfone–Aluminum Chloride Electrolyte Solution

4.1. Introduction

To save energy in the Al electroplating process, not only the electrodeposition reaction on the cathode but also the rapid dissolution of the anodic metal is a key factor. In this chapter, chronopotentiometric measurements were performed in $DMSO_2$–$AlCl_3$ electrolyte solution using Pt disk electrodes to understand the factors affecting the anodic dissolution process of Al in $DMSO_2$–$AlCl_3$ electrolyte. In addition, the effects of NH_4Cl and TMAC on the anodic dissolution reaction were investigated. Cyclic voltammetry using microelectrodes is difficult to interpret because of the complexity of the resulting voltammograms. In chronopotentiometry, the current value during measurement is constant, even when the solution resistance is high, the effect of the iR drop due to the solution resistance during measurement is constant. Further, the results of chronopotentiometry are easier to interpret than those of cyclic voltammetry, and accurate measurement results can be obtained even by using a Pt-disk electrode as the working electrode.

4.2. Experimental

4.2.1. Preparation of the electrolyte solution

To prepare the electrolyte solution, 20.00 g of $DMSO_2$ (Bergstrom Nutrition, purity > 99.0%) and 10.77 g of $AlCl_3$ (KANTO CHEMICAL CO., INC., purity > 98.0%), at a mixing molar ratio of 1:0.38, were placed in a 60 mL glass cell and covered. N_2 gas (purity > 99.99%) was constantly flowed into the glass cell at a rate of 0.1 L min^{-1}. The cell was heated in an oil

bath above 110 °C to completely dissolve each reagent. Then, uniform stirring was performed using a magnetic stirrer, and the resulting mixture was used as a basic electrolyte solution. Depending on the purpose of the experiment, NH_4Cl (KANTO CHEMICAL CO., INC., purity > 98.0%) and TMAC (KANTO CHEMICAL CO., INC., purity > 99.5%) were added to the electrolyte solution. The amount of NH_4Cl and TMAC added ranged from 0.00–0.10 mol per 1 mol of $DMSO_2$, and the molar concentrations of NH_4^+ and TMA^+ were adjusted to a range of 0.20–1.00 mol L^{-1}. Before performing the experiments, the electrolyte solution was bubbled with N_2 gas for 0.5 h, and N_2 gas was constantly flowed during the experiment.

4.2.2. Molar concentration of species in the electrolyte

As shown in Eq. 4-1, Al is present in $DMSO_2$–$AlCl_3$ electrolyte solution as $Al(DMSO_2)_3^{3+}$ and $AlCl_4^-$ [3]. In the cathode, $Al(DMSO_2)_3^{3+}$ is reduced to Al (Eq. 4-2). When Al is used as the anode, Al dissolves to form $Al(DMSO_2)_3^{3+}$ according to Eq. 4-3. Therefore, the $Al(DMSO_2)_3^{3+}$ concentration in the electrolyte solution is maintained at a constant value during Al electrodeposition.

$$4AlCl_3 + 3DMSO_2 \rightleftharpoons Al(DMSO_2)_3^{3+} + 3AlCl_4^- \quad (4\text{-}1)$$

$$Al(DMSO_2)_3^{3+} + 3e^- \rightleftharpoons Al + 3DMSO_2 \quad (4\text{-}2)$$

$$Al + 3DMSO_2 \rightleftharpoons Al(DMSO_2)_3^{3+} + 3e^- \quad (4\text{-}3)$$

As described in chapter 2, the addition of either NH_4Cl or TMAC causes a change in the volume and the ionic equilibrium of the electrolyte. In particular, the ionic equilibrium in the electrolyte solution changes when adding *m* mol of the ammonium salt according to Eq. 4-4, where R is H or CH_3.

$$Al(DMSO_2)_3^{3+} + 3AlCl_4^- + mNR_4Cl$$

$$\rightleftharpoons (1 - \frac{m}{4})\, Al(DMSO_2)_3^{3+} + (3 + \frac{m}{4})\, AlCl_4^- + mNR_4^+ + \frac{3m}{4}DMSO_2 \quad (4\text{-}4)$$

Table 4-1a and 4-1b shows the volume change, and the ionic equilibrium change for the electrolyte solution with various preparation amount of NH_4Cl or TMAC. Table 4-2a and 4-2b shows the molar concentrations of NH_4Cl or TMAC, and the viscosity of the electrolyte solution at different NH_4^+ or TMA^+ concentrations, at 90 °C. The molar concentration was calculated considering the change in the electrolyte volume and the ionic equilibrium according to Eq. 4-4. NH_4Cl and TMAC were assumed to be completely dissociated into NH_4^+ and TMA^+ cations, respectively. The volume of the electrolyte solution was measured using a graduated cylinder with a volume of 0.1 L.

Table 4-1a. Amount of preparation, volume change, and ionic equilibrium change of the electrolyte solution with NH_4Cl.

Amount of preparation/mol (Molar ratio)			Volume /mL	Ionic equilibrium/mol (Molar ratio)			
$DMSO_2$	$AlCl_3$	NH_4Cl	(change ratio)	$DMSO_2$	$Al(DMSO_2)_3^{3+}$	$AlCl_4^-$	NH_4^+
0.531	0.202	0.000	51.67	0.380	0.051	0.151	0.000
(1.000)	(0.380)	(0.000)	(1.000)	(0.715)	(0.095)	(0.285)	(0.000)
0.531	0.202	0.011	51.85	0.388	0.048	0.154	0.011
(1.000)	(0.380)	(0.020)	(1.004)	(0.730)	(0.090)	(0.290)	(0.020)
0.531	0.202	0.027	52.94	0.400	0.044	0.158	0.027
(1.000)	(0.380)	(0.050)	(1.025)	(0.753)	(0.083)	(0.297)	(0.050)
0.531	0.202	0.037	53.73	0.408	0.041	0.161	0.037
(1.000)	(0.380)	(0.070)	(1.040)	(0.768)	(0.078)	(0.302)	(0.070)
0.531	0.202	0.053	54.26	0.420	0.037	0.165	0.053
(1.000)	(0.380)	(0.100)	(1.050)	(0.790)	(0.070)	(0.310)	(0.100)

Table 4-1b. Amount of preparation, volume change, and ionic equilibrium change of the electrolyte solution with tetramethylammonium chloride (TMAC).

Amount of preparation/mol (Molar ratio)			Volume /mL (change ratio)	Ionic equilibrium/mol (Molar ratio)			
$DMSO_2$	$AlCl_3$	TMAC		$DMSO_2$	$Al(DMSO_2)_3^{3+}$	$AlCl_4^-$	TMA^+
0.531	0.202	0.000	51.67	0.380	0.051	0.151	0.000
(1.000)	(0.380)	(0.000)	(1.000)	(0.715)	(0.095)	(0.285)	(0.000)
0.531	0.202	0.011	52.80	0.388	0.048	0.154	0.011
(1.000)	(0.380)	(0.020)	(1.022)	(0.730)	(0.090)	(0.290)	(0.020)
0.531	0.202	0.027	54.66	0.400	0.044	0.158	0.027
(1.000)	(0.380)	(0.050)	(1.058)	(0.753)	(0.083)	(0.297)	(0.050)
0.531	0.202	0.037	55.89	0.408	0.041	0.161	0.037
(1.000)	(0.380)	(0.070)	(1.082)	(0.768)	(0.078)	(0.302)	(0.070)
0.531	0.202	0.053	57.53	0.420	0.037	0.165	0.053
(1.000)	(0.380)	(0.100)	(1.082)	(0.790)	(0.070)	(0.310)	(0.100)

Table 4-2a. Molar concentration of species and viscosity of the electrolyte solution upon addition of NH_4Cl.

Electrolyte Composition	Molar concentration/mol L^{-1}				Viscosity /mPa s
	$DMSO_2$	$Al(DMSO_2)_3^{3+}$	$AlCl_4^-$	NH_4^+	
A	7.351	0.977	2.930	0.000	48.9
B	7.479	0.922	2.970	0.205	36.6
C	7.551	0.828	2.985	0.502	29.0
D	7.588	0.767	2.990	0.692	22.0
E	7.734	0.685	3.034	0.979	20.2

Table 4-2b. Molar concentration of species and viscosity of the electrolyte solution upon addition of tetramethylammonium chloride (TMAC).

Electrolyte Composition	Molar concentration/mol L^{-1}				Viscosity /mPa s
	$DMSO_2$	$Al(DMSO_2)_3^{3+}$	$AlCl_4^-$	TMA^+	
F	7.345	0.905	2.917	0.201	36.9
G	7.313	0.802	2.897	0.486	19.0
H	7.295	0.737	2.875	0.665	16.5
I	7.295	0.646	2.862	0.923	14.7

4.2.3. Viscosity measurements

The viscosity of the electrolyte solution was measured using an electromagnetic spinning–type viscometer (EMS-1000S, Kyoto Electronics Manufacturing) and a spherical Al probe of 2 mm diameter. The target electrolyte solution was placed in a glass tube, heated to 90 °C, and measured at a probe rotation rate of 1000 rpm. The given viscosity value is an average value of a plurality of measurements. To suppress measurement variation due to corrosion of the probe, the probe was immersed in boiling pure water for 1 h to oxidize the probe surface before to the measurements.

4.2.4. Electrochemical measurements

Chronopotentiometry measurements were performed using an electrochemical analyzer (BAS, ALS-660A) and a three-electrode system comprising Pt disk electrodes with a diameter of 1.6 mm as the working electrode (WE), an Al wire as the reference electrode (RE), and an Al coil as the counter electrode (CE). First, a constant cathodic current was applied, and Al was electrodeposited on the Pt disk electrode. After stopping the cathodic electrodeposition, an anodic current was passed through at a constant current density, and the potential change was observed. To avoid the influence of the change in concentration near the electrode after the cathodic electrodeposition, the electrolyte solution was stirred for 30 s after cathodic electrodeposition and then allowed to stand for 30 s before measurement. In this electrolyte solution, the equilibrium potential of Al and Al^{3+} is the reference, so the potential axis of the chronopotentiogram was denoted vs. Al-wire. The temperature of the electrolyte solution was adjusted to 90 °C using an oil bath.

To compare the potential of the anodic dissolution reaction with the literature values, the redox reaction of ferrocene was used as an internal potential standard. Linear sweep voltammetry (LSV) was performed using a $DMSO_2$–$AlCl_3$ electrolyte solution containing 5 mmol of ferrocene. The electrodes used for the measurement were glass-encapsulated Pt disk electrodes as WE, a double-junction Ag|$AgNO_3$ electrode as RE, and an Al coil as CE. As the

internal solution of RE, a propylene carbonate solution mixed with 10 mM $AgNO_3$ and 10 mM tetrabutylammonium tetrafluoroborate was used. The sweep speed was 50 mV s^{-1}.

The Coulombic efficiency (Q_{eff}, %) was calculated using Eq. 4-5, where Q_o is the oxidation Coulomb number. This is given by the accumulated Coulomb number from just before the beginning of the anodic dissolution to a potential higher than +3.0 V. Q_r is the reduction Coulomb number, which corresponds to the accumulated Coulomb number from the beginning to the end of the cathodic electrodeposition.

$$Q_{\text{eff}} = \frac{Q_O}{Q_r} \times 100 \tag{4-5}$$

4.3. Results and Discussion

4.3.1. Anodic dissolution chronopotentiometry in $DMSO_2$-$AlCl_3$ electrolyte solution

Figure 4-1 shows the chronopotentiograms of the cathodic electrodeposition and anodic dissolution of Al in a $DMSO_2$–$AlCl_3$ electrolyte solution. In this measurement, the anodic dissolution was immediately performed after the cathodic electrodeposition. The horizontal axis of the potentiograms shows the elapsed time since the beginning of cathodic electrodeposition. The cathodic electrodeposition time in Figs. 4-1a and 4-1b was 20 s and 300 s, respectively. The current density of the cathodic electrodeposition and anodic dissolution was 0.1 mA mm^{-2}. In Fig. 4-1a, the anodic dissolution potential was +0.2 V until shifting to a potential higher than +3.0 V at an electrolysis time of 17 s. As shown in Fig. 4-1b, the anodic dissolution exhibited a two-wave behavior for a cathodic electrodeposition of 300 s. The anodic dissolution potential increased from +0.2 to 1.5 V at 170 s and then above +3.0 V at 280 s.

Generally, when metals electrodeposited on a Pt electrode dissolve under a constant current condition, the anodic dissolution potential maintains a constant value while the metal

electrodeposition proceeds. When the metal electrodeposition is completely exhausted, the anodic dissolution potential shifts to a positive potential and the anodic dissolution exhibits a one-wave behavior. The one-wave behavior observed in Fig. 4-1a for the anodic dissolution corresponds to the anodic dissolution reaction of Al electrodeposited on the Pt electrode according to Eq. 4-3. The shift to a higher potential than +3.0 V indicates that the electrodeposited Al on the Pt electrode was completely dissolved at this point. In contrast, the two-wave behavior for the anodic dissolution observed in Fig. 4-1b is unlikely to depend on the change in concentration of the reaction species near the electrode and suggests that the anodic dissolution of Al proceeds in a different manner from the normal anodic dissolution reaction.

Figures 4-2a–4-2c shows the chronopotentiograms of the anodic dissolution in $DMSO_2$–$AlCl_3$ electrolyte solution as a function of the cathodic electrodeposition time and the anodic current density. The current density of the cathodic electrodeposition was 0.4 mA mm^{-2}, and the current density of the anodic dissolution was 0.1–0.4 mA mm^{-2}. The horizontal axis shows the elapsed time from the start of the anodic dissolution. In this experiment, to avoid the influence of the composition change near the electrode during electrodeposition, the electrolyte solution was stirred for 30 s followed by static for 30 s when transiting from cathodic electrodeposition to anodic dissolution. At any anodic current density, a one-wave behavior was observed when the cathodic electrodeposition time was short, whereas a two-wave behavior occurred for long cathodic electrodeposition times. Further, the higher the anode current density, the faster the shift to the second stage potential, and the time to shift to the second stage converges to a constant value. Thus, it can be concluded that the shift to the anodic dissolution potential of the second-stage occurs at a anodic dissolution time of about 80 s for an anodic current density of 0.1 mA mm^{-2}, about 20 s for 0.2 mA mm^{-2}, and about 5 s for 0.4 mA mm^{-2}. The time to shift to the second-stage reaction is proportional to the power of −2 of the anodic current density. This indicates that the transition time to the second stage is not simply determined by the anodic charge density, but follows another mechanism. This point will be described later in the discussion of Fig. 4-9.

As shown in Fig. 4-2, the anodic dissolution reaction in the first stage of this measurement starts at higher potential when the anodic current density is high. Since the electrical conductivity of the electrolyte solution is low, superposition of the voltage due to the solution resistance occurs in this measurement using the disk electrode. In the linear sweep voltammetry with potential control, the potential drop between the working and reference electrodes due to the solution resistance vary when the current value change, causing variations in the actual electrode potential. Therefore, the voltammogram becomes distorted and difficult to analyze. On the other hands, in the chronopotentiometry measured at a constant current, if the electrical conductivity of the solution does not change significantly during the measurement, the potential drop due to the solution resistance is constant. Therefore, the distortion of the wave is small, and accordingly the effect on analysis characteristics such as the elapsed time to the potential change is small. As shown in Eqs. 4-2 and 4-3, the electrodeposition and dissolution reaction in $DMSO_2$–$AlCl_3$ electrolyte solution involves $Al(DMSO_2)_3^{3+}$. The cyclic voltammetry measurements using the microelectrode in chapter 3, Al electrodeposition and dissolution occur at 0.0 V vs. Al-wire. The anodic dissolution reaction corresponding to the first wave observed in Figs. 4-1 and 4-2 is the anodic dissolution reaction described by Eq. 4-3. Meanwhile, the anodic dissolution reaction of the second wave occurs at a potential about 1.0 V higher than that of the first wave, which suggests the occurrence of different reactions in the two stages of the dissolution reaction.

In the chronopotentiometry measurements shown in Fig. 4-2, since the current density of the cathodic electrodeposition was set to the same value, the cathodic electrodeposition conditions are the same even under different anodic dissolution currents for the same cathodic electrodeposition time. However, for example, when comparing the anodic dissolution current density of 0.1 mA mm^{-2} in Fig. 4-2a and 0.2 mA mm^{-2} in Fig. 4-2b for a cathodic electrodeposition time of 15 s, a single-wave is observed in the former case and two-waves in the latter. This indicates that the cause for the two-wave chronopotentiograms is the dissolution process rather than the cathodic electrodeposition process. The cathodic electrical charge density at an electrodeposition time of 15 s was 6 mC mm^{-2}, whereas the anodic electrical

charge density of the anodic currents at the end of the second-stage in Figs. 4-2a and 4-2b showed similar values of 5.5 and 5.8 mC mm^{-2}, respectively. This suggests that the anodic current at the end of the second-stage corresponds to the dissolution of electrodeposited Al and that both the first- and the second-stage reactions involve Al dissolution via three-electron-transfer. To analyze this in more detail, the Coulombic efficiency was calculated from the ratio of the electrodeposition Coulomb amount and the dissolved Coulomb amount obtained from Fig. 4-2. Figure 4-3 shows the plots of the Coulombic efficiency with respect to the cathodic electric charge density. The solid-symbol plots represent the single-wave anodic dissolution, and the open-symbol plots correspond to the two-wave anodic dissolution. If the second-stage reaction is a dissolution reaction with one- or two-electron-transfer, the Coulombic efficiency of the second-stage should be 33% or 67%, and the overall Coulombic efficiency should decrease. The Coulombic efficiency was 90% or more regardless of the anodic current density and the anodic dissolution wave behavior. This result confirms that both the first- and the second-stage reactions involve Al dissolution via three-electron transfer. The values of the Coulombic efficiency calculated via chronopotentiometry matched both those obtained via cyclic voltammetry and using the weight of the electrodeposition film as shown in Chapter 2 and 3. From these results, it can be concluded that the reaction at the second-stage potential is an Al dissolution reaction involving a three-electron-transfer different from that described by Eq. 4-3.

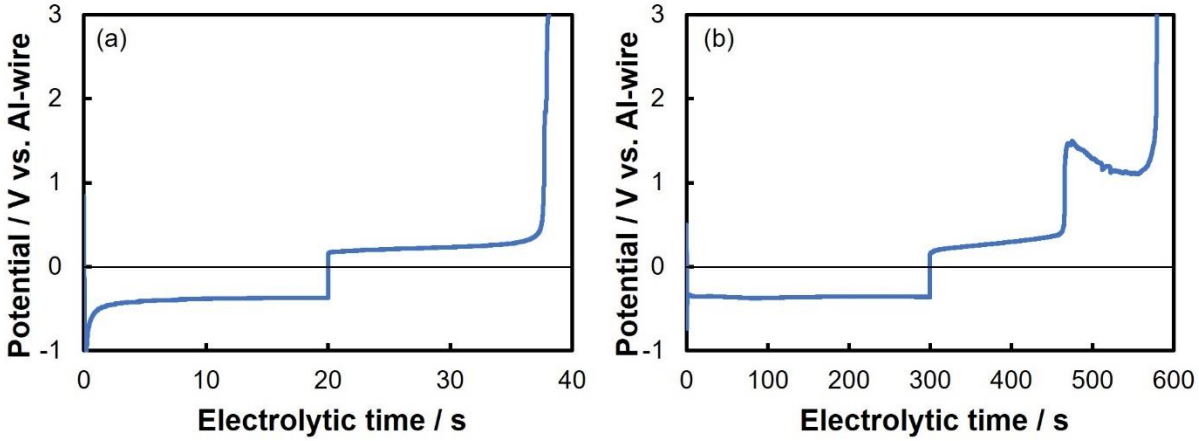

Figure 4-1. Chronopotentiograms of the cathodic electrodeposition and anodic dissolution in $DMSO_2$–$AlCl_3$ electrolyte solution measured by changing the cathodic electrodeposition time. Cathodic electrodeposition and anodic dissolution current density, 0.1 mA mm^{-2}; cathodic electrodeposition time, (a) 20 s and (b) 300 s; temperature, 90 °C.

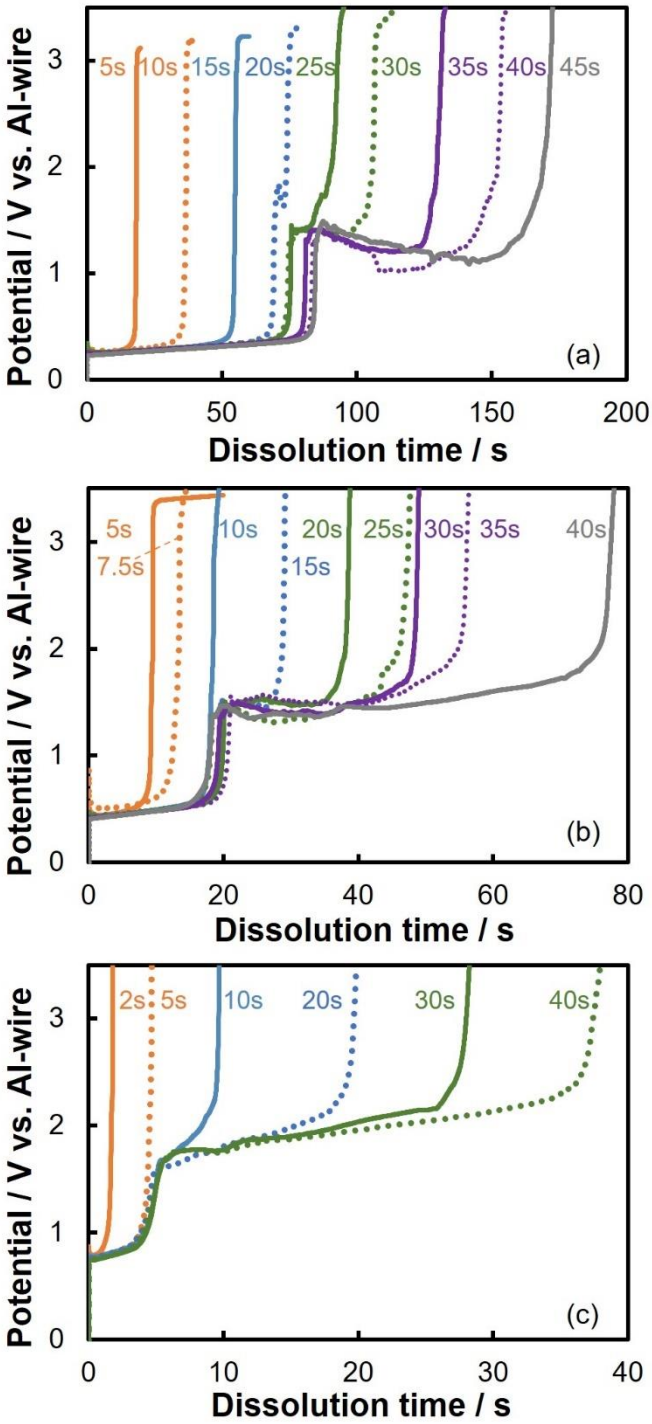

Figure 4-2. Chronopotentiograms of the anodic dissolution in $DMSO_2$–$AlCl_3$ electrolyte solution measured by changing the cathodic electrodeposition time and the anodic dissolution current density. Cathodic electrodeposition current density, 0.4 mA mm^{-2}; cathodic electrodeposition time, (a) 5–45 s, (b) 5–40 s, and (c) 2–40 s; anodic dissolution current density, (a) 0.1, (b) 0.2, and (c) 0.4 mA mm^{-2}; temperature, 90 °C.

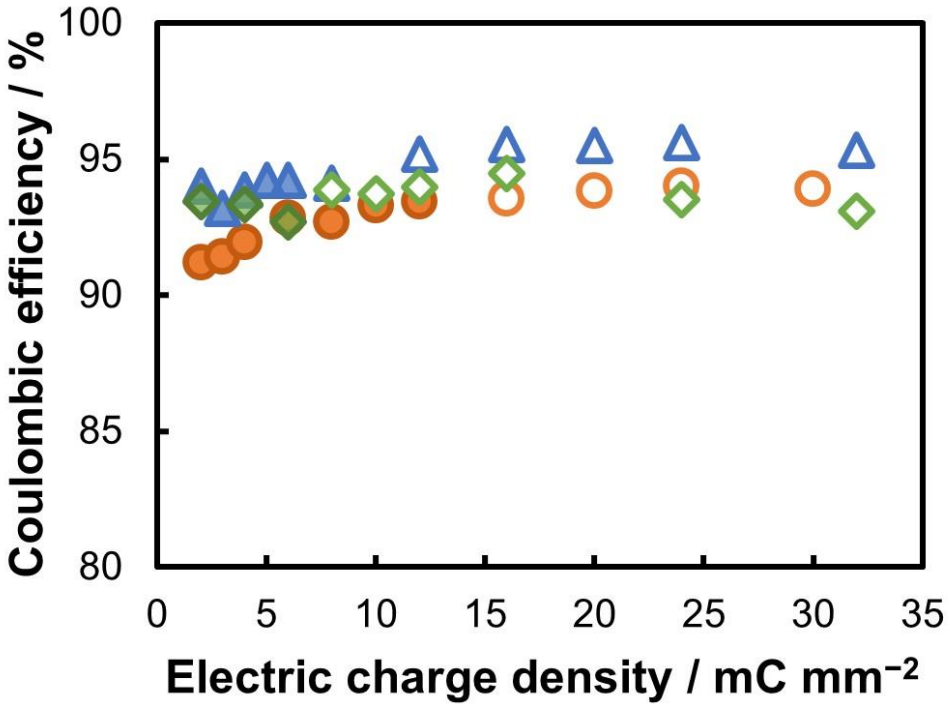

Figure 4-3. Coulombic efficiency calculated using chronopotentiograms in $DMSO_2$–$AlCl_3$ electrolyte solution. Solid-symbols, one-wave anodic dissolution; open-symbols, two-wave anodic dissolution; anodic current density, (orange circles) 0.1, (blue triangles) 0.2, and (green diamonds) 0.4 mA mm^{-2}; $DMSO_2$:$AlCl_3$ = 1:0.38 (mol); temperature, 90 °C.

4.3.2. Assignment of dissolution reactions in the second step

In ionic liquids and molten salts Al electrolyte solutions, another anodic reaction, which is also a three-electron-transfer reaction, proceeds to produce $Al_2Cl_7^-$ from $AlCl_4^-$ according to Eq. 4-6 [1]:

$$Al^0 + 7AlCl_4^- \rightleftharpoons 4Al_2Cl_7^- + 3e^-. \quad (4\text{-}6)$$

As shown on the right side of Eq. 4-1, because $AlCl_4^-$ is present in the $DMSO_2$–$AlCl_3$ electrolyte solution, the second-stage of the dissolution reaction could proceed according to Eq. 4-6. Normally, the reaction described by Eq. 4-6 is not observed because its redox potential is considerably more positive than that of Eq. 4-3. However, the value of the redox potential of Eq. 4-6 in $DMSO_2$ solvent is unknown. According to the literature edited by Ohno [5], the equilibrium potential of the reaction of Eq. 4-6 in various ionic liquids is about −0.3 V vs. the ferrocene|ferrocenium cation couple ($Fc|Fc^+$). To compare the reaction potentials of Eqs. 4-3 and 4-6, LSV measurements were performed for a $DMSO_2$–$AlCl_3$–ferrocene electrolyte using $Fc|Fc^+$ as the internal standard. Figure 4-4a shows the LSV curves obtained for $DMSO_2$–$AlCl_3$ and $DMSO_2$–$AlCl_3$–ferrocene electrolyte solutions. Figure 4-4b shows a magnified view of the vertical axis of Fig. 4-4a to clarify the reaction wave of ferrocene oxidation. When $Ag|AgNO_3$ was used as an RE, the potential of Al-wire of Eq. 4-3 was −1.6 V (vs. $Ag|AgNO_3$), and the potential of $Fc|Fc^+$ was −0.3 V (vs. $Ag|AgNO_3$). Therefore, a potential of Al-wire in Eq. 4-3 can be assigned −1.3 V (vs. $Fc|Fc^+$). This indicates that the electrode potential of Eq. 4-6 is +1.0 V vs Al-wire in $DMSO_2$–$AlCl_3$ electrolyte investigated here. The difference in basicity and temperature of the bath may affect the reaction potential. According to the Nernst formula shown in Eq. 4-7, the activity ratio of the reaction species α_o/α_r has logarithmic term, and the effect of temperature is compressed to 1/3 because Eq. 4-6 is a three-electron reaction. That is, the effect of the basicity and temperature of the bath on the reaction potential is expected to be small. According to these results, the reaction potential of Eq. 4-6 is about 1.0 V higher than

that of Eq. 4-3. This is approximately equivalent to the potential difference between the first and second stages of the anodic dissolution reaction observed in Fig. 4-1b and 4-2. Thus, the second-stage anodic dissolution reaction in $DMSO_2$–$AlCl_3$ electrolyte solution could proceed according to Eq. 4-6.

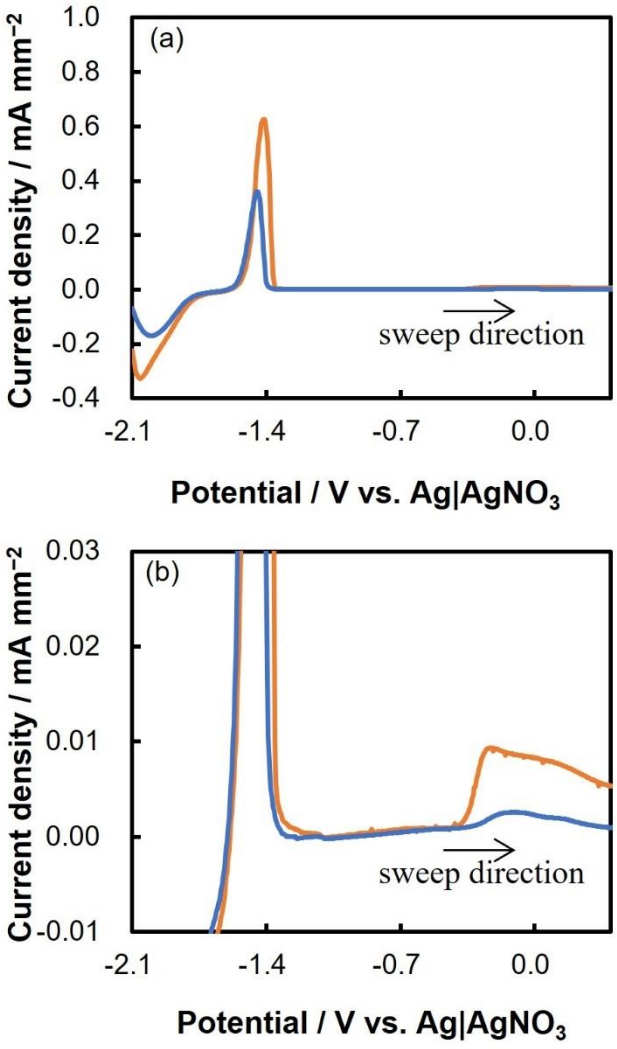

Figure 4-4. Linear sweep voltammograms measured in $DMSO_2$–$AlCl_3$–ferrocene electrolyte solution (a) and its magnified view (b). (Blue line) without ferrocene, (orange line) with 5 mM ferrocene; working electrode, ϕ20 μm Pt microelectrode; reference electrode, Ag|$AgNO_3$ in propylene carbonate; sweep rate, 50 mV s^{-1}; temperature, 90 °C.

4.3.3. Reverse chronopotentiometry in $DMSO_2$-$AlCl_3$ electrolyte solution

$Al_2Cl_7^-$ would be generated near the electrode during the second-stage anodic reaction. In ionic liquids and molten salts electrolyte, the Al electrodeposition reaction occurs from $Al_2Cl_7^-$ [1]. That is, when the current is reversed to cathodic electrodeposition during the second-stage anodic dissolution reaction, the cathodic electrodeposition reaction from $Al_2Cl_7^-$ should occur at a more positive potential than the cathodic electrodeposition reaction from $Al(DMSO_2)_3^{3+}$. To verify this, after performing the chronopotentiometry measurements of the anodic dissolution in $DMSO_2$–$AlCl_3$ electrolyte, reverse chronopotentiometry that reverted to the cathodic current was performed. First, Fig. 4-5 shows a chronopotentiogram of anodic dissolution obtained for a current density of cathodic electrodeposition and anodic dissolution of 0.2 mA mm^{-2} and an electrodeposition time of 120 s. The horizontal axis shows the elapsed time since the anodic dissolution started (t = 0). Under these conditions, the potential of cathodic electrodeposition was approximately −0.6 V, and the anodic dissolution followed a distinct two-wave behavior. Figure 4-6 shows the results of reverse chronopotentiometry. Next, the current was reversed from anodic dissolution to cathodic electrodeposition (a) during the first-stage dissolution reaction, (b) during the second-stage dissolution reaction, (c) just before the end of the second-stage dissolution reaction, and (d) after the completion of the second-stage dissolution reaction; furthermore, the potential change was recorded. The current reversal times were (a) 20, (b) 70, (c) 100, and (d) 120 s from the start of anodic dissolution. The current density of cathodic re-electrodeposition was 0.1 mA mm^{-2}. The horizontal axis of potentiograms shows the elapsed time from the start of anodic dissolution. In the case of (a), the potential after reverting to the cathodic current shifted to near −0.3 V, but in the case of (b) and (c), the potential temporarily stagnated near +0.15 V as shown by the black dashed line described in Fig. 4-6, and then shifted to a more negative potential and converged to near −0.3 V. In the case of (d), potential stagnation was observed near +2.0 V, but not near +0.15 V as in (b) and (c). Thereafter, the potential shifted to a slightly lower potential than in the case

of (a)–(c) and converged to near −0.6 V.

The cathodic electrodeposition potential varies with the cathodic current density. The potential converged to −0.3 V after reverting to the cathodic electrodeposition in Fig. 4-6 is considerably similar to the cathodic electrodeposition potential shown in Fig. 4-1. The cathodic electrodeposition reactions indicate that they are Al electrodeposition reactions described in Eq. 4-2. The reaction with a potential near +0.15 V observed in (b) and (c) is a reduction reaction of the product of the second-stage of the anodic dissolution reaction, which is a different cathode reaction from that of Eq. 4-2. As already discussed, if the second-stage anodic dissolution reaction proceeds according to Eq. 4-6, $Al_2Cl_7^-$ would be formed near the electrode during the anodic dissolution reaction. That is, the reaction near +0.15 V is a cathodic electrodeposition reaction from $Al_2Cl_7^-$, which is a reverse reaction to that of Eq. 4-6. Therefore, the potential stagnation at +0.15 V after reverting to the cathodic current supports that the second-stage anodic dissolution reaction is an anodic dissolution reaction as in Eq. 4-6. The reason for the shift of the re-electrodeposition potential to the more negative side than the potential of the second-stage of the dissolution reaction is the potential drop due to the superimposition of the solution resistance with the opposite polarity. The lack of potential stagnation at +0.15 V under the condition (d) can be attributed to the diffusion of the generated $Al_2Cl_7^-$ to the bulk after the completion of the anodic dissolution reaction.

Furthermore, after reversing the current from anodic dissolution to cathodic electrodeposition immediately after the end of the second-stage of the anodic dissolution reaction, double reverse chronopotentiometry was performed by reverting the current to anodic dissolution while the cathodic electrodeposition reaction proceeded at a potential of near +0.15 V. The results are shown in Fig. 4-7. The current density of the first cathodic electrodeposition and anodic dissolution was 0.2 mA mm^{-2}, and the current density of cathodic re-electrodeposition and anodic re-dissolution was 0.05 mA mm^{-2}. The cathodic electrodeposition time was 120 s, the reversal time to the cathodic current was 105 s from the start of anodic dissolution, and the reversal time to the anodic current was 115 s. The potential during cathodic re-electrodeposition stagnated near +0.15 V as in the results of Fig. 4-6. After

reverting to the anodic current, the potential stagnated near +1.5 V for about 10 s before shifting to a higher potential than +3.0 V. The stagnated potential near +1.5 V after reverting to the anodic current was almost identical to that of the second-stage of the anodic dissolution reaction. This result indicates that the reaction occurring at +0.15 V is the Al re-electrodeposition, which is supported by the potential at the re-dissolution time and the amount of charge.

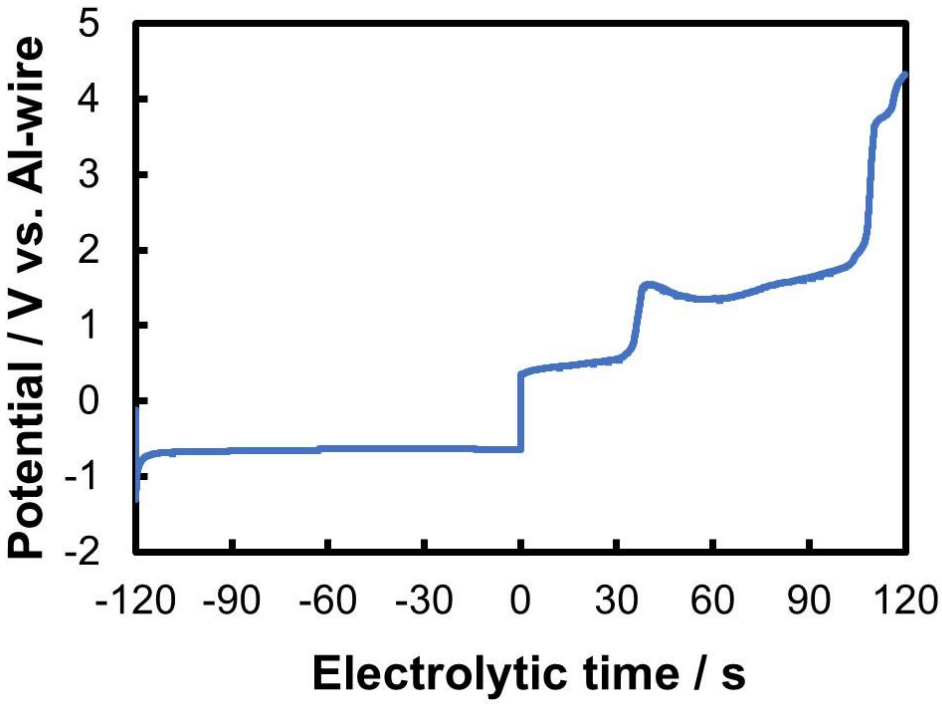

Figure 4-5. Chronopotentiogram of cathodic electrodeposition and anodic dissolution in $DMSO_2$–$AlCl_3$ electrolyte solution. Cathodic electrodeposition and anodic dissolution current density, 0.2 mA mm^{-2}; electrodeposition time, 120 s; temperature, 90 ℃.

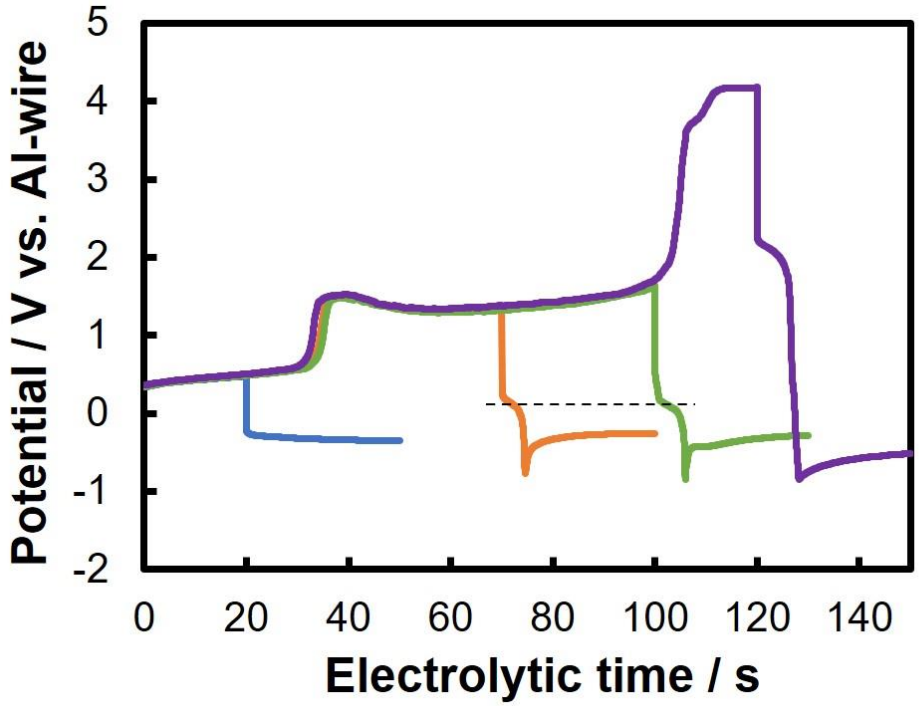

Figure 4-6. Chronopotentiograms of anodic dissolution and cathodic re-electrodeposition in $DMSO_2$–$AlCl_3$ electrolyte solution. Cathodic electrodeposition and anodic dissolution current density, 0.2 mA mm^{-2}; cathodic re-electrodeposition current density, 0.1 mA mm^{-2}; electrodeposition time, 120 s; current reversal time, (blue line) 20 s, (orange line) 70 s, (green line) 100 s, (violet line) 120 s; temperature, 90 °C.

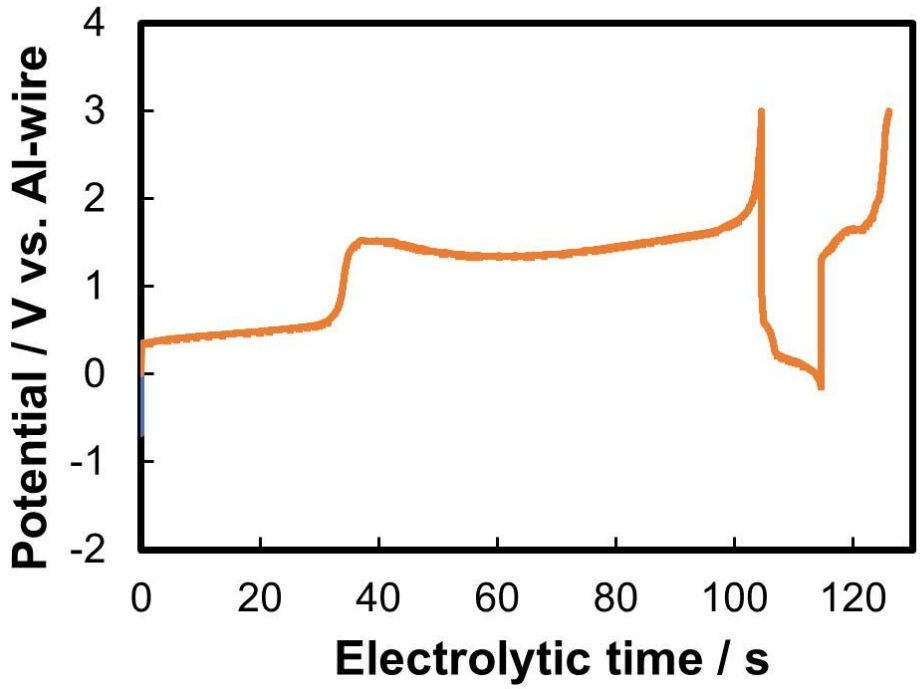

Figure 4-7. Double reverse chronopotentiogram in $DMSO_2$–$AlCl_3$ electrolyte solution. Current density of cathodic electrodeposition and anodic dissolution, 0.2 mA mm^{-2}; current density of cathodic re-electrodeposition and anodic re-dissolution, 0.05 mA mm^{-2}; electrodeposition time, 120 s; current reversal time, 105 s; second current reversal time, 115 s; temperature, 90 °C.

4.3.4. Factors in the transition to the second-stage anodic dissolution reaction

The reason for the transition from the first-stage to the second-stage during the anodic dissolution reaction in $DMSO_2$–$AlCl_3$ electrolyte solution is discussed. In conventional chronopotentiometry, the concentration ratio of the reductant and oxidant near the electrode changes due to the consumption of the reactants and the accumulation of the reaction product. The potential changes according to the Nernst formula are shown in Eq. 4-7:

$$E = E^0 + \frac{RT}{nF} ln \frac{\alpha_o}{\alpha_r}, \tag{4-7}$$

where E is the electrode potential, E_0 is the standard electrode potential, R is the gas constant, T is the absolute temperature, n is the number of electron-transfer, F is the Faraday constant, and α_o and α_r are the activity value of oxidants and reductants. The potential change based on Eq. 4-3, which is the first-stage dissolution reaction, can be calculated using Eq. 4-7. The activity value in the denominator of the logarithmic term is 1 because it is a dissolution reaction of electrodeposited metal. The activity of the oxidant α_o is the product of the activity coefficient and the concentration of the oxidant. The concentration of metal-ions near the electrode surface increases due to metal dissolution during the anodic dissolution reaction. Such concentration changes near the electrodes can affect the concentration and activity of the metal ions. As shown in Table 4-1, the concentration of $Al(DMSO_2)_3^{3+}$, which is the product of the anodic dissolution reaction, before the start of the dissolution is 0.977 mol L^{-1}. According to Eq. 4-3, three $DMSO_2$ molecules per Al atom are solvated in the dissolution reaction. As shown in Table 4-1, there is 7.351 mol L^{-1} of non-solvated $DMSO_2$ in the electrolyte solution before anodic dissolution begins. Even if all this $DMSO_2$ contributes to solvation, the increase in $Al(DMSO_2)_3^{3+}$ concentration due to anodic dissolution is only about 1/3 of that value, i.e., 2.450 mol L^{-1}. Since this electrolyte is a concentrated solution, the activity coefficient of the oxidant is less than 1. Therefore, assuming that an activity coefficient is 1, temperature is 90 °C,

and an electron-transfer number is 3, the potential change due to the concentration change was calculated to be about 30 mV using Eq. 4-7. This result cannot explain the potential change of about 1.0 V during the transition to the second-stage reaction, suggesting that the changes in $Al(DMSO_2)_3^{3+}$ concentration near the electrode is not the main cause for the large potential changes during the anodic dissolution reaction. As shown in Eq. 4-1, $DMSO_2$, $Al(DMSO_2)_3^{3+}$, and $AlCl_4^-$ are present in the $DMSO_2$–$AlCl_3$ electrolyte solution. If the amount of $DMSO_2$ near the electrode is not enough, the reaction of Eq. 4-3 does not occur, and Al^{3+} cannot be stably dissolved in the electrolyte solution. In this case, even if Al remains on the electrode, the potential increases and shifts to the value of the reaction of Eq. 4-6, which occurs at a more positive potential.

In Fig. 4-2, the time from the start of anodic dissolution to the shift to the second-stage is defined as the transition time τ_1, and the time from the start of anodic dissolution to the shift to a potential of +3.0 V is defined as the transition time τ_2. Figure 4-8 shows the results of plotting τ_1 and τ_2 as a function of the cathodic electric charge density, respectively. Even under the condition of the two-wave process, τ_2 increased monotonically with respect to the electrodeposition Coulomb amount. This indicates that the reaction occurring at the potential of the second-stage is an Al dissolution reaction of three-electron-transfer, similar to the anodic reaction of the first-stage. τ_1 converged to a constant value with an increase in the electrodeposition Coulomb amount, and remained at a lower value as the anodic current density is increased. This result confirmed that the transition to the second-stage anodic dissolution reaction is likely to occur under conditions of high anodic current density.

Furthermore, chronopotentiometry measurements for the anodic dissolution were performed by changing the anodic current density to determine the transition time τ_1. Figure 4-9 shows the result of plotting the $-1/2$ power of τ_1 with respect to the anodic current density. In general, the transition time for chronopotentiometry with a disk electrode in a redox system in solution can be expressed according to the Sand formula shown in Eq. 4-8 [6,7]:

$$i\tau^{\frac{1}{2}} = \frac{\pi^{\frac{1}{2}} nFAD^{\frac{1}{2}} C_b}{2}, \quad (4\text{-}8)$$

where i is the current value, τ is the transition time, n is the number of electron-transfer, F is the Faraday constant, A is the electrode area, D is the diffusion coefficient, and C_b is the concentration of bulk reactive species. In a normal redox reaction, the transition time is the time at which the electrode surface concentration of the reactant species that transfers electrons becomes zero. Equation 4-8 can still be used even if the cause of the potential shift is not the concentration change for the electron transfer reactant, but the depletion of $DMSO_2$ as a solvent molecule for solvation. The transition time to the second-stage when the anodic current density changes exhibits good linearity through the origin as shown in Fig. 4-9. This suggests that the transition to the second-stage anodic dissolution reaction is a diffusion-dominated process. Accordingly, the viscosity of the electrolyte solution would affect the anodic dissolution reaction.

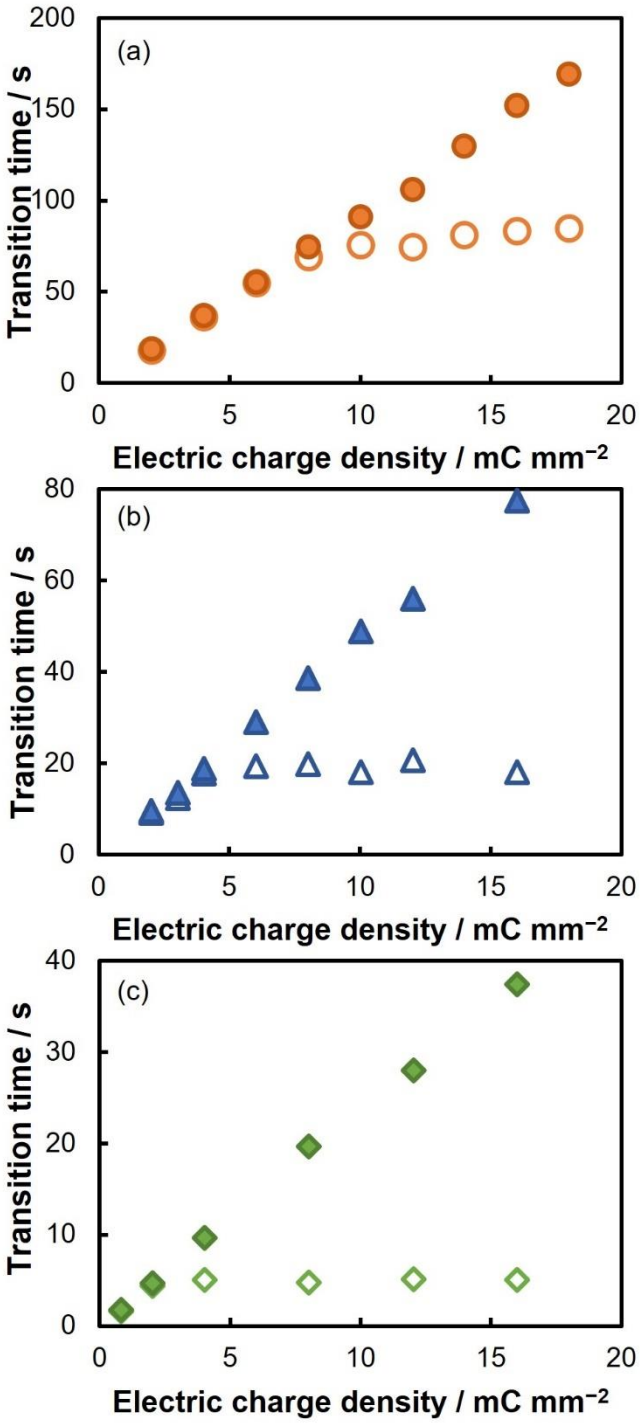

Figure 4-8. Relationship between electrodeposition Coulomb amount and transition time obtained from the chronopotentiograms of the anodic dissolution in $DMSO_2$–$AlCl_3$ electrolyte solution. Open symbols, transition time τ_1; solid symbols, transition time τ_2; cathodic electrodeposition current density, 0.4 mA mm^{-2}; anodic dissolution current density, (a) 0.1, (b) 0.2, and (c) 0.4 mA mm^{-2}; cathodic deposition time, (a) 20–300, (b) 10–160, and (c) 5–80 s; temperature, 90 °C.

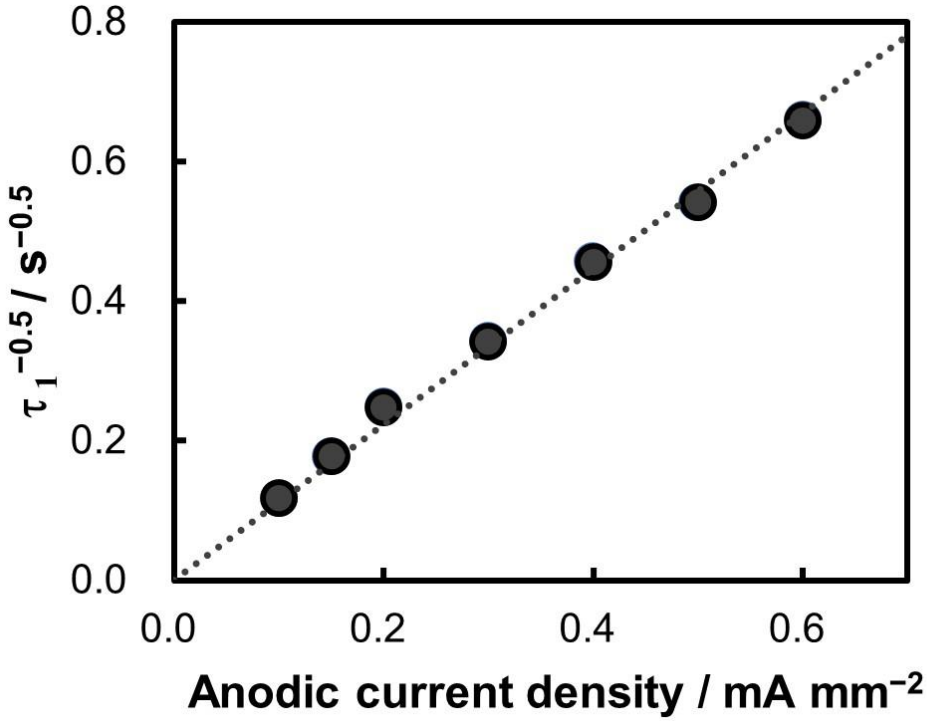

Figure 4-9. Relationship between anodic dissolution current density in $DMSO_2$–$AlCl_3$ electrolyte solution and the −1/2 power of transition time (τ_1) calculated from the chronopotentiograms of anodic dissolution.

4.3.5. Anodic dissolution Chronopotentiometry in $DMSO_2$-$AlCl_3$ electrolyte with NH_4Cl and TMAC

As mentioned in Chapter 2, the addition of NH_4Cl or TMAC decreases the viscosity of the $DMSO_2$–$AlCl_3$ electrolyte solution. Chronopotentiometry of electrolyte solutions with addition of NH_4Cl or TMAC is expected to behave according to the Sand formula. Therefore, chronopotentiometry measurements were performed for anodic dissolution in $DMSO_2$–$AlCl_3$ electrolyte solution with NH_4^+ concentration of 0.205 mol L^{-1} (Fig. 4-10a) and with a TMA^+ concentration of 0.201 mol L^{-1} (Fig. 4-10b) at different cathodic electrodeposition times ranging from 2 s to 40 s. The cathodic and anodic current density was 0.4 mA mm^{-2}. In both cases, for cathodic electrodeposition times of 10 s or more, the anodic dissolution exhibited a two-wave behavior. The transition time τ_1 until the transition to the second-stage potential converged to a constant value for long cathodic electrodeposition times. These results follow the same trend as those of the basic composition bath, as shown in Fig. 4-2.

Figures 4-11, 4-12 show chronopotentiograms for anodic dissolution in electrolyte solution with different concentration of NH_4^+ and TMA^+ at various anodic current densities. Figures 4-13 and 4-14 show the plots of the −1/2 power of the transition time τ_1 with respect to the anodic current density. Regardless of the NH_4^+ or TMA^+ concentrations, all plots fit well a straight line through the origin.

If the anodic dissolution reaction in $DMSO_2$–$AlCl_3$ electrolyte solution satisfies the conditions of the Sand formula, the diffusion coefficient *D* as the controlling factor can be calculated from the Sand formula. Table 4-3 shows the *D* values obtained from the slope of the plots of Figs. 4-9, 4-13, and 4-14. As three molecules of $DMSO_2$ are consumed for each three electrons in Eq. 4-3, the valence *n* in the Sand formula can be deemed 1. The calculated *D* values ranged between 0.4×10^{-11} and 1.8×10^{-11} m^2 s^{-1} and increased with increasing concentration of NH_4^+ or TMA^+ because the viscosity decreased owing to NH_4^+ or TMA^+ addition.

The diffusion coefficient *D* of molecules in solution is given by the Einstein–Stokes

formula shown in Eq. 4-8:

$$D = \frac{k_B T}{6\pi r \eta}, \tag{4-8}$$

where k_B is the Boltzmann constant, T is the absolute temperature, r is the Stokes radius, and η is the solution viscosity. Figure 4-15 shows a plot of the D values calculated using the Sand formula with respect to the reciprocal of the solution viscosity ($1/\eta$). The error bars in the graph reflect variations in viscosity measurements. The plot approximates a straight line through the origin, suggesting that the $DMSO_2$–$AlCl_3$ electrolyte solution follows the Einstein–Stokes equation, regardless of the addition of NH_4Cl or TMAC. By introducing the slope of the plot in Fig. 4-15 (2.33×10^{-13} kg m s^{-2}) into Eq. 4-8, the Stokes radius r was determined to be 1100 pm. This is considerably larger than the molecular size of $DMSO_2$ (about 280 pm) and slightly larger than the size of $Al(DMSO_2)_3^{3+}$. To ensure that sufficient $DMSO_2$ diffuses from the bulk to the electrode, $Al(DMSO_2)_3^{3+}$ must diffuse from near the electrode into the bulk. One of the reasons for the Stokes radius to be larger than the size of $DMSO_2$ and $Al(DMSO_2)_3^{3+}$ may be the simultaneous diffusion of both species. Legrand suggested the possibility of the existence of $Al(DMSO_2)_n^{3+}$ ($n > 3$) as well as $Al(DMSO_2)_3^{3+}$ [2]. In accordance with this, in the ^{27}Al NMR spectrum of the electrolyte shown in Chapter 2, another peak was observed near the peak attributed to $Al(DMSO_2)_3^{3+}$. The large Stokes radius calculated herein also suggests the existence of $Al(DMSO_2)_n^{3+}$ ($n > 3$), in which more than three $DMSO_2$ molecules are solvated.

Table 4-3. Diffusion coefficient in $DMSO_2$–$AlCl_3$ electrolyte solution calculated via chronopotentiometry.

Molar concentration / mol L^{-1}		Diffusion coefficient
NH_4^+	TMA^+	$\times 10^{-11}$ / m^2 s^{-1}
0.000	0.000	0.448
0.205	0.000	0.468
0.502	0.000	0.590
0.692	0.000	0.944
0.979	0.000	1.146
0.000	0.201	0.677
0.000	0.486	0.988
0.000	0.923	1.834

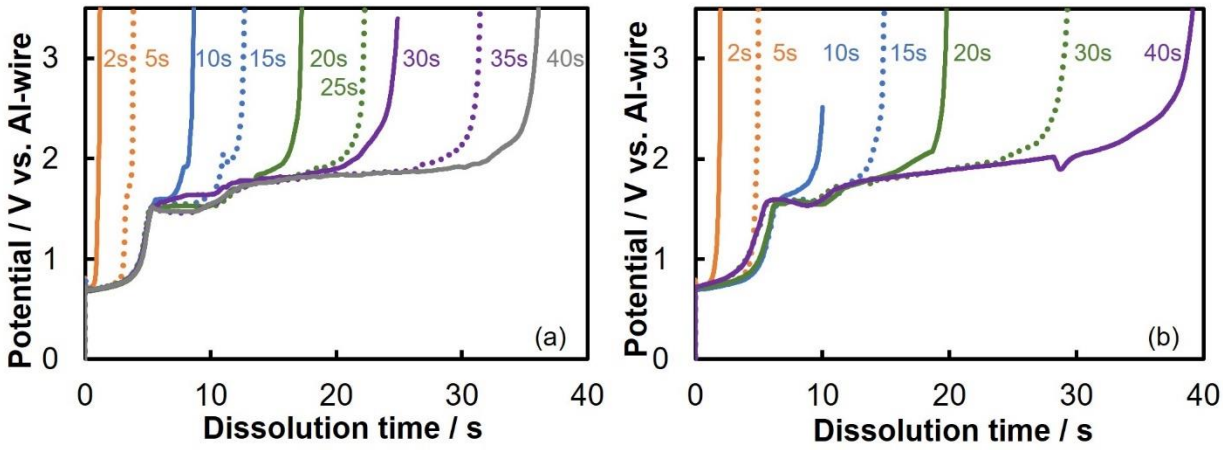

Figure 4-10. Chronopotentiograms of anodic dissolution in $DMSO_2$–$AlCl_3$–NR_4Cl electrolyte solution measured at different cathodic electrodeposition times. (a) NH_4^+ concentration, 0.205 mol L^{-1}; (b) TMA^+ concentration, 0.201 mol L^{-1}; current density of cathodic electrodeposition, 0.4 mA mm^{-2}; cathodic electrodeposition time, 2–40 s; anodic dissolution current density, 0.4 mA mm^{-2}; temperature, 90 °C.

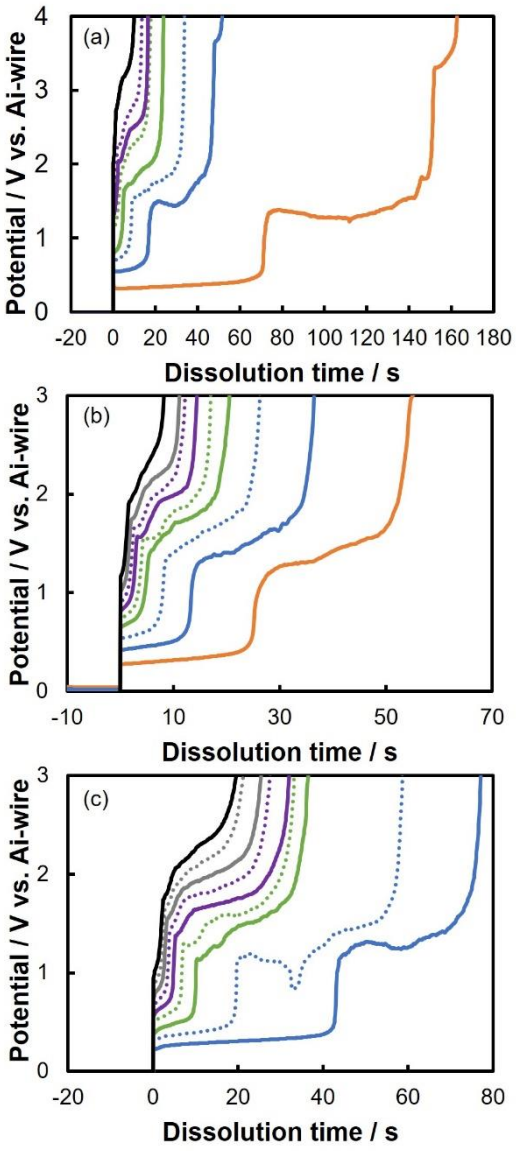

Figure 4-11. Chronopotentiograms of anodic dissolution in $DMSO_2$–$AlCl_3$–NH_4Cl electrolyte at various anodic dissolution current densities. (a) NH_4^+ concentration, 0.205 mol L^{-1}; (b) NH_4^+ concentration, 0.502 mol L^{-1}; (c) NH_4^+ concentration, 0.979 mol L^{-1}; current density of cathodic electrodeposition, 0.4 mA mm^{-2}; cathodic electrodeposition time, 30 s; current density of anodic dissolution, 0.1 mA mm^{-2} (orange solid line), 0.2 mA mm^{-2} (blue solid line), 0.3 mA mm^{-2} (blue dotted line), 0.4 mA mm^{-2} (green solid line), 0.5 mA mm^{-2} (green dotted line), 0.6 mA mm^{-2} (violet solid line), 0.7 mA mm^{-2} (violet dotted line), 0.8 mA mm^{-2} (gray solid line), 0.9 mA mm^{-2} (gray dotted line), 1.0 mA mm^{-2} (black solid line); temperature, 90 °C;.

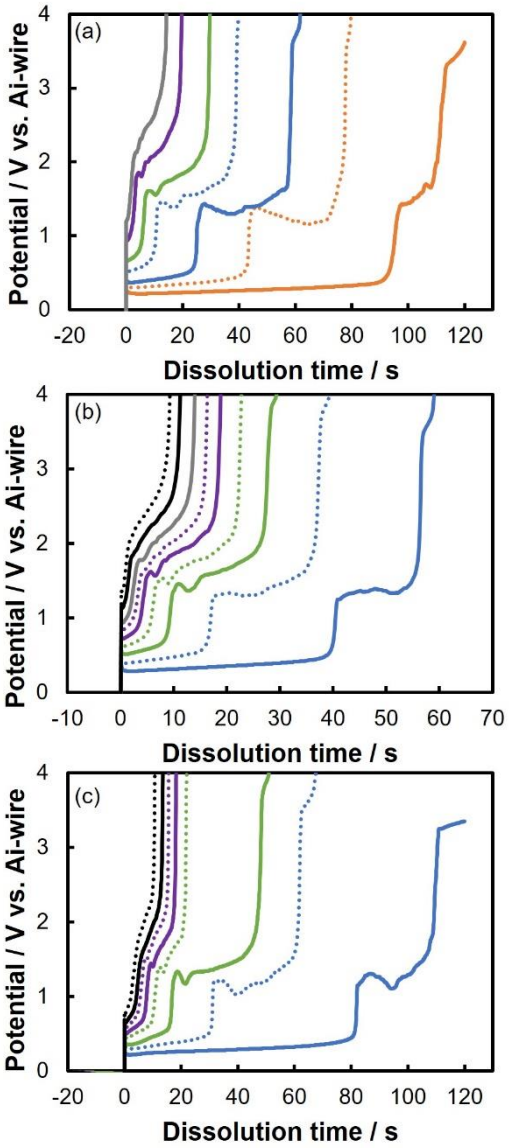

Figure 4-12. Chronopotentiograms of anodic dissolution in $DMSO_2$–$AlCl_3$–tetramethylammonium chloride (TMAC) electrolyte solution at various anodic dissolution current densities. (a) TMA^+ concentration, 0.201 mol L^{-1}; (b) TMA^+ concentration, 0.486 mol L^{-1}; (c) TMA^+ concentration, 0.923 mol L^{-1}; current density of cathodic electrodeposition, 0.4 mA mm^{-2}; cathodic electrodeposition time, 30 s; current density of anodic dissolution, 0.1 mA mm^{-2} (orange solid line), 0.15 mA mm^{-2} (orange dotted line), 0.2 mA mm^{-2} (blue solid line), 0.3 mA mm^{-2} (blue dotted line), 0.4 mA mm^{-2} (green solid line), 0.5 mA mm^{-2} (green dotted line), 0.6 mA mm^{-2} (violet solid line), 0.7 mA mm^{-2} (violet dotted line), 0.8 mA mm^{-2} (gray solid line), 0.9 mA mm^{-2} (gray dotted line), 1.0 mA mm^{-2} (black solid line), and 1.2 mA mm^{-2} (black dotted line); temperature, 90 °C.

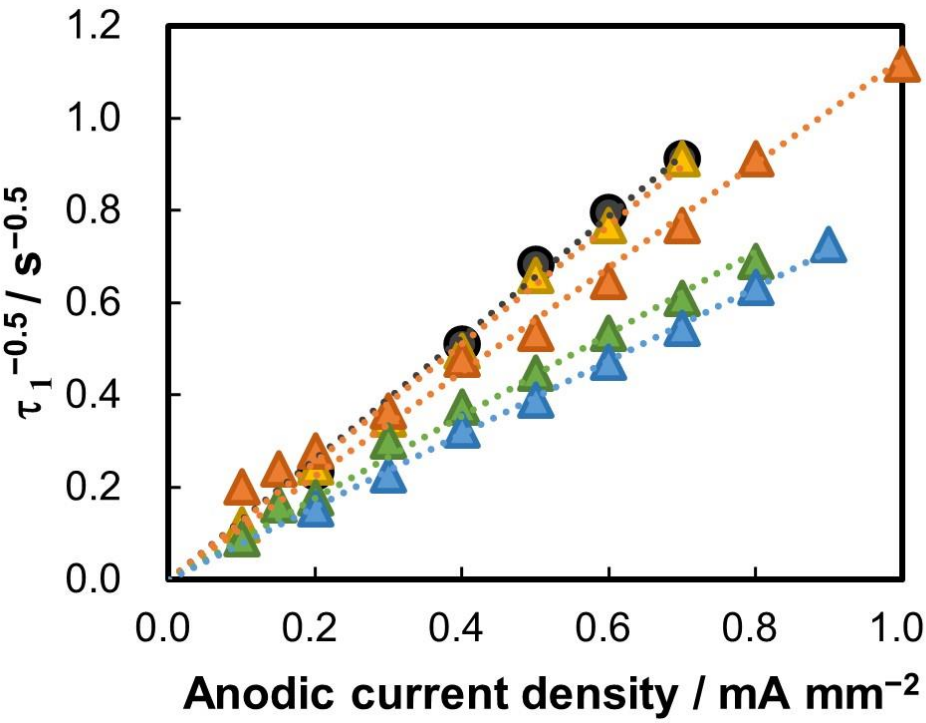

Figure 4-13. Relationship between anodic dissolution current density and the −1/2 power of the transition time (τ_1) in $DMSO_2$–$AlCl_3$–NH_4Cl electrolyte solution. (Black circles) NH_4^+ 0.000 mol L^{-1}; (yellow triangles) NH_4^+ 0.205 mol L^{-1}; (orange triangles) NH_4^+ 0.502 mol L^{-1}; (green triangles) NH_4^+ 0.692 mol L^{-1}; (blue triangles) NH_4^+ 0.979 mol L^{-1}.

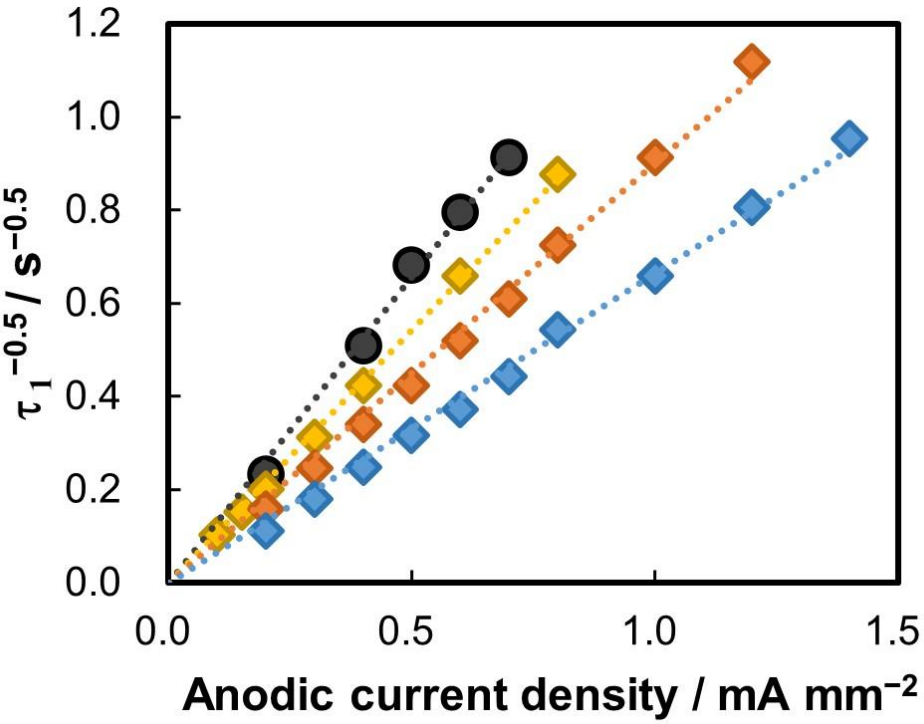

Figure 4-14. Relationship between anodic dissolution current density and the −1/2 power of the transition time (τ_1) in $DMSO_2$–$AlCl_3$–tetramethylammonium chloride (TMAC) electrolyte solution. (Black circles) TMA^+ 0.000 mol L^{-1}; (yellow diamonds) TMA^+ 0.201 mol L^{-1}; (orange diamonds) TMA^+ 0.486 mol L^{-1}; (blue diamonds) TMA^+ 0.923 mol L^{-1}.

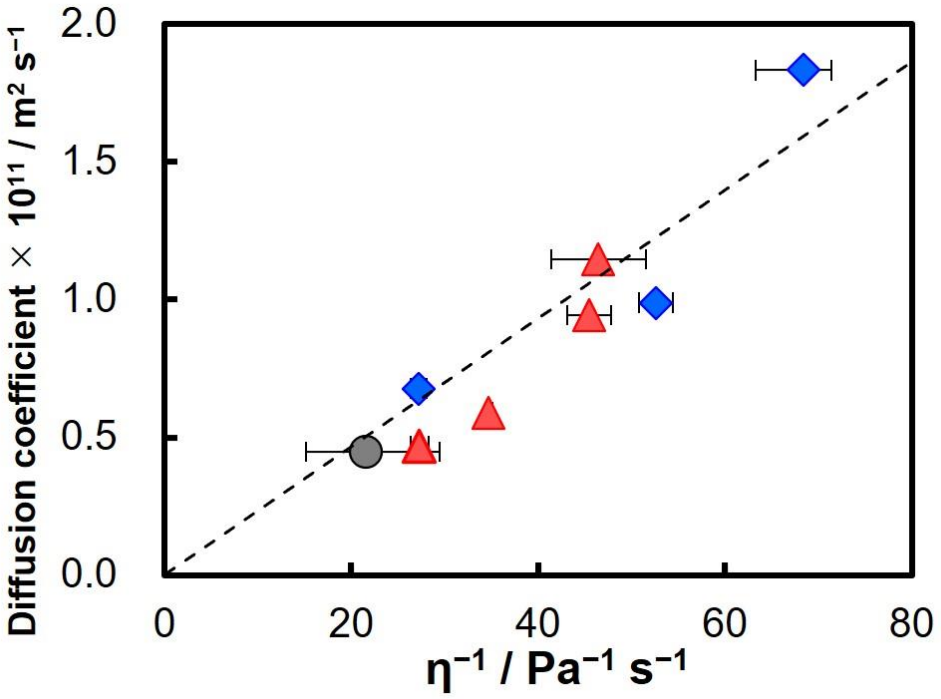

Figure 4-15. Relationship between the diffusion coefficient calculated using the Sand formula and the reciprocal of viscosity ($1/\eta$). (Blue circles) basic composition; (red triangles) NH_4^+ 0.201–0.979 mol L^{-1}; (blue diamonds), TMA^+ 0.201–0.923 mol L^{-1}.

4.4. Summary of findings

In this chapter, to analyze the anodic dissolution reaction in $DMSO_2$–$AlCl_3$ electrolyte solution, cathodic electrodeposition was performed at a constant current using a Pt disk electrode followed by chronopotentiometry measurements of the anodic dissolution. The main conclusions are as follows.

1. The anodic dissolution in $DMSO_2$–$AlCl_3$ electrolyte solution measured via chronopotentiometry exhibits a two-wave behavior at high anodic current density. The anodic dissolving potential of the second stage is about 1.0 V higher than that of the first-stage.
2. The potential of the second-stage reaction and the results of multiple reverse chronopotentiometry measurements suggest that the anodic dissolution reaction of the second-stage involves a three-electron transfer from Al^0 and $AlCl_4^-$ to $Al_2Cl_7^-$.
3. The anodic dissolution reaction involves two stages because $Al(DMSO_2)_3^{3+}$ is not stably formed owing to $DMSO_2$ depletion near the electrode during the anodic dissolution reaction.
4. The transition time until the anodic dissolution potential shifts to the second-stage is proportional to the −0.5 power of the anodic current density and can be described by the Sand formula. This indicates that the transition to the second-stage is a diffusion-dominated process.
5. The addition of NH_4Cl and TMAC promotes the diffusion delivery of $DMSO_2$ by reducing the viscosity of the electrolyte.
6. The diffusion coefficient obtained from the transition time to the second-stage and the anodic current density generally satisfies the Einstein–Stokes formula. The Stokes radius calculated from this slope is larger than the estimated size of $Al(DMSO_2)_3^{3+}$, suggesting the possibility of the existence of $Al(DMSO_2)_n^{3+}$ ($n > 3$).

4.5. References

[1] J. Tang and K. Azumi, *Electrochim. Acta*, **56**, 1130 (2011).

[2] L. Legrand, M. Heintz, A. Tranchant and R. Messina, *Electrochim. Acta*, **40**, 1711 (1995).

[3] L. Legrand, A. Tranchant, and R. Messina, *Electrochim. Acta*, **41**, 2715 (1996).

[4] T. Hirato, J. Fransaer, and J. -P. Celis, *J. Electrochem. Soc.*, **148**, C280 (2001).

[5] H. Ohno (ed.), *Electrochomical Aspects of Ionic Liquids* (Wiley Interscience, New York) (2005).

[6] M. Shinichi, *Electrochemistry*, **67**, 1084 (1999).

[7] Y. Katayama, *Electrochemistry*, **79**, 969 (2011).

Chapter 5. Conclusions and Prospects

5.1. Conclusions

This study aimed to establish an electrolyte composition that has high electrical conductivity and facilitates plating with high Coulombic efficiency and to investigate the key factors required for controlling the anodic dissolution reaction. In brief, this study aimed to achieve conductivity of 0.5 S m^{-1} or more at 100 °C and Coulombic efficiency of 80% or more. In addition, the electroplating and electrochemical properties of $DMSO_2$–$AlCl_3$ electrolyte solution with added additives were estimated in this study. The conclusions are summarized below.

5.1.1. Mechanism of increasing the conductivity of electrolyte solution by adding of additives

The addition of ammonium salts, NH_4Cl and TMAC, were found to effectively increase the conductivity of the electrolyte solution. Conductivity increased in proportion to the amount of NH_4Cl and TMAC added, whereas viscosity decreased. This decrease in viscosity contributed to an increase in conductivity according to Walden's law. The addition of NH_4Cl and TMAC caused an ionic equilibrium change in the electrolyte and increased the concentration of nonsolvating $DMSO_2$ species, thereby decreasing the viscosity.

5.1.2. Effect of NH_4Cl and TMAC on film and electrolyte solution properties

Side reactions occur in an additive-free electrolyte and decrease Coulombic efficiency at potentials lower than −0.8 V vs. Al-wire. $DMSO_2$ remains in large amounts in the electrolyte. However, it is a reduction reaction of $DMSO_2$ molecules solvated with Al^{3+} as $DMSO_2$ is not reduced in this potential region. NH_4Cl shifts the Al electrodeposition potential on the Pt electrode to the positive side and accelerates the Al electrodeposition reaction even at an added

amount of NH_4Cl of 0.02 mol. Consequently, the Al electrodeposition reaction proceeds at a positive potential than the side reaction region, and the electrodeposition film becomes highly pure, uniform, and has an excellent appearance without black deposits. However, the Coulombic efficiency decreases when a high concentration of NH_4Cl is added since NH_4^+ reduction reaction occurs at a more positive potential than that in the Al electrodeposition reaction. Therefore, adding a high concentration of NH_4Cl to increase conductivity is not appropriate. Although TMAC suppresses the Al electrodeposition reaction, the reduction reaction of TMAC itself does not occur in the region where the Al electrodeposition reaction proceeds. Therefore, the Coulombic efficiency does not decrease considerably even if TMAC is added up to 0.1 mol, which is enough to raise the conductivity sufficiently. By adding a small amount of NH_4Cl that does not extensively decrease the Coulombic efficiency and an amount of TMAC that can sufficiently increase the electrical conductivity, the Al electrodeposition promoting action of NH_4Cl can be preferentially expressed over the Al electrodeposition suppressing action of TMAC. Thus, a good Al deposition film similar to the case of adding NH_4Cl alone can be obtained. By adding 0.02 mol of NH_4Cl and 0.10 mol of TMAC together, the conductivity of the electrolyte increased to 0.54 S m^{-1}, and the Coulombic efficiency became 86.6%. Due to the addition of additives, the loss of Coulombic efficiency due to the combined addition of additives was only about 7%. The conductivity increased to about three times that of the additive-free, whereas the tank voltage decreased to about 1/3 of that of the additive-free. Compared to the additive-free electrolyte, this electrolyte consumes about 1/3 times of the power consumption, and thus, the energy saving of the Al electrodeposition process has been realized. Here, the author found an electrolyte composition that has high conductivity and allows plating with high current density by adding NH_4Cl and TMAC together. An excellent film appearance was also obtained with a high current density using this electrolyte.

5.1.3. Factors influencing the anodic dissolution reaction

When there is insufficient $DMSO_2$ in the vicinity of the anode electrode, the anodic

dissolution reaction of Al in the $DMSO_2$–$AlCl_3$ electrolyte solution shifts from the normal dissolution reaction to Al^{3+} to another anodic dissolution reaction that occurs at a more positive potential. The anodic reaction produces $Al_2Cl_7^-$, which increases the tank voltage during electrodeposition. The addition of NH_4Cl and TMAC promotes the diffusion supply of $DMSO_2$ while lowering the viscosity of the electrolyte. Thus, a supply of sufficient $DMSO_2$ to the vicinity of the anode was essential for the anodic dissolution reaction to proceed at a low potential.

5.2. Prospects for the future

In future research, the process scale-up of the Al electrodeposition process needs to be verified using the electrolyte composition established in this study for practical use. As clarified in this study, sufficient supply of $DMSO_2$ to the vicinity of the anode is necessary for the anodic dissolution reaction to proceed stably at low potential. This can be achieved by optimizing the anode structure and ensuring strong solution flow. In addition, the electrochemical measurement method using microelectrodes investigated in this study is a technology useful for controlling the electrolyte solution for stabilizing the quality of the electrodeposited film. By utilizing the knowledge gained in this research, the author intends to develop equipment and mass production technology for the practical application of Al electrodeposition process.

List of Publications and Presentations

Original Papers

1. J. Matsuda, A. Okamoto, Haruo Akahoshi, S. Shironita, M. Umeda, *J. Electrochem. Soc.*, **169**, 042502 (2022). [DOI: 10.1149/1945-7111/ac613c]
2. J. Matsuda, A. Okamoto, Haruo Akahoshi, S. Shironita, M. Umeda, *J. Electrochem. Soc.*, **169**, 112516 (2022). [DOI: 10.1149/1945-7111/aca2ea]
3. J. Matsuda, A. Okamoto, Haruo Akahoshi, S. Shironita, M. Umeda, *J. Electrochem. Soc.*, **170**, 042503 (2023). [DOI: 10.1149/1945-7111/accba6]

Patents

1. J. Matsuda, A. Okamoto; "Electric aluminum plating solution, method for producing aluminum film using the same, and method for manufacturing aluminum foil", JP patent, JP2021-095638, December 7, 2020.

Oral Presentations

1. G. Kamiji, H. Akahoshi, M. Umeda, J. Matsuda, A. Okamoto, T. Shimada; Electrochemical Evaluation of Al Electrodeposition Reaction in Dimethyl Sulfone-Based Electrolyte Using Microelectrodes, *141st Meeting of the Surface Finishing Society of Japan*, B02-09, March 3, 2020.
2. G. Kamiji, H. Akahoshi, M. Umeda, J. Matsuda, A. Okamoto; Electrochemical Evaluation of Al Electrodeposition Reaction in Dimethyl Sulfone-Based Electrolyte Using Microelectrodes (2), *142nd Meeting of the Surface Finishing Society of Japan*, B02-09, September 7, 2020.
3. H. Akahoshi, Y. Sawa, S. Shironita, M. Umeda, J. Matsuda, A. Okamoto; Analysis of Electrochemical Behavior of Ammonium Salts in Dimethyl Sulfone Solvents, *144th Meeting of the Surface Finishing Society of Japan*, 17B-01, September 17, 2021.
4. J. Matsuda, A. Okamoto, Y. Sawa, H. Akahoshi, M. Umeda; Improvement of Conductivity

of Aluminum Plating Solution by Adding Ammonium Salts, *144th Meeting of the Surface Finishing Society of Japan*, 17B-02, September 17, 2021.

5. Y. Sawa, J. Matsuda, A. Okamoto, H. Akahoshi, S. Shironita, M. Umeda; Polarization Behavior of Aluminum Plating Solution with Ammonium Salt, *144th Meeting of the Surface Finishing Society of Japan*, 17B-03, September 17, 2021.
6. H. Akahoshi, J. Matsuda, Y. Sawa, S. Shironita, M. Umeda; Study of Al Anode Dissolution Reaction in Dimethyl Sulfone Solvent, *146th Meeting of the Surface Finishing Society of Japan*, 06A-03, September 6, 2022.
7. H. Akahoshi, J. Matsuda, Y. Sawa, S. Shironita, M. Umeda; Fast Sweep Voltammetry Analysis of Al Electrodeposition/Dissolution Reaction from Dimethyl Sulfone Solvent (1), *147th Meeting of the Surface Finishing Society of Japan*, 07C-08, March 7, 2023.

Acknowledgment

I would like to express my deepest gratitude to Dr. Haruo Akahoshi, Project Professor of the Department of Materials Science and Technology, Nagaoka University of Technology (NUT), for his enthusiastic and careful guidance and appropriate advice throughout the execution of this research and the completion of my dissertation.

I would like to express my heartfelt gratitude to Prof. Minoru Umeda and Associate Prof. Sayoko Shironita of the Department of Materials Science and Technology, NUT, for providing the research space and equipment necessary to conduct this research and provided warm encouragement and accurate advice for this study and dissertation as supervisors.

I would like to thank Prof. Hiroshi Matsubara of the Department of General Education, NUT, and Prof. Takayuki Ishibashi and Prof. Tsuyoshi Honma and Associate Prof. Asami Funatsu of the Department of Materials Science and Technology, NUT, for their helpful discussions and advice on this study and dissertation as examiners.

I would like to take this opportunity to express my gratitude to Mr. Gakuto Kamiji and Mr. Yuma Sawa of the Department of Materials Science and Technology, NUT, who supported me in the electrochemical measurements and analysis in this research.

I would like to offer my deep gratitude to Mr. Kenichi Inoue, Mr. Hirohisa Sano, Dr. Tsunenori Yamamoto, Dr. Hideki Yamaura, Mr. Setsuo Ando, Dr. Takeshi Shimada, Dr. Hajime Murakami, Mr. Yuichi Kusada, Mr. Shin Takahashi, Mr. Hiroshi Onuma, Dr. Kenji Okishiro, Dr. Hisato Tokoro, and Dr. Atsushi Okamoto of Proterial Co., Ltd. (formerly Hitachi Metals Co., Ltd.) for giving me the opportunity to enroll in this doctoral program and many considerations regarding balancing corporate work and doctoral program. I would also like to express my gratitude to the Functional Ceramics Group and related departments.

Finally, I would like to express my sincere gratitude to my wife, daughter, and son, who have always supported me physically and mentally.

Junichi Matsuda

August 2023